

COBALT RECOVERY FROM THE IRON CREEK DEPOSIT USING PHYSICAL BENEFICIATION

By
Emma Bishop

© Copyright by Emma Bishop, 2023
All Rights Reserved

A thesis submitted to the Faculty and the Board of Trustees of the Colorado School of Mines in partial fulfillment of the requirements for the degree of Master of Science (Earth Resource Development Engineering).

Golden, Colorado

Date: _____

Signed: _____
Emma Bishop

Signed: _____
Dr. Corby Anderson
Thesis Advisor

Golden, Colorado

Date: _____

Signed: _____
Professor M. Stephen Enders
Department Head
Mining Engineering

ABSTRACT

Cobalt is defined as a critical mineral by the U.S. Department of Energy, commonly used in lithium-ion batteries, jet turbines, and steel alloys. Currently, the U.S. is nearly completely dependent on imports for its cobalt supply. Due to this, efforts to mine and refine cobalt domestically are being pursued. This thesis describes part of the effort of Electra Battery Materials to create a functional cobalt mine at the Iron Creek deposit, located in the Idaho Cobalt Belt. The focus of this research is to examine the feasibility of physical beneficiation methods on different mineral samples in an attempt to improve the cobalt grade, and to create an economically feasible flowsheet when combined with the other research sections of this project. Specifically, the physical beneficiation methods tested were magnetic separation, heavy liquid separation, and electrostatic separation. The feed materials tested were a deposit sample, a bulk flotation concentrate, a thermal decomposition product of the bulk flotation concentrate, a differential flotation concentrate, and a thermal decomposition product of the differential flotation concentrate. Bond work index testing and sortation sampling was also performed on the deposit samples. It was determined that magnetic separation of the thermal decomposition products showed the most success in increasing the cobalt grade in the concentrate of all methods tested and is the most likely to be used in a flowsheet. Testing of the deposit samples and bulk flotation concentrate also showed promising results in the heavy liquid separation and electrostatic separation but are less likely to be used due to being less efficient than other already established methods. Preliminary leaching testing was then performed on the magnetic product of the thermal decomposition magnetic separation testing to examine the response.

TABLE OF CONTENTS

ABSTRACT.....	iii
TABLE OF CONTENTS.....	iv
LIST OF FIGURES	ix
LIST OF TABLES	xi
LIST OF EQUATIONS	xiv
ACKNOWLEDGEMENTS	xv
CHAPTER 1. INTRODUCTION	1
1.1 Critical Materials	1
1.2 Criticality of Cobalt	2
1.3 Idaho Cobalt Belt	3
1.4 Content of Work	3
CHAPTER 2. LITERATURE REVIEW	4
2.1 Discovery of Cobalt	4
2.2 Properties of Cobalt	4
2.3 Applications of Cobalt	4
2.4 Global Cobalt Production	5
2.5 Cobalt Deposit Types.....	7
2.5.1 Stratiform Sediment-hosted (SSH) Cu-Co Deposits.....	7
2.5.2 Ni-Co laterites.....	8
2.5.3 Magmatic Ni-Cu-Co sulfide deposits.....	8
2.5.4 Hydrothermal and volcanogenic deposits	8
2.5.5 Underwater deposits.....	9
2.6 Cobalt Recovery Methods.....	9
2.6.1 Sediment Hosted Cu-Co Deposits.....	9
2.6.2 Ni Laterites.....	11
2.6.3 Magmatic Ni Sulfides	13
2.6.4 Cobalt Arsenides	14
2.6.5 Recycling	15
2.7 Magnetic Separation	16
2.7.1 Magnetic Behavior.....	16
2.7.2 Magnetic Separation Theory.....	17
2.7.2 Magnetic Separation of Pyrite.....	18

2.7.3 Magnetic Separation of Pyrrhotite	18
2.7.4 Effects of Microwave Heating on Magnetic Separation	19
2.8 Gravity Separation	19
2.8.1 Specific Gravity	19
2.8.2 Gravity Separation Theory	20
2.8.3 Gravity Separation of Pyrite	20
2.9 Electrostatic Separation	21
2.9.1 Electrical Conductivity	21
2.9.2 Electrical Charging Methods	21
2.9.4 Electrostatic Separation of Pyrite.....	25
2.10 Sulfuric Acid Leaching of Pyrite and Pyrrhotite.....	26
2.10.1 Factors Effecting Leaching of Pyrite and Pyrrhotite.....	26
CHAPTER 3. CHARACTERIZATION OF IRON CREEK DEPOSIT.....	28
3.1 Iron Creek Deposit.....	28
3.2 Iron Creek Deposit Characterization.....	28
3.3 Previous Testing.....	30
3.4 Sample Preparation	36
3.4.1 Sample Storage Preparation.....	36
3.4.2 3-Acid Digestion Procedure.....	39
CHAPTER 4. BOND WORK INDEX TESTING.....	40
4.1 Bond Work Index.....	40
4.2 Bond Work Index Testing Procedure.....	40
4.3 Bond Work Index Data	42
4.4 Bond Work Index Discussion	43
CHAPTER 5. SORTATION.....	44
5.1 Scanning Type Determination	44
5.2 Scanning Testing Procedure.....	45
5.3 Sortation Sample Analysis	46
5.4 Sortation XRT Scan Data.....	48
5.5 Sortation Cobalt and Copper AAS Data	49
5.6 Sortation XRT and ASS Data Combined.....	50
5.7 Sortation Discussion	51
CHAPTER 6. MAGNETIC SEPARATION	52
6.1 Testing Conditions.....	52
6.1.1 Testing of Thermal Decomposition Products	54

6.2 Wet High Intensity Magnetic Separation Testing Procedures	55
6.2.1 Deposit Sample Testing Procedure	55
6.2.2 Bulk Flotation Testing Procedure	55
6.2.3 Thermal Decomposition Bulk Flotation Product Testing Procedure	56
6.2.4 Differential Flotation Product Testing Procedure	56
6.2.5 Thermal Decomposition Differential Flotation Product Testing Procedure	56
6.3 Preparation of Magnetic Separation Sample for Analysis	56
6.3.1 AAS Preparation	56
6.4 Magnetic Separation AAS Data.....	57
6.5 Magnetic Separation Washability Curves.....	62
6.6 Mineralogy of Thermal Decomposition Products.....	64
6.7 Magnetic Separation Statistical Analysis.....	66
6.7.1 Statistical Analysis on Feed Materials Testing	66
6.7.2 Statistical Analysis on Flotation and Thermal Decomposition Materials Testing	68
6.8 Magnetic Separation Discussion.....	74
CHAPTER 7. GRAVITY SEPARATION.....	76
7.1 Testing Conditions	76
7.2 Gravity Separation Testing Procedures.....	77
7.2.1 Deposit Sample Testing Procedure	77
7.2.2 Bulk Flotation Testing Procedure	77
7.2.3 Deposit Sample Washability Curve Testing Procedure	77
7.2.4 Bulk Flotation Washability Curve Testing Procedure	78
7.3 Preparation of Gravity Separation Sample for Analysis	78
7.4 Gravity Separation AAS Data.....	78
7.5 Heavy Liquid Separation Washability Curves.....	79
7.6 Gravity Separation Statistical Analysis.....	83
7.6.1 Statistical Analysis on RPM Testing.....	83
7.6.2 Statistical Analysis on Particle Size Testing.....	84
7.7 Gravity Separation Discussion.....	85
CHAPTER 8. ELECTROSTATIC SEPARATION.....	87
8.1 Testing Conditions	87
8.2 Electrostatic Separation Testing Procedures.....	88
8.2.1 Deposit Sample Testing Procedure	88
8.2.2 Bulk Flotation Testing Procedure	89
8.3 Preparation of Electrostatic Separation Sample for Analysis	89

8.4 Electrostatic AAS Data	89
8.5 Electrostatic Washability Curve.....	90
8.6 Electrostatic Statistical Analysis	92
8.7 Electrostatic Separation Discussion	93
CHAPTER 9. SULFURIC ACID LEACHING	95
9.1 Pourbiax Diagrams.....	95
9.1.1 Iron Pourbaix Diagram.....	95
9.1.2 Sulfur Pourbaix Diagram	96
9.2 Leaching Testing Conditions	97
9.3 Leaching Testing Procedure.....	98
9.4 Leaching AAS Data	98
9.5 Leaching Statistical Analysis	99
9.5.1 Analysis of Cobalt Recovery	99
9.5.2 Analysis of Copper Recovery	101
9.5.3 Analysis of Iron Recovery	103
9.6 Leaching Discussion	105
CHAPTER 10. ECONOMIC ANALYSIS	106
10.1 Model Assumptions	106
10.1.1 Operation Assumptions.....	106
10.1.2 Elemental Value Assumptions	106
10.1.3 Assumptions for Testing Conditions.....	107
10.1.4 Consumable Operating Cost Assumptions.....	107
10.1.5 Employee Number, Wage, and Salary Assumptions	107
10.1.6 Model Discount Rate	108
10.1.7 Model Timeline.....	108
10.2 Model Capital Expenditures (CAPEX).....	108
10.2.1 Gravity Separation CAPEX	108
10.2.2 Electrostatic Separation CAPEX	109
10.3 Model Recoveries of Separation Methods	109
10.4 Gravity Separation Model Output.....	110
10.5 Electrostatic Separation Model Output.....	110
10.6 Model Sensitivity Analysis	111
10.6.1 Gravity Separation Sensitivity Analysis	111
10.6.2 Electrostatic Separation Sensitivity Analysis.....	113
10.7 Combined Economic Model	114

10.7.1 Combined Model Assumptions.....	114
10.7.2 Combined Model Output	115
10.7.3 Sensitivity Analysis.....	117
10.9 Model Comparisons and Conclusions.....	118
CHAPTER 11. CONCLUSIONS	119
11.1 Proposed Flowsheets.....	120
11.2 Further Work.....	122
11.2.1 Magnetic Separation Further Work.....	122
11.2.2 Gravity Separation Further Work	123
11.2.3 Electrostatic Separation Further Work.....	123
11.2.4 Leaching Further Work.....	123
REFERENCES	125
APPENDICES	130
APPENDIX A. Elemental Characterization	130
APPENDIX B. Bond Work Index G_{pr} , F_{80} , P_{80} Data	132
APPENDIX C. Additional Magnetic Separation Washability Curves	135
APPENDIX D. Additional Magnetic Separation Statistical Analysis Data.....	137
APPENDIX E. Additional Gravity Separation Washability Curves.....	139
APPENDIX F. Additional Electrostatic Separation Data.....	142
APPENDIX G. Additional Electrostatic Separation Washability Curves	144
APPENDIX H. Grade Calculations	146
APPENDIX I. Recovery Calculations	147
APPENDIX J. Combined Economics Design Criteria and Model Assumptions	148
APPENDIX K. Refined Flowsheet with Mass Balances	158

LIST OF FIGURES

Figure 2.1: Map of major cobalt deposits [13].....	7
Figure 2.2: Example flowsheet used to process sediment hosted Cu-Co deposits [13].....	10
Figure 2.3: Example flowsheet used to process nickel laterite deposits [13].	12
Figure 2.4: Example flowsheet used to process magmatic Ni sulfides deposits [13].	13
Figure 2.5: Example flowsheet used to process Cobalt arsenides deposits [13].....	15
Figure 2.6: Rotational drum separator, inductive charging.....	22
Figure 2.7: Rotational drum separator, corona charging.....	22
Figure 2.8: Particle-particle triboelectric charging.	23
Figure 2.9: Drum separator diagram	24
Figure 2.10: Multi-electrode drum separator diagram.	24
Figure 2.11: Belt separator diagram.....	25
Figure 2.12: Free fall separator diagram.	25
Figure 3.1: Color key for the identified images of samples IC 18-07, IC 18-09, and IC 18-27.	28
Figure 3.2: Identified image for sample IC 18-07.....	29
Figure 3.3: Identified image of sample IC 18-09.....	29
Figure 3.4: Identified image for sample IC 18-27.....	30
Figure 3.5: Laboratory scale jaw crusher unit.....	37
Figure 3.6: Laboratory scale jaw crusher unit.....	38
Figure 5.1: Sortation samples on tarps before XRT scanning.	46
Figure 5.2: Ring and puck mill used for grinding.....	47
Figure 5.3: Ro-tap used for particle size analysis.	48
Figure 5.4: XRT scan of all 4 samples showing density differences by different colors.....	48
Figure 6.1: Bench scale WHIMS diagram.	53
Figure 6.2: WHIMS washability curve of the cobalt response of the magnetic fraction of the deposit sample.	63
Figure 6.3: WHIMS washability curve of the copper response of the magnetic fraction of the deposit sample.	64
Figure 6.4: Identified image of thermal decomposition product of bulk flotation concentrate magnetic fraction.....	65
Figure 6.5: Identified image of thermal decomposition product of bulk flotation concentrate non-magnetic fraction.....	65
Figure 6.6: Half-normal plot for magnetic separation cobalt grade effects.	69
Figure 6.7: Half-normal plot for magnetic separation cobalt recovery effects.	69

Figure 6.8: Magnetic Separation cobalt grade Pareto chart.	70
Figure 6.9: Magnetic Separation cobalt recovery Pareto chart.	70
Figure 6.10: Half-normal plot for magnetic separation copper grade effects.	72
Figure 6.11: Half-normal plot for magnetic separation copper recovery effects.	72
Figure 6.12: Magnetic Separation copper grade Pareto chart.	73
Figure 6.13: Magnetic Separation copper recovery Pareto chart.	73
Figure 7.1: Washability curve of the cobalt response of the deposit sample.	80
Figure 7.2: Washability curve of the cobalt response of the bulk flotation concentrate.	81
Figure 7.3: Washability curve of the copper response of the deposit sample.	82
Figure 7.4: Washability curve of the copper response of the bulk flotation concentrate.	82
Figure 8.1: High tension roll separator.	87
Figure 8.2: Electrostatic washability curve of the cobalt response of the deposit sample.	91
Figure 8.3: Electrostatic washability curve of the copper response of the tailings in the deposit sample. .	91
Figure 9.1: Iron Eh-pH diagram.	96
Figure 9.2: Sulfur Eh-pH diagram.	97
Figure 9.3: Half-normal plot for sulfuric acid cobalt effects.	100
Figure 9.4: Sulfuric acid cobalt Pareto chart.	100
Figure 9.5: Half-normal plot for sulfuric acid copper effects.	102
Figure 9.6: Sulfuric acid copper Pareto chart.	102
Figure 9.7: Half-normal plot for sulfuric acid iron effects.	104
Figure 9.8: Sulfuric acid iron Pareto chart.	104
Figure 11.1: First possible proposed flowsheet for the concentration of cobalt at the Iron Creek Deposit.	121
Figure 11.2: Proposed flowsheet for the concentration of cobalt at the Iron Creek Deposit.	122

LIST OF TABLES

Table 2.1: Global cobalt production capacity by country in 2019 [27]. 6

Table 2.2: Global refining capacity by country in 2019 [28]..... 6

Table 3.1: Analytical Report of key elements from as-received samples..... 30

Table 3.2: McClelland ICP metal analysis results. 31

Table 3.3: Summary of McClelland 2018 Rougher Flotation Testing..... 32

Table 3.4: Cleaner Test Results for Bulk Sample 4313-001..... 33

Table 3.5: Cleaner Test Results for Bulk Sample 4313-002..... 34

Table 3.6: Cleaner Test Results for Bulk Sample 4313-003..... 35

Table 3.7: Details on Iron Creek deposit samples received from Electra. 36

Table 4.1: BWIs for various minerals in the tested deposit samples [51, 52]..... 40

Table 4.2: Ball charge and mass of balls for bond work index test. 41

Table 4.3: BWI data for sample IC 18-07..... 42

Table 4.4: BWI data for sample IC 18-09..... 42

Table 4.5: BWI data for sample IC 18-27..... 42

Table 4.6: BWI test results from Hazen for sample IC 18-07. 43

Table 5.1: Densities of major mineral constituents in Iron Creek deposit samples. 45

Table 5.2: Average percent area of the 4 sortation samples. 49

Table 5.3: Average cobalt and copper content from sortation samples. 49

Table 5.4: Combined percent area and elemental analysis data to model sortation..... 50

Table 5.5: Percent of rock data at differing % area cut off grades..... 51

Table 6.1: Magnetic properties of target and gangue materials. 52

Table 6.2: Testing conditions for the run-of-mine trials. 53

Table 6.3: Testing conditions for the bulk flotation concentrate trials. 54

Table 6.4: Testing conditions for the differential flotation concentrate trials..... 54

Table 6.5: Testing conditions for the thermal decomposition product of the bulk flotation concentrate. .. 55

Table 6.6: Testing conditions for the thermal decomposition product of the differential flotation concentrate. 55

Table 6.7: AAS data for deposit sample IC 18-07 magnetic separation tests..... 58

Table 6.8: AAS data for deposit sample IC 18-09 magnetic separation tests..... 59

Table 6.9: AAS data for deposit sample IC 18-27 magnetic separation tests..... 60

Table 6.10: AAS data for bulk flotation concentrate magnetic separation tests. 61

Table 6.11: AAS data for differential flotation concentrate tests. 61

Table 6.12: AAS data for thermal decomposition product of bulk flotation test..... 62

Table 6.13: AAS data for thermal decomposition of differential flotation tests.....	62
Table 6.14: Minerals present in magnetic separation thermal decomposition products by quantity.	66
Table 6.15: Magnetic separation feed material cobalt grade ANOVA for sample IC 18-07.....	67
Table 6.16: Magnetic separation feed material cobalt recovery ANOVA for sample IC 18-07.....	67
Table 6.17: Magnetic separation feed material copper grade ANOVA for sample IC 18-07.....	67
Table 6.18: Magnetic separation feed material copper recovery ANOVA for sample IC 18-07.....	67
Table 6.19: Magnetic separation flotation material cobalt grade ANOVA.	71
Table 6.20: Magnetic separation flotation material cobalt recovery ANOVA.	71
Table 6.21: Magnetic separation flotation material copper grade ANOVA.	74
Table 6.22: Magnetic separation flotation material copper recovery ANOVA.	74
Table 7.1: Specific gravities of target and gangue materials.	76
Table 7.2: Test conditions for heavy liquid separation trials using deposit sample IC 18-07.	77
Table 7.3: AAS data for gravity separation particle size testing.....	79
Table 7.4: AAS data for gravity separation RPM testing.	79
Table 7.5: AAS data for gravity separation RPM testing.	83
Table 7.6: RPM testing feed material cobalt recovery ANOVA.	83
Table 7.7: RPM testing feed material copper grade ANOVA.	84
Table 7.8: RPM testing feed material copper recovery ANOVA.	84
Table 7.9: RPM testing feed material cobalt grade ANOVA.	84
Table 7.10: RPM testing feed material cobalt recovery ANOVA.	85
Table 7.11: RPM testing feed material copper grade ANOVA.	85
Table 7.12: RPM testing feed material copper recovery ANOVA.	85
Table 8.1: Expected electrical conductivities of target and gangue materials.	88
Table 8.2: Test conditions for electrostatic separation trials.....	88
Table 8.3: AAS data output for electrostatic separation.	90
Table 8.4: Electrostatic separation testing feed material cobalt grade ANOVA.	92
Table 8.5: Electrostatic separation testing feed material cobalt recovery ANOVA.	92
Table 8.6: Electrostatic separation testing feed material copper grade ANOVA.	93
Table 8.7: Electrostatic separation testing feed material copper recovery ANOVA.	93
Table 9.1: Test conditions for leaching trials.....	98
Table 9.2: AAS data for sulfuric acid leach test leachates.....	99
Table 9.3: Sulfuric acid cobalt recovery ANOVA.....	101
Table 9.4: Sulfuric acid copper recovery ANOVA.....	103
Table 9.5: Sulfuric acid iron recovery ANOVA.	105

Table 10.1: Pricing data for each element.....	107
Table 10.2: Consumables pricing.....	107
Table 10.3: Employee type, number, and wage information [53, 54, 55].....	108
Table 10.4: Gravity Separation CAPEX.....	107
Table 10.5: Electrostatic separation CAPEX.....	108
Table 10.6: Gravity separation value per tonne.....	107
Table 10.7: Electrostatic separation value per tonne.....	108
Table 10.8: Gravity separation model output, USD per annum.....	111
Table 10.9: Electrostatic separation model output, USD per annum.....	111

LIST OF EQUATIONS

Equation 2.1:	Homogenous magnetic field strength in a solenoid.....	17
Equation 2.2:	Magnetic flux density in a vacuum.....	17
Equation 2.3:	Magnetic flux of a material placed in a magnetic field.	17
Equation 2.4:	Magnetic flux density.....	17
Equation 2.5:	Magnetic susceptibility of a material.....	17
Equation 2.6:	Relationship between magnetic flux and an applied magnetic field.	17
Equation 2.7:	Specific magnetic susceptibility of a material.....	17
Equation 2.8:	Concentration criterion.....	20
Equation 2.9:	Pyrrhotite leaching in non-oxidative environment.....	26
Equation 2.10:	Pyrrhotite leaching in oxidative environment	26
Equation 2.11:	Water decomposition.....	26
Equation 2.12:	Iron oxidation.....	26
Equation 4.1:	Bond Work Index equation.....	40
Equation 4.2:	Bond Work Index Cycle equation.....	41
Equation 6.1:	Pyrite decomposition.....	54
Equation 6.2:	Bonferroni limit equation.....	68
Equation 6.3:	t-value equation.....	68
Equation 9.1:	Lower limit for water stability.....	94
Equation 9.2:	Upper limit for water stability.....	94

ACKNOWLEDGEMENTS

I am grateful for the assistance and guidance of my faculty advisor Dr. Corby Anderson, as well as the rest of my thesis committee, Professor Erik Spiller and Dr. Emmanuel De Moor, and my colleagues in the Kroll Institute of Extractive Metallurgy.

I would like to thank the Critical Minerals Institute and Electra Battery Materials for sponsoring this research and providing samples.

I would also like to thank my family and friends for their continued support.

CHAPTER 1. INTRODUCTION

Cobalt, commonly used in lithium-ion batteries, jet turbines, and steel alloys, is defined by the Department of Energy as a critical element. This means that the United States does not have a secure supply and the government sees a disruption to the supply chain as an unacceptable hindrance. Currently, the U.S. imports 100% of its cobalt. The U.S. does, however, contain a moderately sized cobalt deposit that has produced cobalt ore in the past that could start production again. This report examines one possible method of refining this deposit.

Cobalt is generally exclusively produced as a by-product of copper and nickel mining, as cobalt is usually associated with either copper or nickel and cobalt prices in the past were not high enough to make it economical to mine cobalt as a target material. No copper or nickel operations in the U.S. currently produce cobalt.

Electra Battery Materials (Electra) is a battery material refining and recycling company located in Toronto, Canada. The Iron Creek deposit owned by Electra is a low-arsenic sulfide deposit known to contain cobalt. This makes it an option for a domestic supply of cobalt production, as the low amounts of arsenic allow for it to be refined in North America. As the refining plant is located in Canada, the grade of the cobalt needs to be increased before it is shipped to make the operation economically viable. Hence, several deposit samples with a range of cobalt contents were sent from Iron Creek for testing to attempt to increase the cobalt grade by a range of different methods.

This research aims to examine various physical beneficiation methods that could be used in conjunction with flotation and thermal decomposition to produce a flowsheet that would produce a cobalt concentrate that would be economical to ship to Canada. To do this, an understanding of element criticality, cobalt applications, cobalt mineralogy, and cobalt and pyrite processing is necessary. Contained in this report are the above, as well as the physical benefactions methods developed. The flotation and thermal decomposition methods examined for this research are not looked at in depth here, as that was the focus of other students during this project.

1.1 Critical Materials

The United States Energy Act of 2020 describes a critical mineral as a non-fuel element that is essential for economic or national security and has a supply chain that could be disrupted [1]. A mineral is considered essential if the loss of access to said critical mineral could have significant consequences on a national level. Supply chain disruption can stem from any number of political, geological, or economic

factors, including one country or company controlling the majority of the supply of one mineral, civil or social unrest, and natural disasters.

In 2022, the United States Geological Survey (USGS) increased the number of elements as critical minerals to 50, up from 35 in the first list released in 2018, due to rare earth elements and platinum group elements no longer being listed as a group [1]. Five elements were also removed from the list in 2022: helium, potash, rhenium, uranium, and strontium. Uranium was removed as it is considered a fuel mineral and as of the initial list, fuel minerals were not excluded [2].

1.2 Criticality of Cobalt

Cobalt is one of the critical minerals listed in the USGS 2022 report and is a metallic element used in batteries, turbines, and magnets [1] [3]. With the sudden increase in demand for electric cars worldwide, the demand for cobalt has significantly increased. The United States considers cobalt a critical mineral because the supply chain is heavily dominated by two countries, the Democratic Republic of the Congo (DRC) and China, and there are nearly no mining productions that produce cobalt as the primary mineral, resulting in the overall production of cobalt being limited by the demand for other metals. The DRC produces approximately 60%-70% of the world's cobalt ore, mainly as a byproduct of copper mining, with roughly 20% coming from artisanal mining. Artisanal mining in the DRC is often seen as dangerous and unethical to its workers, with poor labor laws and environmental practices often being reported [4]. China dominates cobalt processing and processes approximately two-thirds of the world's cobalt. As of writing this master's thesis in 2023, recent U.S. relations with China have degraded for multiple reasons, and further degradations could see China begin to limit refined cobalt products for diplomatic leverage [5]. The US also has a very limited supply of domestically produced cobalt, with Jervois operating the last operational cobalt mine in Idaho in 2023, but the concentrate was planned to be shipped to Brazil to be processed due to its high arsenic content [6].

Cobalt is used in lithium-ion batteries (LIBs) to help stabilize the cathode during discharge [7]. While other materials can be used, such as nickel and aluminum, cobalt has the best combination of stability and conductivity. Cobalt is also good at preventing oxygen from becoming liberated in the battery, which would otherwise result in a thermal runaway reaction that can cause a LIB to combust [8].

Work has been done to develop batteries that use a significantly reduced amount of cobalt, if any. Presently, the most researched so far and promising are LiNiO_2 (LNO) batteries, which can store a higher charge capacity than LiCoO_2 under the same conditions [7]. The primary issue with LNOs is that, while they have a high theoretical energy density, the Ni lacks the lattice stability that comes from the Co, leading to safety hazards [8]. The magnetic moment of the Ni also can interact with the Li and cause a

decrease in the thickness of the LiO_2 layers, making it more difficult for the Li ions to move and causes the LNO to degrade faster [8]. Other minerals have been researched in their effectiveness in replacing Co and Ni in the LNOs, primarily Mg, Mn, and Al. In testing done in 2021, both LNOs doped with Mn and Al showed improved thermal stability compared to LNOs [7]. These doped batteries, however, had greatly reduced performance rates and capacities [7]. With electrical vehicles looking to increase their range and price to that more similar to those with internal combustion engines (ICE), having batteries with large capacities and low costs are vitally important.

1.3 Idaho Cobalt Belt

The Idaho Cobalt Belt is a copper-cobalt deposit in the Salmon River Mountains in east-central Idaho. The 50 km long deposit trends northwest and 10 km wide at its central point [9]. The primary minerals in the southeast end of the deposit are pyrite and chalcopyrite, with increasing amounts of arsenopyrite, pyrrhotite, and cobaltite as the deposit moves to the northwest [10]. The four main deposits in the Idaho Cobalt belt are the Blackbird, Blackpine, Iron Creek, and Salmon Canyon deposits, with Blackbird being the most important and well-researched [10]. The Blackbird mine produced copper and cobalt in the early 1900's before its shutdown in the late 1960s [11].

The last operating site in the Idaho Cobalt Belt was the Idaho Cobalt Operation (ICP), which is owned by Australia-Based Jervois Mining and started operation in the fall of 2022. The deposit is estimated to contain 34.5 Milb of cobalt, as well as 49.76 Milb of copper and 53 koz of gold [12]. The projected mine life was 12.5 years [12]. Operations were stopped in early 2023 due to falling cobalt prices.

1.4 Content of Work

The content of this work is separated into the following chapters. Chapter 2 is a literature review. Chapter 3 is a characterization of the Iron Creek deposit. Chapter 4 details bond work index testing done on some of the material initially received. Chapter 5 shows the results of sortation testing done on some of the material. Chapter 6 through Chapter 8 discuss the physical beneficiation methods tested. Chapter 9 covers the initial leaching testing done on some promising concentrate produced by the separation methods. Chapter 10 presents basic economic models for each beneficiation method and discusses potential economic viability. Chapter 11 provides conclusions for the methods presented and their possible potential for industrial use.

CHAPTER 2. LITERATURE REVIEW

2.1 Discovery of Cobalt

Before its elemental discovery, cobalt was used as a dark blue pigment and dye in jewelry, glass, pottery, and painting [3] [13]. Elemental cobalt was discovered in 1739 by Georg Brandt, when he was able to isolate cobalt and prove that the element coloring some glass blue was not bismuth [3] [14] [13]. It was named after 'kobolds', creatures that cursed German miners looking for copper [15]. This name was first given to ores thought to contain copper in the area but turned out to be poisonous arsenic-bearing cobalt ores that appeared similar [15].

2.2 Properties of Cobalt

Cobalt is a transition group-VI element [3]. It has a density of 8.86 g/cm³ [3]. It has a Mohs hardness of 5 [16]. Cobalt has a melting point of 1495 °C and a boiling point of 2927°C [16]. It has an electrical conductivity of 0.172×10^6 S/m, classifying it as a conductor [16]. Cobalt is ferromagnetic [16]. Its tensile strength is 800 MPa, Poisson's ratio is 0.31, modulus of elasticity is 220 MPa, and shear modulus is 82.6 GPa [16] [17] [18].

Cobalt has the highest known elemental Curie temperature at 1121°C [13]. This is the temperature at which a material's magnetic properties are sharply changed if exceeded, and generally, regardless of its magnetic properties below the temperature, become paramagnetic [19]. This allows for cobalt to retain its properties at high temperature, making it ideal to be used in alloys that experience extreme heat.

Cobalt has a similar atomic radius to other transition elements and can substitute for them in many minerals, namely iron and nickel [20]. Atomic substitutions can occur if the size difference of the atoms is less than 30%, if the substituting atom can fit on the crystallographic site, and the charge of the ions cannot differ by more than 1 [21].

2.3 Applications of Cobalt

The primary use of cobalt is for batteries, accounting for approximately 58% of the world's cobalt use in 2019 [22]. In comparison, in 1999, only 10% of the world's cobalt was used for batteries [13]. This is caused by the growth of powerful electronic, primarily electric vehicles. This type of growth is not expected to slow down anytime soon, as many countries are highly promoting the sale of electric cars as a part of new climate change regulations. As discussed earlier, cobalt is used as a stabilizer in LIBs and has no ready replacement.

A major secondary use of cobalt is that of superalloys, which accounts for 46% of the U.S.'s cobalt use in 2019 [22]. This was the dominant use of cobalt until it began to be used as a component in

batteries [13]. Superalloys are nickel-, iron-, and/or cobalt- based alloys that can be used at temperatures greater than 70% of their melt temperature [23]. These alloys are used in jet turbines, wind turbines, the aerospace industry, and various medical devices [13]. Cobalt alloys were first used in 1907 in automobile part manufacturing parts to help increase the life of the steel cutting tools, with the first superalloy being used in prototype jet engines in the 1950s [23]. Co-based superalloys are able to function at higher temperatures than Ni-based ones, allowing for the possibility of higher efficiency engines that function at high temperature [24]. Cobalt superalloys are also able to be created in larger single crystals than Ni-based ones with fewer defects, which is required in applications that need to achieve high temperature creep resistance [24].

Other uses include prosthetic limbs, hard facing materials, low expansion alloys, chemicals, and dyes [20]. Cobalt is an important component of catalysis used in the oil and natural gas refining industry, used to remove sulfur from crude oil and to process natural gas to synthetic diesel [20]. A radioactive isotope of cobalt, cobalt-60, is commonly used in the medical industry for cancer treatment, a medical tracer, and as an external radiation source [25].

The use of cobalt in the U.S. differs from the general world's use. As of a USGS report released in 2020, minimal cobalt is used to create batteries within the U.S. [22]. Therefore, the industry that uses the most cobalt in the U.S. is the superalloys industry, followed by various chemical applications at 31% and 14% in various metallic operations [22].

2.4 Global Cobalt Production

Given its low concentration in ores, cobalt is generally considered a companion metal with limited economic interest. It is almost always produced as a byproduct of copper, nickel, and arsenic mining. This results in the recoverability of the cobalt depending on the typical recovery efficiencies of the companion metal and the relative cost and benefit of the cobalt recovery. There is only one active mine where cobalt is the primary commodity, the Bou Azzer mine in Morocco. There are several closed cobalt mines, some of which include the cobalt mine in Ontario, Canada, the Black Bird district in Idaho, United States, and Mount Cobalt Mine in Queensland, Australia [13].

It is estimated that 25 million tons of terrestrial cobalt resources exist in the world [26]. Of that, currently 7.6 million tons are classified as reserves, with most being in the Democratic Republic of Congo (DRC), Australia, and Indonesia [26].

The world leader in cobalt production from primary sources is the DRC, with them producing over 100 kt of cobalt, or approximately 70% of the world's supply, in 2019 [13]. The top ten countries in cobalt production capacity are shown in Table 2.1.

Table 2.1: Global cobalt production capacity by country in 2019 [27].

Country	Cobalt Production Capacity (tons)
DRC	100,000
Russia	6,100
Australia	5,100
Philippines	4,600
Cuba	3,500
Madagascar	3,300
Papua New Guinea	3,100
Canada	3,000
South Africa	2,400
Morocco	2,100

China is the leader in cobalt refining by far, accounting for two-thirds of the world's total production in 2019. Shown below in Table 2.2 is the refining capabilities by country as of 2019 [13].

Table 2.2: Global refining capacity by country in 2019 [28]

Country	Cobalt Refining Capacity (tons)
China	170,000
Finland	16,500
Zambia	9,500
Canada	8,020
Russia	7,520
Australia	6,700
DRC	6,050
Madagascar	5,600
Japan	5,500
Norway	5,200
Belgium	3,000
South Africa	2,900

2.5 Cobalt Deposit Types

Most cobalt is found in 3 major types of deposits: stratiform sediment-hosted Cu-Co deposits, Ni-Co laterites, and magmatic Ni-Cu-Co sulfide deposits. Cobalt can also be found in several other types of deposits which are generally grouped together and referred to as hydrothermal and volcanogenic deposits [13]. A map of the major cobalt deposits can be seen below in Figure 2.1.

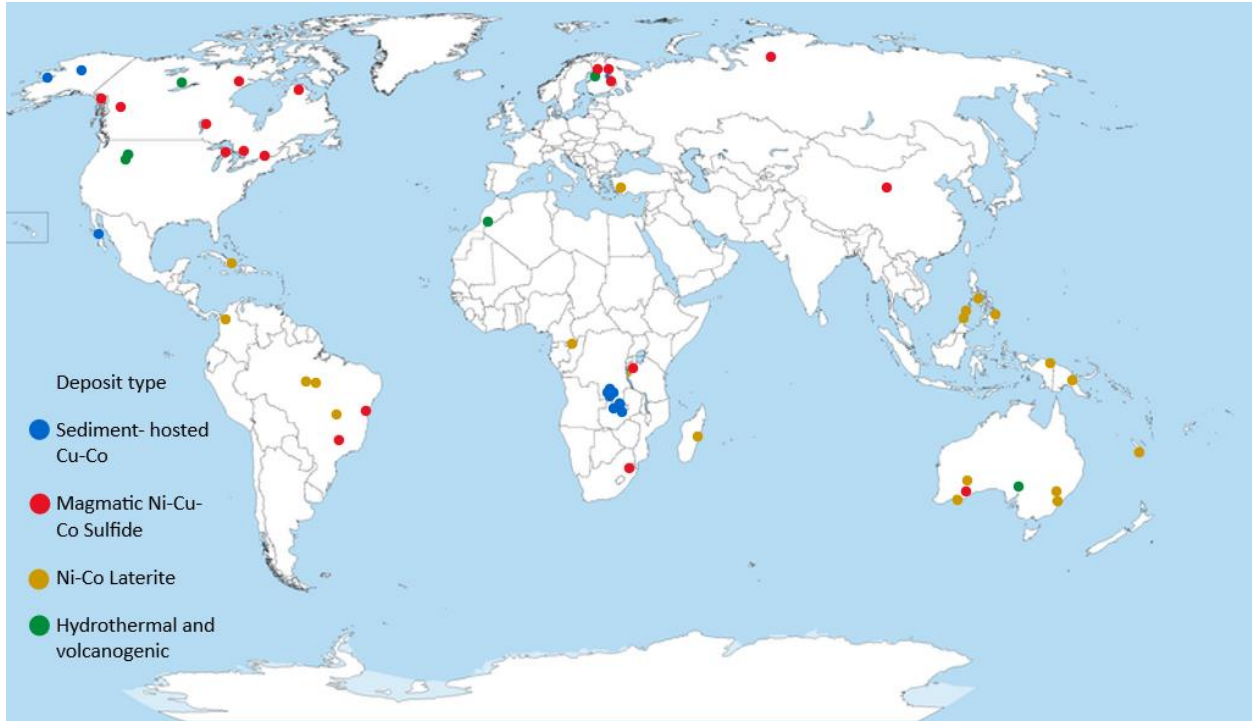


Figure 2.1: Map of major cobalt deposits [13].

2.5.1 Stratiform Sediment-hosted (SSH) Cu-Co Deposits

Most stratiform sediment-host (SSH) Cu-Co deposits are in the Central Africa Copper Belt (CAC). The largest deposit outside of Africa is the European Kuferschiefer, extending from northeast England to Poland and central Germany [20]. Finding ways to improve recovery in this type of deposit is important as nearly 50% of the cobalt mined in the world comes from this type of deposit [20]. These deposits generally consist of three zones: the weathered oxide zone on the surface, the mixed oxide-sulfide zone, and a sulfide zone [13]. Cobalt can be concentrated in the weathered zone and is most abundant in the mineral heterogenite, while in the sulfide zone the most common cobalt mineral is carrollite. These types of deposits can be tens of meters deep and cobalt and copper do not always coincide [13].

2.5.2 Ni-Co laterites

Nickel-cobalt laterites are the second most important type of cobalt containing deposits. The primary target mineral mined from this type of deposit is nickel, with cobalt being considered a secondary product. These are formed by weathering bedrock by groundwater, typically in tropical and subtropical climates, which enriches some minerals while removing others [20]. Concentrations of cobalt and nickel in the weathered zones are commonly upwards of 10 times greater than that of the bedrock [13]. There are three types of Ni-Co laterite deposits: hydrous silicate deposits, clay silicate deposits, and limonite deposits. The formation of each depends on the climatic conditions, with the cobalt concentrating where primary sulfide and silicate ores are subjected to atmospheric leaching, with the rate of chemical weathering needing to be higher than the rate of erosion [13]. Saprolite zones at the base of these deposits can be difficult to remove cobalt from, as the lack of weathering reduces cobalt enrichment and requires more grinding to liberate the target minerals [20]. Notable examples of this deposit are located in New Caledonia and Cuba, due to the ideal weather conditions [20].

2.5.3 Magmatic Ni-Cu-Co sulfide deposits

Magmatic deposits are formed by high temperature magmatic processes. Cobalt is often found in these deposits in mafic or ultramafic intrusions that occur as lenses that settle in depressions at the bottom of the magmatic host bodies [20]. There are three sub-morphologies that fall under magmatic sulfide deposits: basal deposits, startabound deposits, and deposits in extrusive ultramafic rocks. Each of these has its own unique mineralogy and the location of the cobalt and nickel-bearing sulfide differs for each [20].

Nickel is most commonly the economic commodity in this type of deposit, with copper, cobalt, and platinum group metals (PGMs) being minor by-products or secondary commodities [13]. The major cobalt bearing minerals in this type of deposit are pentlandite, chalcopyrite, and pyrrhotite, all of which can contain cobalt substituted for other elements [13] [20]. The largest magmatic sulfide deposits are located in Russia, South Africa, Western Australia, and Canada [20].

2.5.4 Hydrothermal and volcanogenic deposits

Hydrothermal and volcanogenic deposits show a wide range of formation types and mineralogy. The common point between them is how they were formed, with minerals precipitating from hydrothermal fluids passing through host rock sourced from volcanic activity [20]. Common examples are Cu (-Zn-Co-Ag-Au) Volcanogenic Massive Sulfides (VMS), Iron Oxide Copper Gold (IOCG), Mississippi Valley Type (MVT) Zn-Pb (-Co-Ni) sulfides, and polymetallic (Ag-Ni-As-Bi) -Co-rich vein deposits, the latter of which is the only deposit type where cobalt is extracted as the primary commodity [13]. This type of deposit can be found all over the world, with notable examples including Bou Azzer

deposit in Morocco, Outokumpu district in Sweden, the Idaho Cobalt belt in the U.S [20]. Mining operations that have cobalt as the primary product have only come from this type of deposit.

2.5.5 Underwater deposits

Underwater mineral deposits are not currently considered in total world resource calculations, as there is no way to economically mine them. It is estimated that there is 121 Mt of Co on the seafloor, with between 16 and 34 Mt of that being recoverable cobalt, based on current and expected technology advancements [13]. If sea floor resources were included in total cobalt resources, it would represent approximately 80% of the total cobalt [13]. There are three metal-rich mineral deposits that appear the most viable, each with their own distinct mineralogy: ferromanganese nodules, ferromanganese crusts, and seafloor massive sulfides [29]. These deposits are not expected to be mined in the near future, as there are more easily accessible deposits on the surface and the environmental impact of such a mining operation is impossible to determine given the lack of understanding of the deep-sea biosphere [29].

2.6 Cobalt Recovery Methods

With cobalt being a secondary product from nearly all mines, the recovery often depends on the process of the primary element and ore mineralogy.

2.6.1 Sediment Hosted Cu-Co Deposits

Processing of sediment hosted Cu-Co deposits largely depends on the type of ore. Oxide ores are processed using leaching-solvent extraction-electrowinning, while sulfide ores are processed through flotation. Mixed ores are processed using a mixture of both. After leaching, solvent extraction is used to separate cobalt and copper and to remove impurities. After impurity removal, the cobalt can be precipitated as an intermediate product, such as cobalt hydroxide [13]. Electrowinning can also be used to get a higher degree of separation between cobalt and the other elements. When cobalt is a target element in sulfide ores, a roast leach route is used over the conventional copper smelting and converting process as it reduces cobalt losses [13]. Mixed ores are the most complex Cu-Co to process, and usually are treated with a two-stage differential sulfide-oxide flotation process. Typical recoveries of mixed ores range from 50% to 70% from the sulfide mineral and 30% to 40% from the oxide minerals [13]. An example flowsheet can be seen in Figure 2.2.

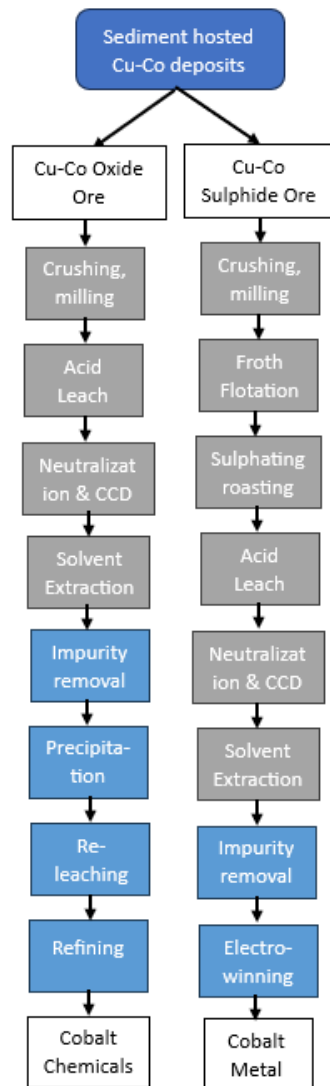


Figure 2.2: Example flowsheet used to process sediment hosted Cu-Co deposits [13].

The cobalt recovery in this type of deposit is the most variable and generally the lowest of the four deposit types discussed here. The grade of the cobalt recovered is dependent on the complexity of the copper extraction flowsheet. The leaching process focuses on maximizing the copper recovery, so cobalt recoveries are generally less than 75% [13]. Mineralogical department of cobalt can also influence the recovery of cobalt. In sulfides, where cobalt and copper are often hosted in the same mineral, there is a correlation between copper and cobalt recovery in flotation. In oxides and mixed ores, there is less of a correlation between copper and cobalt recovery in flotation due to the minerals hosting the cobalt being more difficult to float [13].

2.6.2 Ni Laterites

The two primary ways that nickel laterites are processed are pyrometallurgically and hydrometallurgically [13]. Cobalt is only recovered in the hydrometallurgy process, however, as the cobalt is lost and reports to the slag in the pyrometallurgy process [13]. There are two hydrometallurgical processes, High-Pressure Acid Leaching (HPAL) for limonite ore, and the Caron process for mixed saprolite-limonite ores [13]. HPAL is the preferred method for cobalt recovery and is recovered as a mixed nickel-cobalt sulfide or a nickel-cobalt hydroxide. The Caron process uses reductive roasting, ammonia leaching, and solvent extraction to produce a cobalt sulfide [13]. Other processing methods currently being tested for saprolite ore include enhanced pressure acid leaching, heap leaching, and chloride leaching [13]. Recovery rates for HPAL are approximately 93%, while the recovery for the Caron process is estimated to be less than 80%, though no plants using the Caron process report cobalt recoveries [13]. Other processing methods currently being tested for saprolite ore include enhanced pressure acid leaching, heap leaching, and chloride leaching [13]. Most Ni-laterite operations do not include pre-concentration due to the small particle size of the Ni-Co-bearing and oxide gangue minerals preventing separation [13]. An example flowsheet can be seen in Figure 2.3.

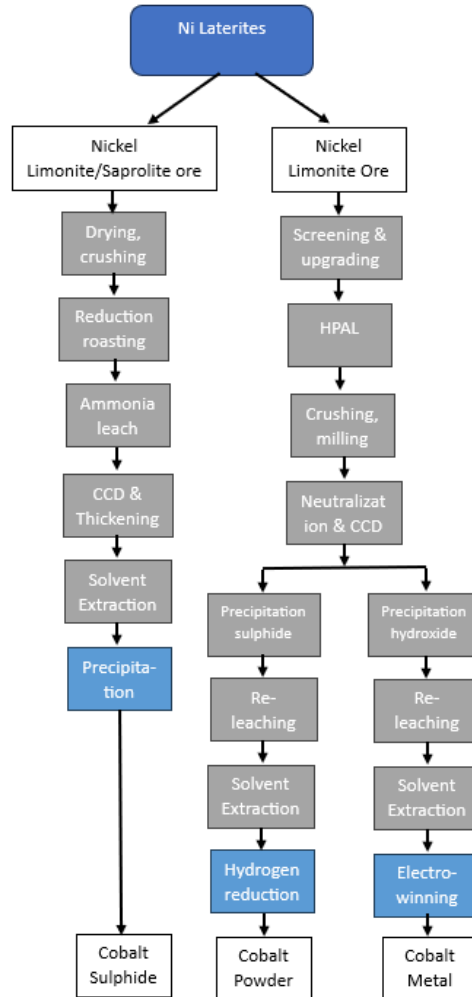


Figure 2.3: Example flowsheet used to process nickel laterite deposits [13].

The ratio of the ore type affects the recovery of cobalt, with recovery typically decreasing with increasing saprolite fed to the plant. This is due to the location of the cobalt with the saprolite, as cobalt is disseminated in the Mg-silicates, and it is very difficult to remove the cobalt at normal temperatures [13]. In limonite ores that are considered cobalt rich, the majority of the cobalt is in asbolane and lithiophorite. In cobalt-poor limonite ores, the cobalt is in the weathered materials, with the amount depending on what the dominant mineral phase in the ore is [13].

Nickel laterites are also processed in China as nickel pig iron (NPI), a low-cost feed stock for stainless steel, using various roasting and pyrometallurgical methods. Experiments have been done to test the viability of processing the waste slag created to recovery elements such as cobalt, lead, and copper using solvent extraction and electrowinning. Initial optimization testing done in Indonesia has shown some promising results, with cobalt recoveries of approximately 70% [30, 31].

2.6.3 Magmatic Ni Sulfides

Cobalt in magmatic Ni sulfides is separated from the copper via froth flotation, either by producing a bulk sulfide concentrate or by sequential floatation of copper, then cobalt and nickel. The resulting concentrate is converted into a Co-Ni-S matte either by flash furnace or by drying/roasting and an electric furnace. The matte is then leached and processed by solvent extraction to remove the nickel. To remove the cobalt, hydrogen reduction is used to produce cobalt powder or by electrowinning to produce a cobalt metal [13]. An example flowsheet can be seen in Figure 2.4.

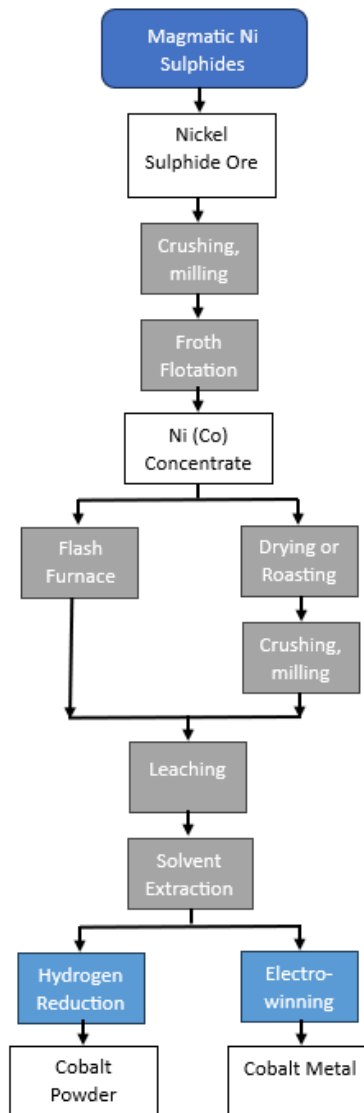


Figure 2.4: Example flowsheet used to process magmatic Ni sulfides deposits [13].

Overall cobalt recovery rates in this process are approximately 40%, with most of the loss coming from the smelting process [13]. In comparison, the recoveries of nickel and copper are both greater than

95%. Cobalt recovery could be increased by using one of several post-smelting processes, namely smelting at a higher temperature, using slag additives, or producing a secondary matte in a slag-cleaning electric arc furnace [13].

The mineralogical deportment of the cobalt can also play a role in reducing the recovery [13]. When the cobalt is hosted in the same mineral phases as the nickel, usually Ni-pentlandite, the recovery is higher than normal, as the cobalt reports to the same fraction as the nickel. When the cobalt is hosted in another mineral, such as iron sulfides or silicates, the recovery of cobalt drops greatly, as these minerals are normally seen as gangue materials and report to tailing [13].

2.6.4 Cobalt Arsenides

Cobalt arsenides are only being processed in Morocco currently, though this type of ore was also mined at the Blackbird mine in Idaho, USA when it was in production. This type of ore is first upgraded using screening and gravity separation. It then undergoes froth flotation and roasting. The roasted product then is acid leached and the leachate is used in solvent extraction and electrowinning. The result of this process is cobalt metal [13]. Pressure leaching was also used in some operational flowsheets [32]. An example flowsheet can be seen in Figure 2.5. There used to be several cobalt arsenides operations during the 20th century but due to health and environmental issues, nearly all have closed [32].

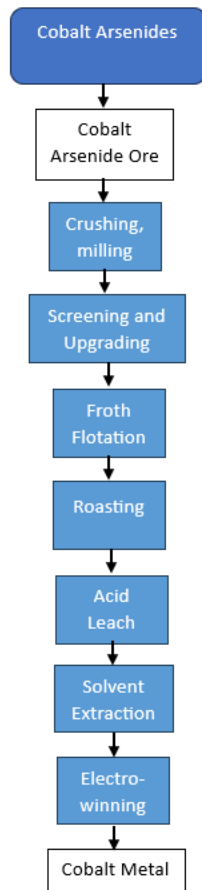


Figure 2.5: Example flowsheet used to process Cobalt arsenides deposits [13].

2.6.5 Recycling

Recycling has the potential to be a major source of cobalt in the future. It was estimated that in 2012, 69% of cobalt was sent to landfills [13]. The challenge with cobalt recycling is that it requires the recycling process to be on par with if not better than mining in terms of economics, environmental impact, and volume in order for it to be competitive [13]. Types of material fed into the recycling can be classified into two different categories, new scrap, which is waste from processing and manufacturing, and old scrap, which is post-consumer waste [20]. Old scrap is much hard to process as it is combined with other materials that maybe make processing difficult [20].

The recycling process for cobalt depends on the type of material being processed. Cobalt used in alloys will typically not be removed and instead re-melted to be used again as the alloy [20]. If it is removed, double membrane electrolytic cells (DMEC) are used with several solvent extraction processes to produce a high purity cobalt cathode [25]. Batteries are incinerated, with the copper, cobalt, iron, and

nickel melting into an alloy that is then processed and separated into individual metals [20]. Spent catalysts from petroleum refining are melted down with other spent catalysts in an arc furnace and sold to nickel and cobalt refineries [25].

2.7 Magnetic Separation

Magnetic separation is a mineral processing method that uses the differences in the magnetic properties of an element or a mineral to achieve a separation or concentration. This physical beneficiation method is commonly used in iron refining but can be used for other minerals if there is a large enough difference in magnetic response between the target and gangue minerals.

2.7.1 Magnetic Behavior

A magnetic dipole is a microscopic magnet, equivalent to a flow of an electric charge around a loop, such as electrons circulating around an atomic nucleus [33]. A magnetic field exerts a force on magnetic dipoles, making them align with the magnetic field. As the forces are equal in all directions, the magnetic field is uniform, and the net force on the dipole is zero. If the magnetic field has a gradient however, the magnetic force on the dipole varies within the field and will be proportional to the magnetic dipole moment and the magnetic of the gradient, allowing for separations depending on the materials [34].

The effect that an external magnetic field has on a mineral placed in it depends on the behavior of its electrons. Most materials can be classified as diamagnetic, paramagnetic, or ferromagnetic. Diamagnetic materials have no unpaired electrons, are weakly repelled by magnetic fields, and report to the non-magnetic fraction. Paramagnetic materials have some unpaired electrons, are weakly attracted by magnetic fields, and can report to either fraction, depending on the strength of the magnetic field and how reactive the material is. Ferromagnetic materials have unpaired electrons and report to the magnetic fraction. In addition, ferromagnetic materials have a net magnetic moment that results in them being strongly attracted by magnetic fields and can stay magnetized after being removed from the field [35].

A material's magnetic behavior can also affect how effective adjustments to the magnetic field can be. Ferromagnetic materials are quickly saturated and increasing the magnetic field strength will not increase the magnetization beyond a certain strength. With paramagnetic materials, the induced magnetization is proportional to the magnetic field strength applied and it is theoretically impossible to saturate the material [34].

2.7.2 Magnetic Separation Theory

The homogenous magnetic field strength in a solenoid can be determined by the equation:

$$H = nI \quad (2.1)$$

Where H is the magnetic field strength, n is the turns per meter, and I is the current per turn [34].

The measurement of magnetic forces on particles is called magnetic flux density. In a vacuum, the relationship between magnetic flux density and magnetic field strength is

$$B_0 = \frac{\Phi}{A} = \mu_0 H \quad (2.2)$$

Where B is the magnetic flux density, Φ is the magnetic flux, A is the cross-sectional area of the coil, and μ_0 is the permeability of the vacuum, which is $\mu_0 = 4\pi \times 10^{-7} \text{ N/A}^2$ [34]. The SI unit for magnetic flux density is the Tesla (T).

The magnetic flux of a material placed in a magnetic field is given by

$$B = \mu H \quad (2.3)$$

Where μ is the permeability of the material.

Magnetic flux density can also be calculated using

$$B = \mu_0 (H + M) \quad (2.4)$$

Where M is the induced magnetization of the material when it is placed in the field.

The magnetic susceptibility of a material is the ratio of induced magnetization to the magnetic field strength:

$$\chi = \frac{M}{H} \quad (2.5)$$

When substituted into Equation 2.4, it gives:

$$B = \mu_0 H (1 + \chi) \quad (2.6)$$

The specific magnetic susceptibility of a material is given by

$$\psi = \chi/\rho \quad (2.7)$$

Where ρ is the density of the material.

Materials with a positive magnetic susceptibility ($\mu > 1$) are called paramagnetic while materials with a negative magnetic susceptibility ($0 < \mu < 1$) are called diamagnetic. From equation 2.5, it can be seen that materials that have a positive susceptibility have a positive effect and strengthen flux density of the magnetic field while materials with a negative susceptibility have a negative effect and weaken the flux density [34]. Magnetic susceptibilities of certain materials can be seen in Table 5.1.

Magnetic separation can be done wet or dry and can be done at a low intensity, with magnetic field strength typically being below 0.5 tesla, or a high intensity, with magnetic field strengths up to 2 Tesla. Low intensity magnetic separation typically targets ferromagnetic materials while high intensity magnetic separation targets paramagnetic materials.

2.7.2 Magnetic Separation of Pyrite

The primary testing focus of magnetic separation of pyrite is to remove it from coal to lower the sulfur content, typically as an alternative to flotation. Coal is considered diamagnetic while coal-associated pyrite is weakly paramagnetic [36]. Testing done in 1980 showed that at finer particle sizes, high-gradient magnetic separation was much more effective than flotation at removing the pyrite, but difficulties were expected in replicating the recovery on an industrial scale due to the lack of development [36].

Testing on removing arsenopyrite from pyrite was done in China to attempt to improve sulfur recovery and grade. Results showed that pulsating high gradient magnetic separation was effective in upgrading the pyrite and reducing arsenic content over a range of magnetic inductions, feed weights, and grinding fineness [37]. This experiment was also upgradeable to a full-scale level with similar results [37].

2.7.3 Magnetic Separation of Pyrrhotite

Testing done by South Central University in China in 2022 looked at magnetic separation of pyrrhotite for nickel processing. They found that as the proportion of fine particles, here considered less than 0.040 mm in diameter, increased, the grade and recovery ratio to the concentrate increased, while the grade and recovery ratio of other, non-targeted elements decreased slightly. Increasing the fineness of the particles did not affect the grade or recovery ratio [38].

They also found that weak magnetic fields, considered to be less than 400 Gauss, only had small amounts of pyrrhotite reporting to the concentrate. As the magnetic field strength increased, the iron grade in concentrate slightly decreased and the recovery ratio increased, while the grade of the non-targeted elements slightly increased [38].

2.7.4 Effects of Microwave Heating on Magnetic Separation

Various testing looked at the effects of heating a sample containing pyrite on the effectiveness of magnetic separation. Pyrite on its own does not usually have a magnetic response, but it can be decomposed into pyrrhotite, which does have some magnetic properties.

One experiment in Turkey in 2003 looked at how heating pyrite to a range of temperatures in different atmospheres affected its reaction in different magnetic fields. The general trend observed was that as the temperature of the treatment increased, the amount of magnetic material in the sample increased [39]. The lower magnetic field intensities, approximately 0.1 Tesla, recovered particles that were only considered ferromagnetic, while higher magnetic field intensities recovered both ferromagnetic and paramagnetic materials [39]. Products created during the heating included pyrite, pyrrhotite, troilite, alpha-hematite, and gamma-hematite, though no hematite was formed when the pyrite was heated in a non-oxygen atmosphere [39].

Another test done in 2007 looked at the effects of microwave heating on the magnetic separation response of several minerals, including pyrite, chalcopyrite, galena, and sphalerite. Results showed that the magnetic field intensity where the minerals started showing a magnetic response was different for each, with pyrite and chalcopyrite reacting at the lowest field intensities [40]. Additionally, only the pyrite and chalcopyrite showed improvement in magnetic response after heating. A side effect of the microwave heating, however, was that flotation was negatively affected in all minerals affected by the microwaves due to the creation of oxides on the surface of the particles [40].

2.8 Gravity Separation

Gravity separation is a mineral processing method that uses the differences in the densities or specific gravity of an element or a mineral to achieve a separation or concentration. While its use has declined with the increase of flotation and magnetic separation methods, it remains one of the primary physical beneficiation methods, especially in coal processing. Gravity separation is also attracting more attention recently as a more environmentally conscious alternative, as some gravity methods use fewer chemicals than other separation methods, notably flotation and leaching, resulting in a smaller environmental impact.

2.8.1 Specific Gravity

Specific gravity, also known as relative density, is the ratio of the density of a substance to that of a standard substance [41]. In mining, the reference substance is typically water, which has a density of 1 kg/L. The exact specific gravity of many minerals can only be approximated when pulling data from literature, as the exact composition of each mineral can vary from source to source.

2.8.2 Gravity Separation Theory

Important factors that determine the viability of gravity separation are relative density, mass, size, and particle shape. In a two-mineral system, the theoretical ease of separation can be determined by the concentration criterion, which is defined by the following:

$$CC = \frac{d_h - d_f}{d_l - d_f} \quad (2.8)$$

Where d_h is the relative density of the heavy mineral, d_l is the relative density of the light mineral, and d_f is the density of the separating fluid [42]. If the concentration criterion is greater than 2.5, separation should be relatively easy. If it is less than 1.25, however, separation using gravity methods is unlikely to be effective [42].

Particles also need to be able to move past one another in order for a separation to occur. There are four different mechanisms for this, though every gravity separation technique uses at least two; density, stratification, flowing film, and shaking [42]. Density uses a viscous fluid that has a relative density that is in between the two materials to be separated. This results in one mineral floating while the other sinks. Stratification is the intermittent fluidization of a bed in a vertical plane and is the major driver in jigs [42]. Flowing films use an incline plane to separate particles in a slurry by their relative movements and are used in a wide range of separation techniques. Shaking stratifies particles by exerting a horizontal force on a flowing film, either in an oscillating or orbital motion [42].

The most widely applied and efficient method of gravity separation is dense-medium separation (DMS). It is a process in which particles of different densities are separated using a liquid of a pre-determined density that is in between the targeted materials such that the lighter materials float while the heavier materials sink. The two main areas of DMS applications are pre-concentration and final cleaning for a salable end product [43]. Pre-concentration is used to remove waste rock and allows for a significant reduction in the quantity of ore that requires grinding and allows for the processing of lower grade ore that otherwise would not be economically viable to process. DMS is different from other gravity separation methods in that it requires a system of processes rather than being a stand-alone unit process. The feed materials need to be prepared, added to the dense medium, separated into heavies and lights, recovered, washed, and then the heavy medium needs to be recovered and recycled [43].

2.8.3 Gravity Separation of Pyrite

Testing done with a hydrocyclone, heavy medium unit, and a concentrating table was done attempting to compare the response of ¼" coal. Results showed that the concentrating table's efficiency decreased at lower specific gravities and that the lower the separating gravity, the larger the difference between the theoretical and actual yields [44]. The heavy medium unit was more effective than the

concentrating table, especially at lower gravities. The differential between the float and sink fraction decreased with finer size and the efficiency increased [44]. The hydrocyclone had similar results to the heavy medium unit, however, it was found that using the hydrocyclone before the heavy medium unit reduced the cost and improved the efficiency [44].

Tests completed in 1982 were also done to determine if it was possible to remove pyritic sulfur from coal using a spiral concentrator and flotation. Testing two different samples, it was determined that it was possible to remove approximately 95% of the pyritic sulfur and 80% of the total sulfur using these two operations in sequence [45]. Bench float-sink tests also showed that it was possible to achieve good coal and sulfur recoveries under optimal conditions [45].

2.9 Electrostatic Separation

Electrostatic separation is a mineral processing method that uses the differences in the conductivities of an element or a mineral to achieve a separation or concentration. It is primarily used for cleaning beach sands, recycling electronic waste and plastic, and processing coal and titanium ore.

2.9.1 Electrical Conductivity

Electrical conductivity is the degree to which a material conducts electricity [46]. Minerals are conductors if they can pass electricity. Minerals are semi-conductors as they can produce electricity in proper conditions. Materials are insulators if they are unable to have electricity pass through them. Few minerals are good conductors, primarily just the metallic elements and the mineral graphite, while most are insulators [46].

2.9.2 Electrical Charging Methods

The process of electrostatic separation consists of two steps, charging and separating [47]. Charging is the primary factor in the separation and can occur in three different ways; induction, discharging, and triboelectrification [47].

Charging by induction is typically done by feeding the mixture to be separated onto a drum and passing it through an electric field generated by a high-voltage electrode that is negatively charged [47]. An attractive force is imposed on the conductive materials, causing them to be lifted off the drum. Nonconductive particles stay on the drum until the force of gravity causes them to fall off. A diagram of this process is shown in Figure 2.6. The particles need to be in contact with the drum for the charge to be transferred, so the material needs to be fed in a single layer to achieve proper separation. This method of separation can only be used to separate conductive material from nonconductive materials, and while this can be done if the difference in conductivity between the target materials and waste materials is high enough, it has never been used on a large scale in practice [47].

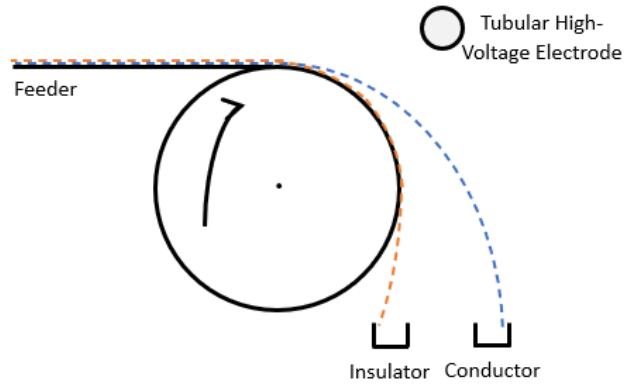


Figure 2.6: Rotational drum separator, inductive charging.

Charging by corona discharge is similar to induction charging, however, all particles are charged, regardless of their conductivity. This is done using an ionizing corona electrode generating an ionic stream, usually a wire or needle [47]. The charge on the conductive and semi conductive materials dissipates quickly to the drum, while the nonconductive materials stay on the drum for longer due to their higher surface resistivity, as shown in Figure 2.7 [47]. Corona separators can be used in a wider range of applications than induction separators due to the stronger electric field used.

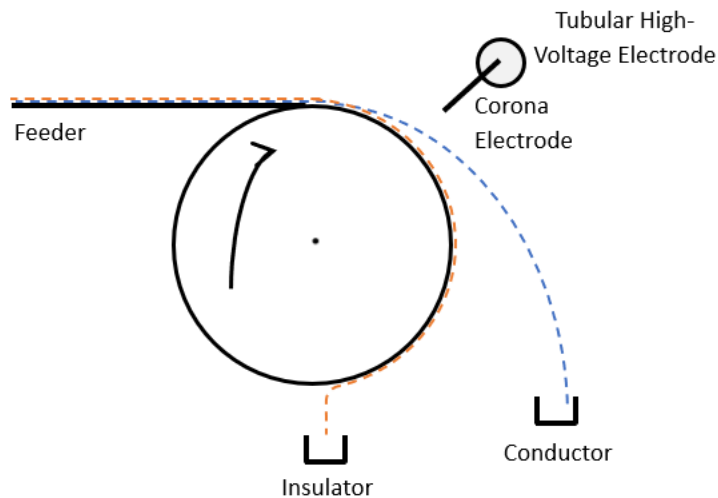


Figure 2.7: Rotational drum separator, corona charging.

Triboelectric charging uses friction between different types of particles or particles and the walls to create the charge used for separation, shown in Figure 2.8 [47]. Due to the complexity of this process and the variety of factors that can affect the charging process, prediction of material behavior is difficult, and the overall process is not well understood [47]. Research is generally done to prevent triboelectric

charging, as it can cause damage to electrical equipment or initiate explosions when unwanted, though when it is used selectively, it is a key step in electrostatic separation [47].

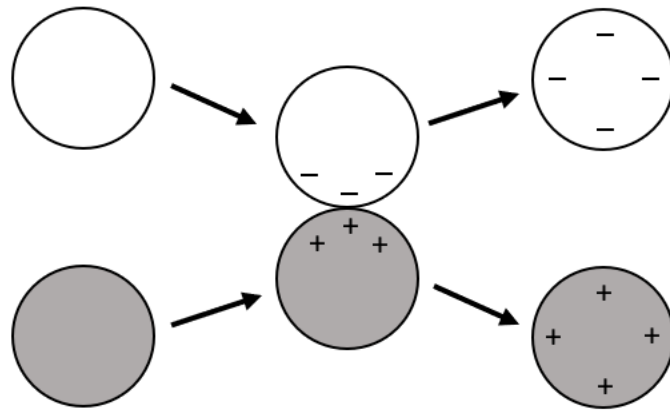


Figure 2.8: Particle-particle triboelectric charging.

Charging of a particle occurs on its surface, so the main property of importance of a particle is the surface conductivity [47]. Conductivity and the surface work function, the amount of energy needed to remove an electron from a solid a to point just outside the solid surface, are not unique properties for a given material and are highly dependent on external factors, such as temperature, humidity, chemicals present, and particle size [47] [48]. The presence of adsorbed water in a particle can result in can cause rapid discharge of charged particles, so preheating materials at 100 to 150 C is required to remove the water [47]. All particles must also be sufficiently liberated to prevent them from being misclassified during separation.

Industrial electrostatic separators can be grouped into three different types: drum, roll, and free falling. Drum separators, as seen in Figure 2.9, are widely used in the beneficiation of mineral sands, iron ore, and electric waste recycling [47]. Metallic tube electrodes are usually used, with non-conductivity coats and vacuum discharge tubes being used when voltages are higher [47]. Wire and needle electrodes in corona separators are also equipped with tubular high-voltage electrodes to enhance separation when nonconductive particles are deflected [47]. Multiple electrodes can also be used to ‘pin’ the nonconductive material and lift the conductive material more effectively, as seen in Figure 2.10.

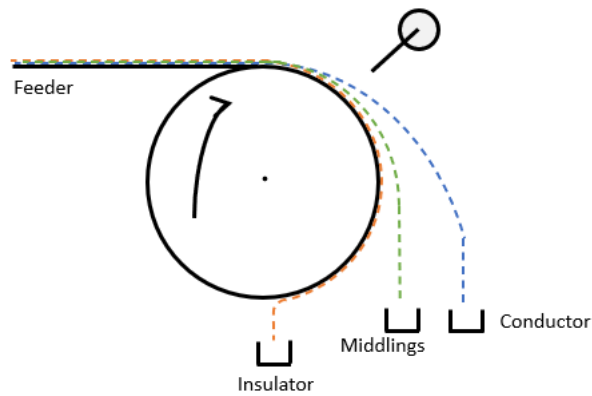


Figure 2.9: Drum separator diagram

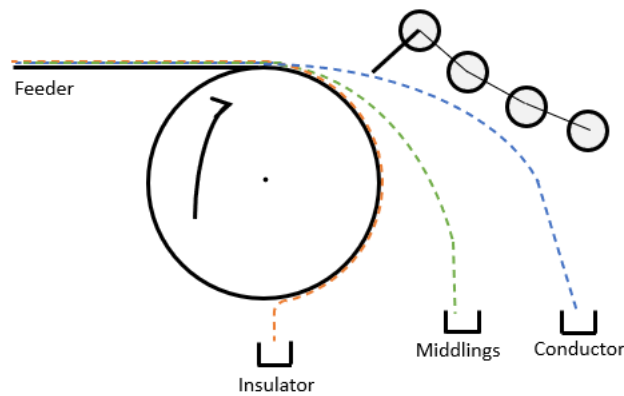


Figure 2.10: Multi-electrode drum separator diagram.

Belt separators are used on fine materials, typically less than 0.1 mm [47]. The particles are charged by the triboelectric effect as they drop into a space between two belts moving in opposite directions. The top belt is a negatively charged electrode and attracts the positively charged particles, while the bottom belt is positively charged, attracting the negatively charged particles [47]. A diagram of this can be seen in Figure 2.11. This results in two products, a concentrate and a tailings, with no middling fraction, which is common in other methods.

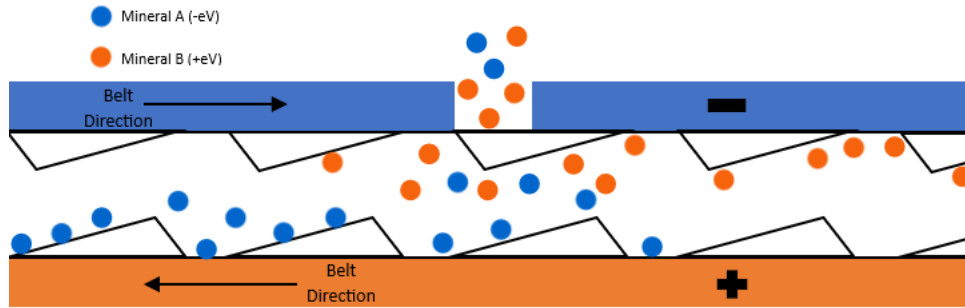


Figure 2.11: Belt separator diagram.

Free falling separators are typically used for coarse materials, up to several mm in diameter. Material falls between two oppositely charged electrodes and material is pulled to one side or the other depending on their conductivity, as seen in Figure 2.12 [47]. Plate electrodes are usually used, though dust can become a problem, as it causes decreases in magnetic field strength as it sticks to the electrodes [47]. In cases where there is a lot of dust, a tubular mode is used, where the electrode is encased in tubes that have brushes to remove any duct [47].

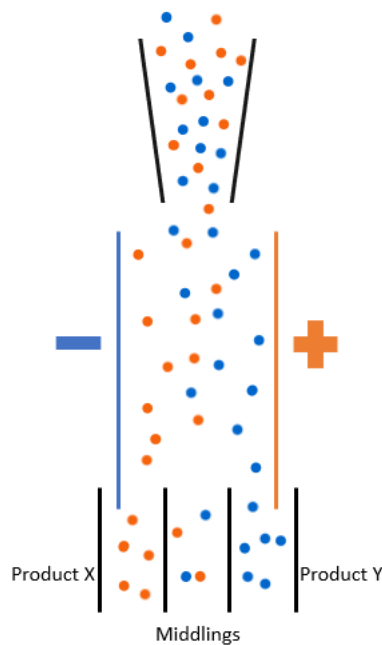


Figure 2.12: Free fall separator diagram.

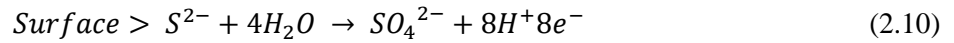
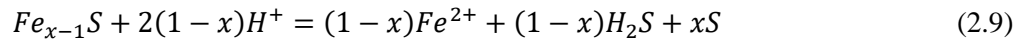
2.9.4 Electrostatic Separation of Pyrite

A test done in 1995 in Canada using artificial mixtures of galena, pyrite, and sphalerite was performed to test the feasibility of using electrostatic separation to remove sulfide minerals from a gangue

material such as quartz. Results from the test showed that pyrite responded the best, with a maximum of 70% of the pyrite recovered in 15% of the mass [49]. Galena also had some response, with a 40% recovery in 11% of the mass, while sphalerite showed no significant beneficiation [49].

2.10 Sulfuric Acid Leaching of Pyrite and Pyrrhotite

Pyrite and pyrrhotite leaching can occur in both non-oxidative and oxidative leaching environments and the reactions can be seen below in Equation 2.9 for non-oxidative leaching and equations 2.10 through 2.12 for oxidative leaching [50]. While oxidative leaching is slower, non-oxidative leaching creates sulfur layers on the particles, slowing down leaching by passivation and requiring these layers to be removed before leaching can begin again [51]. In an oxidative leaching environment, it is possible for pyrrhotite to consume all the oxidants and create non-oxidative conditions. This could result in additional acid being consumed or slowing or halting the leaching of the target minerals [50].



with either



Or



Pyrrhotite is a nonstoichiometric compound and therefore, its thermodynamic characteristics can change based on its composition, affecting its behavior in hydrometallurgical processes. When pyrrhotite has a high sulfur content, its stability in aqueous solutions increases, requiring a higher acidity and oxidation potential to successfully leach compared to pyrrhotite with a lower sulfur content [52].

2.10.1 Factors Effecting Leaching of Pyrite and Pyrrhotite

Testing done by the University of Belgrade looked at several factors that can have an effect on leaching with hydrogen peroxide and pyrite.

2.10.1.1 Effects of Stirring Speed

Testing done on stirring speed was done at 0, 500, and 1000 rpm with a sulfuric acid concentration of 0.3 M and a hydrogen peroxide concentration of 2.0 M. Pyrite dissolution increased with decreasing stirring speed, with hydrogen peroxide consumption decreasing at higher rpm. The reason for this is not clear but it is expected that more oxygen is generated by hydrogen peroxide at the beginning of

the reaction in the presence of stirring and that this oxygen is adsorbed by pyrite particles, which caused a decrease in the pyrite/hydrogen peroxide contact area [53].

2.10.1.2 Effect of Temperature

To test the effect of temperature, temperatures in the range of 293 to 323K were tested with a sulfuric acid concentration of 0.3 M and a hydrogen peroxide concentration of 2.0 M. Overall, the leaching rate increased with increasing temperature. The dissolution curves were linear below temperatures of 313K and parabolic above 313K, caused by the dissolution of hydrogen peroxide, as it decomposes at temperatures above 313K [53].

2.10.1.3 Effect of Particle Size

Testing on particle size was done on four different size fractions sulfuric with an acid concentration of 0.3 M and a hydrogen peroxide concentration of 2.0 M. The results showed that as particle size decreased, the leaching rate increased. This is due to the increase in surface area as particle size decreases, allowing for a greater pyrite/hydrogen peroxide contact surface [53].

2.10.1.4 Effect of Hydrogen Peroxide Concentration

Hydrogen peroxide was used in this testing in concentrations of 0.5, 1, 2, 3, 4, and 5 M at a temperature of 303K in 0.3M sulfuric acid. It was found that there was a linear dependence between the pyrite conversion and hydrogen peroxide except at the 4 and 5 M concentrations. It was also noted that there was a rapid consumption of hydrogen peroxide that led to a decrease in its concentration, reducing the leaching rate. The absorption of O₂ from the decomposed hydrogen peroxide also led to a decreased leach rate [53].

2.10.1.5 Effect of Sulfuric Acid Concentration

Testing on acid concentration was done with six different sulfuric acid concentrations at 303K with 2.0 M hydrogen peroxide. The results showed that as sulfuric acid concentrations increased, pyrite leaching decreased. This could be due to sulfate ions adsorbing on to the surface pyrite particles and reducing the pyrite/hydrogen peroxide contact area. This is supported by further testing done that shows hydrogen peroxide consumption rates decreased with increasing sulfuric acid concentrations [53].

CHAPTER 3. CHARACTERIZATION OF IRON CREEK DEPOSIT

3.1 Iron Creek Deposit

The Iron Creek deposit is a licensed location in the south-eastern corner of the Idaho Cobalt Belt. This site is estimated to contain 12.3 Mt of cobalt and 29 Mt of copper [54]. The primary minerals are pyrite, chalcopyrite, and arsenopyrite, with the cobalt occurring in the deposit primarily as cobaltiferous pyrite [10].

3.2 Iron Creek Deposit Characterization

Three core samples, labeled IC 18-07, IC 18-09, and IC 18-27, were received and sent to Eagle Engineering for AMICS analysis. Modal mineralogy was determined from the samples. The major phases in the samples were determined to be biotite, orthoclase, pyrite, and quartz. Minor phases were albite, allanite, arsenopyrite, calcite, chalcopyrite, iron oxides, and orthoclase. Cattierite was the only cobalt mineral observed. Figures 3.2, 3.3, and 3.4 show the AMICS identified images for each sample. Figure 3.1 shows the color key for the identified images. Cobalt was determined to be associated with pyrite and iron oxides in samples IC 18-07 and IC 18-09. In sample IC 18-27, cobalt was associated with pyrite, chalcopyrite, and orthoclase. The cobalt particles were also found to be very small, approximately 5 microns. An analytical report was performed by Hazen Laboratories for elemental concentrations in the as-received samples and the results of major elements can be seen in Table 3.1. Cobalt concentrations ranged from 2100 to 3400 ppm, while copper concentrations ranged from 1250 to 14000 ppm.

Mineral	Color
Albite	Cyan
Allanite	Magenta
Arsenopyrite	Teal
Biotite	Black
Calcite	Light Green
Cattierite	Purple
Chalcopyrite	Dark Green
Iron Oxides	Orange
Orthoclase	Pink
Pyrite	Red
Quartz	Yellow

Figure 3.1: Color key for the identified images of samples IC 18-07, IC 18-09, and IC 18-27.

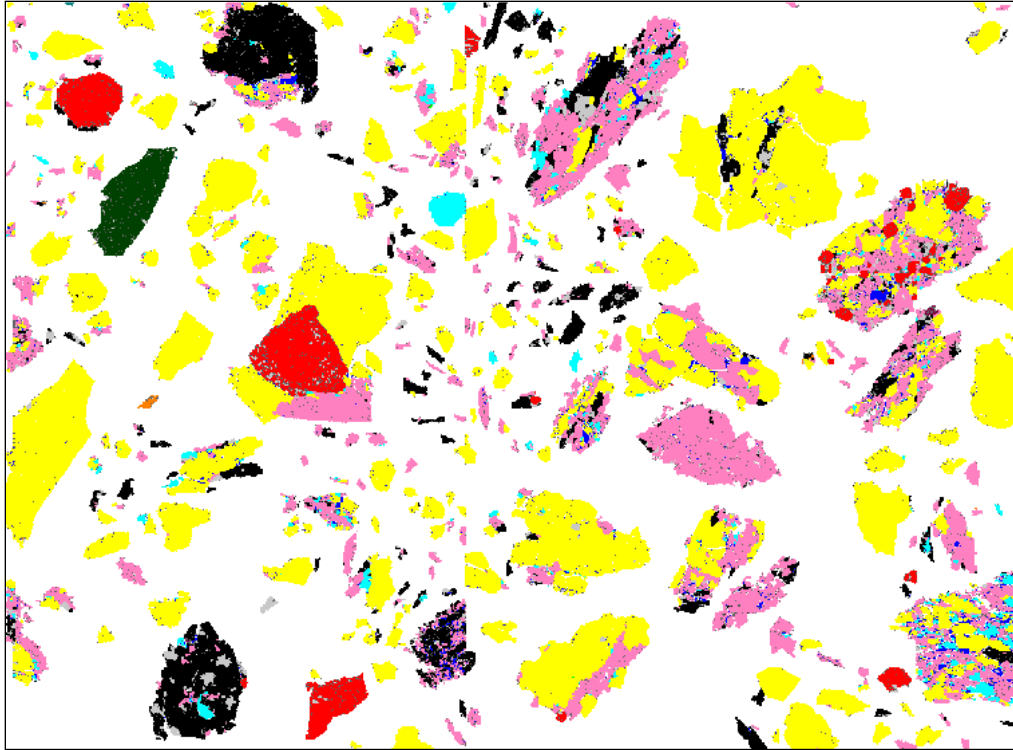


Figure 3.2: Identified image for sample IC 18-07.

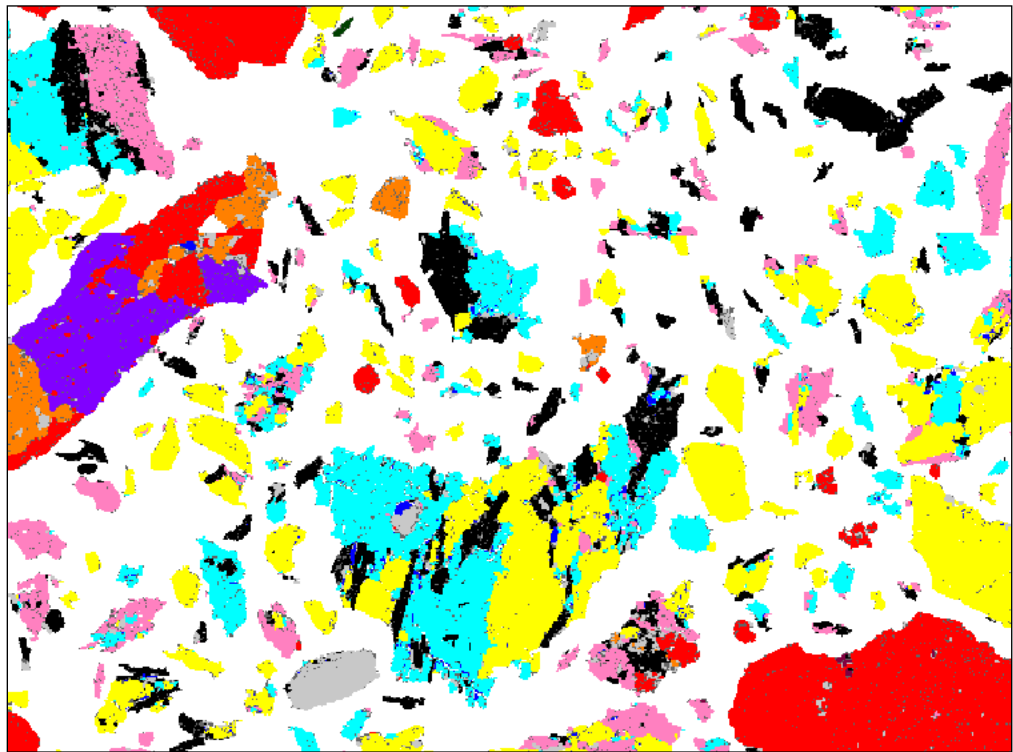


Figure 3.3: Identified image of sample IC 18-09.



Figure 3.4: Identified image for sample IC 18-27.

Table 3.1: Analytical Report of key elements from as-received samples.

Atomic Number	Element Name	Element Symbol	IC 18-07 Conc (ppm)	IC 18-09 Conc (ppm)	IC 18-27 Conc (ppm)
16	Sulfur	S	61600	52100	93400
26	Iron	Fe	100000	94600	123000
27	Cobalt	Co	2685	2083	3404
29	Copper	Cu	2476	1248	13987

3.3 Previous Testing

Previous testing was performed on Iron Creek deposit samples by several companies over the past 50 years, primarily for floatation testing.

Testing was first performed by Hanna and its subsidiary Coastal in the 1970s. No original copies of the reports were made available and the only sources are summaries. The work showed that the coarse sulfides were well liberated and could be floated in a bulk concentrate. The cobalt was rejected to the

tailings with the pyrite, and analysis showed that the cobalt was contained within the pyrite as cobaltian pyrite. The cobalt concentrate ranged from 2.0 to 4.0%.

Testing was done by McClelland in 2018 on behalf of First Cobalt (now Electra). McClelland first received four drill hole samples drilled in 2017, but the cobalt and copper content was low and the samples were not tested. First Cobalt then sent two bulk samples from Adit-1 and one from Aduit-2 in May of 2018. Samples were placed in a freezer to prevent sulfide oxidation during storage.

Each sample was tested in triplicate for cobalt and copper, with single tests for gold, arsenic, C-total, C-organic, S-Total, and S-Organic. An ICP metals analysis was done on each of the samples for the remaining metals, including iron. Results can be seen in Table 3.2 below.

Table 3.2: McClelland ICP metal analysis results.

Analyte, Units	McClelland Bulk Sample Identification		
	4313-001	4313-002	4313-003
Ag, ppm	5	5	<1
As, ppm	619	426	713
Ave. Co, ppm	4,287	2,596	2,653
C – Total, %	0.15	0.13	0.09
C – Organic, %	0.06	0.02	0.04
Fe – Total, %	14.60	11.55	12.00
S – Total, %	11.4	7.84	10.3
S – Sulfide, %	8.63	4.47	6.06
S – Sulfate, %	2.77	3.37	4.24

Mineralogical evaluations were performed on all three bulk samples. Pyrite was the dominant sulfide in the all the samples, followed by chalcopyrite, which together accounted for 56% to 82% of the total sample mass, respectively. Copper oxides and other sulfides were only found in trace amounts. The principal gangue materials were quartz, muscovite/illite, and biotite/phlogopite.

McClelland also performed some initial flotation testing on the samples. Rougher flotation tests were carried out to determine if bulk sulfide concentrates could be recovered that contained high percentages of cobalt and copper. All bulk samples responded well to the rougher flotation testing, with approximately 28% of the mass and 96% of the cobalt reporting to the concentrate. Results can be seen in Table 3.3.

Table 3.3: Summary of McClelland 2018 Rougher Flotation Testing.

Sample	4313-001		4313-002		4313-003	
Test No.	F-1	F-2	F-3	F-4	F-5	F-6
Wt. %						
Concentrate	28.1	30.4	32.3	23.0	25.9	26.9
Tail	71.9	69.6	67.7	77.0	74.1	73.2
Cu ppm						
Concentrate	30,876	29,093	30,758	42,871	4,641	4,498
Tail	621	385	206	164	170	88
Cu Distribution %						
Concentrate	95.1	97.1	98.6	98.7	90.5	94.9
Tail	4.9	2.9	1.4	1.3	9.5	5.1
Co ppm						
Concentrate	15,270	14,736	7,854	10,891	10,510	10,419
Tail	247	211	126	146	157	174
Co Distribution %						
Concentrate	96.0	96.8	96.7	95.7	95.9	95.6
Tail	4.0	3.2	3.3	4.3	4.1	4.4
S Distribution %						
Concentrate	96.3	97.4	98.2	97.6	96.6	96.2
Tail	3.7	2.6	1.8	2.4	3.4	3.8

Cleaner flotation tests were also performed, testing the effects of pH and regrinding the feed material on the results. Results can be seen in Tables 3.4, 3.5, and 3.6. Overall, the regrind with a pH of 12 gave the best results. The two high-grade samples recorded average copper recoveries of 75 to 85% with grades of 27.5 to 30%. The lower grade did not respond as well and only had a recovery of 40%. After testing it was discovered that the samples used had been exposed to the atmosphere for years before being received by McClelland and that oxidation may have occurred, affecting the flotation results, though the impact was thought to be small.

Table 3.4: Cleaner Test Results for Bulk Sample 4313-001.

Test No.	F-22	F-25	F-28
Test Conditions	No Regrind/ Nat. pH	No Regrind/ pH 12	Regrind/ pH 12
Weight %			
Recleaner Conc.	22.7	3.4	2.5
Cleaner Tail #2	1.9	4.5	0.8
Cleaner Tail #1	4.5	21.2	25.8
Rougher Tail	70.9	70.9	70.9
Cu Content, ppm			
Recleaner Conc.	35,600	117,000	275,000
Cleaner Tail #2	12,300	34,400	107,000
Cleaner Tail #1	6,100	16,700	4,470
Rougher Tail	347	347	347
Cu Distribution, %			
Recleaner Conc.	91.5	42.7	75.3
Cleaner Tail #2	2.6	16.6	9.4
Cleaner Tail #1	3.1	38.0	12.6
Rougher Tail	2.8	2.7	2.7
Co Content, ppm			
Recleaner Conc.	19,500	15,800	3,400
Cleaner Tail #2	12,600	19,700	12,800
Cleaner Tail #1	6,610	16,900	18,100
Rougher Tail	225	225	225
Co Distribution, %			
Recleaner Conc.	86.0	10.4	1.7
Cleaner Tail #2	4.7	17.2	2.0
Cleaner Tail #1	5.8	69.4	93.1
Rougher Tail	3.1	3.0	3.2

Table 3.5: Cleaner Test Results for Bulk Sample 4313-002.

Test No.	F-23	F-26	F-29
Test Conditions	No Regrind/ Nat. pH	No Regrind/ pH 12	Regrind/ pH 12
Weight %			
Recleaner Conc.	12.9	3.8	3.0
Cleaner Tail #2	3.3	3.8	0.7
Cleaner Tail #1	7.4	16.0	19.9
Rougher Tail	76.4	76.4	76.4
Cu Content, ppm			
Recleaner Conc.	60,000	127,000	303,000
Cleaner Tail #2	40,800	40,500	55,400
Cleaner Tail #1	15,900	24,100	4,900
Rougher Tail	253	253	253
Cu Distribution, %			
Recleaner Conc.	74.0	46.3	85.4
Cleaner Tail #2	12.9	14.8	3.6
Cleaner Tail #1	11.3	37.0	9.2
Rougher Tail	1.8	1.9	1.8
Co Content, ppm			
Recleaner Conc.	15,700	12,900	2,180
Cleaner Tail #2	13,000	16,000	13,000
Cleaner Tail #1	5,100	11,900	14,500
Rougher Tail	190	190	190
Co Distribution, %			
Recleaner Conc.	68.0	15.6	2.1
Cleaner Tail #2	14.4	19.3	2.9
Cleaner Tail #1	12.7	60.5	90.5
Rougher Tail	4.9	4.6	4.6

Table 3.6: Cleaner Test Results for Bulk Sample 4313-003.

Test No.	F-23	F-26	F-29
Test Conditions	No Regrind/ Nat. pH	No Regrind/ pH 12	Regrind/ pH 12
Weight %			
Recleaner Conc.	12.0	1.6	0.5
Cleaner Tail #2	4.8	1.3	1.3
Cleaner Tail #1	8.7	22.6	23.7
Rougher Tail	74.5	74.5	74.5
Cu Content, ppm			
Recleaner Conc.	7,700	62,800	107,000
Cleaner Tail #2	5,200	10,400	29,700
Cleaner Tail #1	2,060	1,000	1,200
Rougher Tail	142	142	142
Cu Distribution, %			
Recleaner Conc.	63.3	68.3	40.8
Cleaner Tail #2	17.1	9.2	29.4
Cleaner Tail #1	12.3	15.3	21.7
Rougher Tail	7.3	7.2	8.1
Co Content, ppm			
Recleaner Conc.	15,700	13,200	7,190
Cleaner Tail #2	15,000	15,300	10,200
Cleaner Tail #1	6,240	13,200	12,600
Rougher Tail	190	190	190
Co Distribution, %			
Recleaner Conc.	57.4	6.0	1.1
Cleaner Tail #2	22.0	5.6	4.0
Cleaner Tail #1	16.6	84.6	90.8
Rougher Tail	4.0	3.8	4.0

The mineralogical evaluation also included a QEMSCAN particle analysis, x-ray diffraction analysis, and electron microprobe analysis. The results from the tests concluded that the deportment of cobalt, copper, and arsenic is similar in all samples. It also showed that pyrite is the main carrier for cobalt, containing more than 90% of the total cobalt. There is also cobalt in the chalcopyrite, but it is unrecoverable and will be lost to the copper fraction in flotation. Pyrite is also the primary carrier of arsenic, but there may be other arsenic-bearing minerals unaccounted for.

3.4 Sample Preparation

Three shipments of deposit samples from Iron Creek were sent by Electra Battery Materials for testing. Table 3.7 shows the name and basic information of the samples. As the size the samples arrived at were too large to store and tested without possible complications, they needed to be further processed before testing could begin.

Table 3.7: Details on Iron Creek deposit samples received from Electra.

Sample Name	Shipment number	Date Received	Sample Type	Weather/Oxidation	Sample Mass (kg)	Sample Storage Conditions	Intended Experimental Application
IC 18-07	1	02/12/21	HQ Core	Potentially	131.1	<30 °F	Magnetic/Gravity/ Electrostatic Separation
IC 18-09	1	02/12/21	HQ Core	Potentially	74.2	<30 °F	Magnetic Separation
IC 18-27	1	02/12/21	HQ Core	Potentially	34.7	<30 °F	Magnetic Separation
IC 21-02	3	03/09/22	HQ Core	No	20.6	<30 °F	Flotation
IC 21-02 Cu	3	03/09/22	HQ Core	No	5.3	<30 °F	Flotation
Co High Grade	2	07/20/21	Audit	Potentially	51.1	<30 °F	Sortation
Co & Cu High Grade	2	07/20/21	Audit	Potentially	44.7	<30 °F	Sortation
Low Grade	2	07/20/21	Audit	Potentially	50.9	<30 °F	Sortation
Waste Grade	2	07/20/21	Audit	Potentially	42.4	<30 °F	Sortation

3.4.1 Sample Storage Preparation

When the samples from Electra were received, the materials were crushed to a more workable size. The samples received were prepared in two different methods depending on the testing purpose.

Samples used for sortation were crushed to 1 inch, while all other samples were crushed to -6 Tyler mesh or 336 microns.

3.4.1.1 HQ Core Sample Preparation

The core samples were received in sealed 5-gallon buckets. Upon receiving, the buckets were massed and taken to a comminution lab to reduce the particle size to make storage simpler. Samples had to be stored in a freezer to reduce the potential for oxidation and space for large samplers was limited.

The first crusher used was a 4' x 6' laboratory jaw crusher manufactured by Mine & Smelter Supply Company, shown in Figure 3.5. The gap width was set to ½ inch and samples were fed into the machine one rock at a time. The crushed material was screened using a ½ inch aperture to ensure that the material was adequately crushed for the next stage, with any oversized material being fed back into the jaw crusher until it was able to pass through the screen.



Figure 3.5: Laboratory scale jaw crusher unit.

The next crusher used was laboratory scale roll crusher manufactured by Joy Manufacturing Company, shown in Figure 3.6. The gap in the roll crusher was set to 1/8 inch. Care was taken when

feeding the material into the roll crusher so as not to jam the machine. Once crushed, the material was screened at 6 Tyler mesh, with oversized material passing through the roll crusher again until it passes 6 Tyler mesh. The size was chosen as no plan tests needed material coarser than 6 mesh.



Figure 3.6: Laboratory scale jaw crusher unit.

After all material passed 6 Tyler mesh, it was split into 1 kg samples using a Riffle splitter, as to remove any bias in the sampling. Care was taken to keep the core samples separate. Each 1 kg split t was put into storage bags and labeled with the sample name, spilt number, and mass and placed in a freezer with a temperature below 30 °F to reduce the chance of oxidation.

3.4.1.2 Audit Sample Preparation

Audit samples were used to perform sortation testing to determine the viability of using it for pre-concentration on the Iron Creek deposit samples. Samples were received in 5-gallon buckets with an average diameter of 8-10 inches.

Crushing started with the jaw crusher with a set gap width of 2 inches. The crushed material was sieved through a screen with a 2-inch sieve aperture size. Oversized material was fed through the jaw crusher again. This process continued until 100% of the material passed through the 2-inch screen.

The material was sieved again through a 1-inch screen to remove the undersized product. The remaining product was counted and placed on a large table. Once the total number of particles were calculated, 20 particles were randomly selected from each sample and sent out for sortation testing. The particles that were not selected and the undersized particles were placed back into buckets and stored for further testing.

3.4.2 3-Acid Digestion Procedure

All samples were analyzed using atomic absorption spectroscopy (AAS). For this to occur, all samples had to be dissolved into an aqueous solution. This was done by digesting the samples using the method of 3-acid digestion, using hydrochloric acid, nitric acid, and hydrofluoric acid.

The methodology of the 3-acid digestion is to combine 0.5 g of sample, 10 mL of hydrochloric acid, 10 mL of nitric acid, 10 mL of hydrofluoric acid, and 5 mL of deionized (DI) water in a beaker. This beaker is then transferred to a hot plate set to 100 °C and is agitated with a magnetic stir bar for 30 minutes. At the conclusion of the 30 minutes, another 10 mL of hydrochloric acid, 5 mL of nitric acid, and 5 mL of DI water are added to the beaker and agitated for another 30 minutes or until the sample is fully dissolved.

Samples containing high amounts of iron and/or silica were unable to dissolve using the above method. The only difference to the methodology from the one described above is that an additional 3 mL of hydrofluoric acid was added.

Once the sample is fully dissolved, it is filtered using Wattman 44 filter paper to remove any solid particles.

After dissolution, all samples were diluted with 2% nitric acid until the estimated ppm was within the testable range of the AAS.

CHAPTER 4. BOND WORK INDEX TESTING

The first three samples received from Electra, IC 18-07, IC 18-09, and IC 18-27, underwent Bond Work Index (BWI) testing to assist in producing grindability curves to be used for deposit sample processing later in testing.

4.1 Bond Work Index

The Bond Work Index is the amount of energy required to reduce one ton of material from a large size to 100 microns. It can be calculated by Equation 4.1 below. This is important to know as it allows for the most efficient grind of material.

$$W_i = \frac{44.5}{P_i^{0.23}} \times G_{pr}^{0.92} \left(\frac{10}{\sqrt{P_{80}}} - \frac{10}{\sqrt{F_{80}}} \right) \quad (4.1)$$

Where W_i is the Work index in kWh/st, P_i is the sieve opening in microns, G_{pr} is the grindability in g/revolutions, and p and f are the 80% passing sizes in microns of the product and feed respectively.

Table 4.1 shows the range of BWIs from literature for minerals in the tested deposit samples. Based on these values and the density of the samples, the expected BWI for the tested samples would be in the range of 15-17.

Table 4.1: BWIs for various minerals in the tested deposit samples. Table created based on data from [55] and [56].

Mineral	BWI Range (kWh/ton)
Chalcopyrite	15
Feldspar	9-14
Iron Oxides	2-31
Kaolinite	12
Molybdenite	10-16
Pyrite	7-13
Pyrrhotite	9-11
Quartz	11-21

4.2 Bond Work Index Testing Procedure

Before testing could begin, the p80 of the feed materials needs to be calculated. Approximately 200g of sample was split out from material previously crushed to minus 6 Tyler mesh and placed in a sieve stack containing sieves of 6, 8, 10, 12, 16, 20 Tyler mesh. The sieve stack was put into a ro-tap and ran for 15 minutes. The fraction from each sieve was massed and used to calculate the size distribution.

To determine the initial feed mass, a 1000 mL plastic graduated cylinder was used. Approximately 200 mL of material was placed into the cylinder and tapped down to compact it. This was repeated 2-3 times until there was 700 mL of compacted material in the cylinder. The mass of the compacted material was taken, and this number was used as the starting mass for each test cycle. This mass was also divided by 3.5 to calculate the 250% circulating load.

The ball charge for the mill was counted out and the mass checked as seen in Table 4.2. This mass was checked throughout the test to ensure that it stayed within 3% of the initial mass. If the mass does drop by more than 3%, balls are replaced until the mass is back with the 3%.

Table 4.2: Ball charge and mass of balls for bond work index test.

Size (in.)	Number
1.45	43
1.17	67
1.0	10
0.75	71
0.61	94
Total weight	20.125 kg

The ball charge was placed in the Bond work index ball mill. The massed out deposit material was placed in the mill next. The lid was placed and tightened down with the 2 holding nuts. The timer was set to 100 revolutions and allowed to run. The ground material and balls were then removed and separated, with the balls being cleaned to remove any dust. The material was roughly split in half, with each half placed in a sieve stack with a 100 Tyler mesh screen. Each sieve stack was run in the ro-tap for 15 minutes and each fraction was massed and recorded. The undersized was set aside. The oversized was placed on a scale and new material was added until the total mass was equal to the starting mass of the first cycle.

The number of cycles after the first was determined using Equation 4.2 below, rounded to the nearest whole number.

$$R = \frac{CL - (m_f * \frac{U}{100})}{R_p} \quad (4.2)$$

Where R is the number of revolutions for the next cycle, CL is the 250% circulating load, m_f is the mass of the new feed added, U is the % undersized material in the feed, and R_p is the number of the revolutions from the pervious test.

The testing continued until at least 7 cycles have been completed, a reverse in the grams per revolution has occurred in the last three cycles, and the difference between the three cycles is less than 3%. The average of the last three cycles is the grindability in grams per revolution.

The undersized material from the last three cycles was then blended and an approximately 200-gram sample was split out. The sample was then placed in a sieve stack containing screen sizes of 100, 115, 150, 200, 270, and 400 Tyler mesh. The sieve stack was put into a ro-tap and ran for 15 minutes. The fraction from each sieve was massed and used to calculate the size distribution of the product.

The work index is then calculated using Equation 4.1 using the data collected.

4.3 Bond Work Index Data

The data used to calculate the BWI for each sample can be seen in Tables 4.3 through 4.5. The full data used to calculate G_{pr} , P_{80} , and F_{80} can be found in Appendix B.

Table 4.3: BWI data for sample IC 18-07.

Variable	Value	Units
P_1	149	microns
G_{pr}	3.064	g/rev
P_{80}	85.2	microns
F_{80}	2850	microns
BWI	6.27	kWh/st

Table 4.4: BWI data for sample IC 18-09.

Variable	Value	Units
P_1	149	microns
G_{pr}	2.048	g/rev
P_{80}	100.72	microns
F_{80}	3000	microns
BWI	9.61	kWh/st

Table 4.5: BWI data for sample IC 18-27.

Variable	Value	Units
P_1	149	microns
G_{pr}	2.716	g/rev
P_{80}	91.35	microns
F_{80}	2910	microns
BWI	7.21	kWh/st

The BWI of the samples was in the range of 6 to 10 kWh/st, with the average BWI was 7.7 kWh/st. This was much lower than the expected BWI of 15-17 kWh/st, as seen in Table 4.1. Therefore,

material from sample IC 18-07 was sent to Hazen to confirm the results and the testing procedure. The result of that test is in Table 4.6.

Table 4.6: BWI test results from Hazen for sample IC 18-07.

Variable	Value	Units
P₁	149	microns
G_{pr}	3.42	g/rev
P₈₀	105	microns
F₈₀	2505	microns
BWI	6.6	kWh/st

The BWI calculated by Hazen was 6.6 kWh/st. This value is close enough to the test results done at Mines that is assumed that the results from the testing performed at Mines are reliable.

4.4 Bond Work Index Discussion

The average BWI of the samples tested at Mines was 7.7 kWh/st. With the expected BWI being around 15, the actual values are much lower, meaning that the material is much softer than expected based off of mineral composition. This may be due to the samples being oxidized, as the samples were left outside for years at the mine site before they were shipped to Mines. This would have broken down the material slightly or changed the mineral composition before testing, resulting in less energy being required to break down the materials. Knowing that the material requires less energy for crushing and grinding than would be expected is important, as it is possible to over-grind the material if literature BWI values are used.

CHAPTER 5. SORTATION

Sortation in the mining industry is used as a pre concentration step to remove waste rock before grinding and/or processing to reduce operating costs. Before sortation is tested on Iron Creek material at an industrial scale it must be determined whether the material is viable for any sortation techniques.

5.1 Scanning Type Determination

There were several scanning technologies that were considered for the initial sortation testing of Iron Creek deposit samples including color, light transmission, and X-ray transmission (XRT) scanning.

Color scanning was the first scanning technology considered for sortation testing due to its low cost. This is because it requires less computation and scanning hardware. However, it was determined that color scanning would not be viable due to the material surface needing to be prepared by washing before scanning to remove any dust on the surface of the particles that could interfere with scanning. This eliminates color sortation from consideration as washing the material would cost more than would be saved by sortation and makes the sortation operation much more complex.

Light transmission scanning was the next sortation method considered. Similar to color scanning, light transmission scanning is cheap and has a wide range of uses. Pyrite reflects light so it could be used by the scanner to identify the particles that contain pyrite. However, as with color scanning, washing would be required to remove fine material that could interfere with the scanner.

XRT scanning was the next method considered for sortation testing. It was considered as no washing is required as XRT is penetrative and not dependent on the surface of the material. Another reason was the density between the target material and the waste material was large enough that it could be easily noticeable. Table 5.1 below shows the major minerals present and their density and how much of the sample they make up. With the density of the target materials, pyrite, and chalcopyrite, being much larger than the waste materials, biotite, orthoclase, and quartz, it was determined that XRT sortation technology was likely the most viable and was therefore prioritized in testing.

Table 5.1: Densities of major mineral constituents in Iron Creek deposit samples.

Chemical Formula	Mineral	Density of Mineral g/cm³	Percent of Sample Composition
Biotite	K(Mg,Fe) ₃ AlSi ₃ O ₁₀ (OH)	3.09	12.94
Orthoclase	KAlSi ₃ O ₈	2.56	25.74
Cattierite	CoS	4.8	0.51
Chalcopyrite	CuFeS ₂	4.19	1.79
Pyrite	FeS ₂	2.01	12.36
Quartz	SiO ₂	2.65	38.96

5.2 Scanning Testing Procedure

Testing for the 4 samples (cobalt high grade, copper and cobalt high grade, low grade, and waste rock) was done by Saskatchewan Research Council (SRC) in Saskatoon, SK. Sample were sent in large 2-gallon sample bag and pictures of each sample rock sample were taken so that a comparison could be made to the original sample condition later.

After arriving at SRC, the samples were taken from the sample bags and inspected to ensure that no breakage or size reduction occurred during shipping. This was done using the pictures taken before shipping. Mineralogical and elemental data were consulted to determine the best sortation scanning method had the most potential for separating ore grade material from waste grade material. XRT scanning was determined to be the most suitable for this material, as described in Section 5.1.

For the sortation testing, each 20-rock sample was placed in rows of 4 onto clear plastic tarps and held in place with duct tape. Figure 5.1 below shows an example of the sample placed onto clear plastic tarps before XRT scanning. Each tarp was then placed on a small conveyor belt and analyzed using TOMRA's COM Tertiary XRT system. This system used an X-ray source and an X-ray camera to get a whole rock scan for each sample focusing on material density. Once the scan was completed the material was removed from the tarps and placed into 4 separate buckets labeled by sample name. The buckets were then shipped from SRC to Colorado School of Mines (CSM) so that they could be further analyzed.



Figure 5.1: Sortation samples on tarps before XRT scanning.

5.3 Sortation Sample Analysis

Once the samples were returned to CSM, each of the 4 samples were prepared for elemental analysis via AAS. Samples were digested using 3-acid digestion, but the samples first had to be crushed to reach the recommended size of 150 microns. All the rocks were passed through a jaw crusher with a gap width of $\frac{1}{2}$ inch. Once the samples were crushed, the resulting samples were individually fed through a roll crusher with a gap width of 6 Tyler mesh, or 3.327 mm. The resulting material was then sieved using a 6 Tyler mesh screen, with any oversized material returning to the roll crusher to be crushed again. This process continued until all material passed through the 6 Tyler mesh screen.

In order to reach the target size of 150-micron, grinding was used to efficiently reduce the material to particle size. A ring and puck grinding mill was used as it requires the least preparation for use and the effect of particle geometry resulting from the ring and puck mill would not affect the digestion or elemental analysis. Figure 5.2 shows the ring and puck mill used. Material was placed into the mill and

the mill was sealed to limit the amount of material lost as dust during grinding. The mill was then switched on and set for 2 minutes.



Figure 5.2: Ring and puck mill used for grinding.

After grinding the material was sieved using an 8, 10, 14, 20, 28, and 35 sized Tyler mesh screens stacked on top of each other and placed into a ro-tap shaker, seen in Figure 5.3. Screen shaking lasted for 20 minutes to ensure all particles had sufficient time to pass through all possible screens and end in the correct size range. After shaking, the screen stack was removed from the ro-tap and each resulting size fraction was massed. From the recorded mass for each size fraction the overall p80 of the rock was calculated to ensure that the recommended particle size for digestion was achieved. After grinding and size analysis was completed, each rock underwent 3-acid digest outlined in section 3.4.2.



Figure 5.3: Ro-tap used for particle size analysis.

4.4 Sortation XRT Scan Data

The XRT scan of each sample was computed and the data for the density measurements of each rock was output as an image showing areas of high- and low-density material. Figure 5.4 below the output density images for each rock in the 4 tested samples. The red areas in Figure 5.4 are areas of predominantly low-density while the blues areas are areas of predominantly medium- to high-density material.

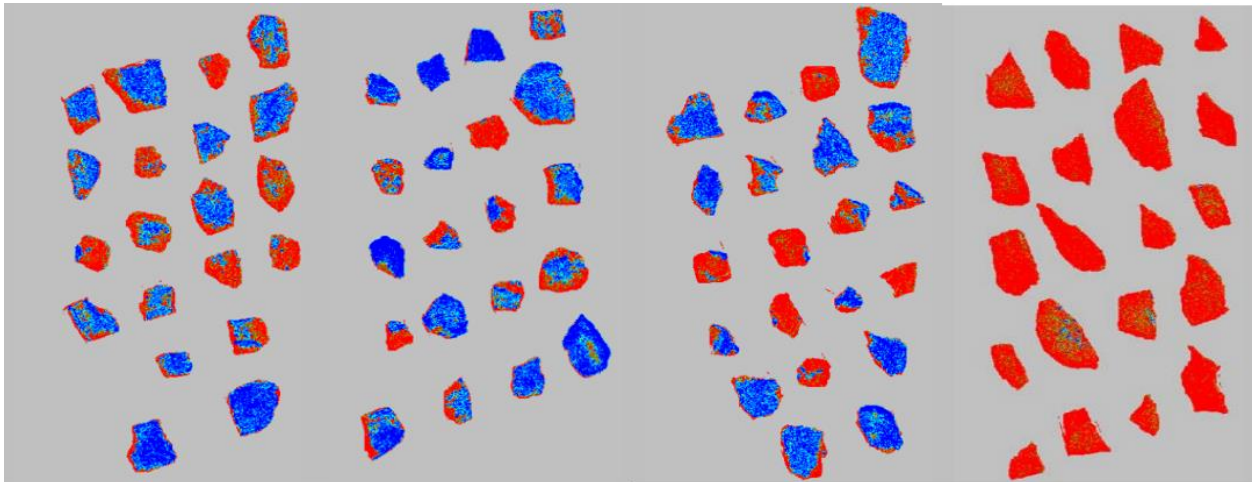


Figure 5.4: XRT scan of all 4 samples showing density differences by different colors.

As stated earlier, the pyrite should be in the high-density areas, with little to none being in the low-density areas. As the cobalt is contained within the pyrite, the cobalt should be in the blue areas.

Just an image showing the different densities is not enough to make a reliable separation, therefore, a numerical representation of the different densities is needed. This was calculated by measuring the percent area of the high-density material for each rock in the scanned images. Table 5.2 below shows the average percent area of high-density material in a rock from each sample.

Table 5.2: Average percent area of the 4 sortation samples.

Sample Name	Average Percent Area of High-Density Material
Cobalt High Grade	63.10
Copper and Cobalt High Grade	48.37
Low Grade	44.40
Waste Grade	0.44

The cobalt high-grade rocks had the highest average percent area, with the high-density material making up 63.1% of the particles on average. Copper and cobalt high-grade rocks and low-grade samples had similar percent areas, with 48.37% and 44.40% respectively. The waste rocks had the lowest average high-density area by far with 0.44%. This data shows that the difference in density observed in the mineralogical analysis can be quantified by XRT scanning and in the form of average percent area calculations of high-density area in the scanned images. It also shows that it is possible to separate waste rocks from all other materials using this scanning and calculation method.

5.5 Sortation Cobalt and Copper AAS Data

AAS was used to collect cobalt and copper grades on each rock sample in each sample group. Table 5.3 shows the average cobalt and copper grade for the sample. The cobalt high-grade sample had the highest average cobalt grade, 0.77%, while the copper and cobalt high grade had the highest average copper grade, 1.25%. The waste samples had the lowest average cobalt and copper grades, 0.005% and 0.016% respectively. This data supports the findings of the XRT scans, as the sample that had the highest high-density percent area, the high-grade cobalt, also had the highest cobalt grade. The copper and cobalt high grade had a lower cobalt grade than the high grade and similarly had a lower average high-density area. The waste rock had little to no cobalt and copper and this was reflected with little to no high-density areas in the XRT scanning.

Table 5.3: Average cobalt and copper content from sortation samples.

Sample Name	Co%	Cu%
Cobalt High Grade	0.774266	0.682813
Copper and Cobalt High Grade	0.350387	1.248502
Low Grade	0.229038	0.749281
Waste Grade	0.004744	0.016181

5.6 Sortation XRT and ASS Data Combined

Previous sections in this chapter discussed and confirmed the potential of using XRT scanning as an effective sortation method for the Iron Creek deposit. However, additional work is needed to determine what the high-density percent area cutoff needs to be to maximize cobalt and copper grade and recovery. Increasing the percentage area cut off would increase the concentrate grade of copper and cobalt but decrease the recovery. Likewise, decreasing the percent area cutoff would increase recovery but decrease the grade in the concentrate. Table 5.4 shows a model of various cutoff percentages using the combined percent area and elemental analysis data.

Table 5.4: Combined percent area and elemental analysis data to model sortation.

% Area Cut Off	Concentrate Grade Co (%)	Concentrate Grade Cu (%)	Co Recovery (%)	Cu Recovery (%)	Predicted Flotation Feed Co Grade (%)	Predicted Flotation Feed Cu Grade (%)
10	0.499	1.004	94.23	94.62	0.43	0.79
20	0.516	1.059	90.05	92.12	0.44	0.82
30	0.531	1.093	86.79	89.15	0.45	0.83
40	0.563	1.022	81.90	74.09	0.46	0.76
50	0.596	1.134	75.78	71.90	0.47	0.81
60	0.664	1.044	69.99	54.89	0.5	0.71
70	0.841	1.119	61.15	40.57	0.55	0.68
80	0.984	1.218	53.64	33.11	0.56	0.66
90	1.36	1.151	24.72	10.43	0.48	0.44

As the sortation is a pre-concentration set, the effects on the next unit operations also need to be considered. Table 5.5 below is data received regarding the expected effects of sortation on flotation. The data from Table 5.4 with the data from Table 5.5 can be used to find the best conditions to balance cobalt and copper grade and recovery. At least 6.2% of the material that underwent sortation scanning would report to flotation, with a maximum of 64.2%. The goal of the sortation was to use it as a pre-concentration step to remove waste materials with minimal grinding to upgrade the flotation feed material. This would nearly double the cobalt and copper grade in the concentrate while maintaining good recovery values, with recoveries of 87% and 89% for cobalt and copper respectively.

Table 5.5: Percent of rock data at differing % area cut off grades.

XRT Dual % Cut Off	% of Rocks to Concentrate	% of Feed Screening at 1/4"	Overall % of Rocks to Float Feed
10	64.2	50.718	71.718
20	59.3	46.847	67.847
30	55.6	43.924	64.924
40	49.4	39.026	60.026
50	43.2	34.128	55.128
60	35.8	28.282	49.282
70	24.7	19.513	40.513
80	18.5	14.615	35.615
90	6.2	4.898	25.898

5.7 Sortation Discussion

Overall, the use of sortation can be considered successful. XRT scanning was selected as the preferred testing method and found to be a suitable method, as it showed a large difference in density between the target and the waste material. It is recommended that other scanning methods should be tested to compare the scanning technology to further gauge the effectiveness of the XRT scanning method.

The XRT scanning results showed that the differences in densities between the target material and the waste were large enough that easily visible on the scan results. Combined with the elemental results from the AAS analysis, the grade of the target and waste materials could be verified, and a high-density percent area cutoff grade could be calculated. This was determined to be 30% as it provided the best balance between the cobalt and copper grade and recovery in the concentrate. The predicted cobalt grade in the concentrate was 0.531% with a recovery of 86.79%. The predicted copper grade in the concentrate was 1.093% with a recovery of 89.15%. The 30% area also reduced the amount of material rejected from crushing, with only 32.1% being rejected.

CHAPTER 6. MAGNETIC SEPARATION

6.1 Testing Conditions

Magnetic separation testing of the deposit material was done in a wet high intensity magnetic separator (WHIMS). This was due to the expected magnetic response of all materials tested and the particle sizes of the samples produced by other experiments. The WHIMS contains two copper coils powered by a transformer with a 2-inch gap between them, where a magnetic field is created. A matrix is placed in this gap to capture the magnetic material in the sample. A calibration curve provided by the manufacturer is used to determine the current needed to produce the target magnetic field intensity. The magnetic properties of some of the materials in the samples tested are shown in Table 6.1.

Table 6.1: Magnetic properties of target and gangue materials.

Mineral	Magnetic Response
Biotite	Paramagnetic
Chalcopyrite	Paramagnetic
Chlorite	Paramagnetic
Feldspar	Non-Magnetic
Galena	Non-Magnetic
Iron Oxides	Ferromagnetic
Jaipurite	Paramagnetic
Kaolinite	Paramagnetic
Molybdenite	Paramagnetic
Muscovite	Non-Magnetic
Pyrite	Non-Magnetic
Pyrrhotite	Paramagnetic
Quartz	Diamagnetic

There are several different options available to use for the matrix, with finer matrixes having the ability to pull larger amounts of magnetic material due to the greater number of sharp contact points and surface area. The particle size is the determining factor in how fine a matrix can be used though, as if too fine a matrix is used, it can become clogged, trapping material in the matrix regardless of its magnetic properties.

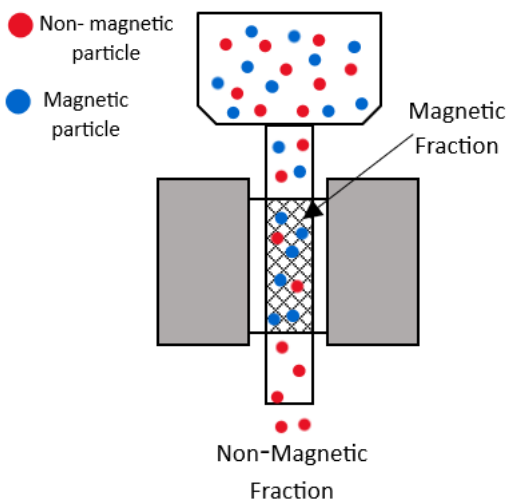


Figure 6.1: Bench scale WHIMS diagram.

Testing in the WHIMS was performed on seven different samples, 3 deposit samples, a bulk flotation concentrate, the product of thermal decomposition on the product of the bulk flotation concentrate, a differential flotation concentrate, and the thermal decomposition product of the differential flotation concentrate. Deposit samples were labeled IC 18-07, IC 18-09, IC 18-27. Testing conditions for the run-of-mine and flotation samples can be found in Tables 6.2 through 6.4.

Table 6.2: Testing conditions for the run-of-mine trials.

Trial number	Magnetic Field Intensity (Tesla)	IC 18-07 mass used (g)	IC 18-09 mass used (g)	IC 18-27 mass used (g)
1	0.3	39.5	39.9	39.6
2	0.4	40.3	40.2	40.1
3	0.5	39.9	40.3	39.9
4	0.6	39.5	39.8	39.7
5	0.7	39.4	39.2	39.8
6	0.8	40.5	40.2	40.0
7	0.9	40.0	40.0	39.2
8	1.0	39.9	40.0	39.7

Table 6.3: Testing conditions for the bulk flotation concentrate trials.

Trial number	Magnetic Field Intensity (Tesla)	Bulk float conc. mass used (g)
1	0.3	15.9
2	0.4	16.5
3	0.6	18.8
4	0.8	19.0

Table 6.4: Testing conditions for the differential flotation concentrate trials.

Trial number	Magnetic Field Intensity (Tesla)	Differential float conc. mass used (g)
1	1.0	24.9
2	0.5	24.7

6.1.1 Testing of Thermal Decomposition Products

Thermal decomposition of pyrite is an important step in making magnetic separation viable. Pyrite is a sulfide mineral with the chemical formula FeS_2 , though it is possible for elements with similar atomic radii to iron, like cobalt, to substitute in for the iron. Pyrite does not respond to a magnetic field according to literature, so magnetic separation of deposit samples and flotation concentrate should be ineffective. However, pyrite decomposes into pyrrhotite and troilite, two other iron sulfide minerals, by the removal of sulfur as seen in Equation 6.1 below:



Troilite is also non-magnetic, but the intermediate product of pyrrhotite does respond to a magnetic field. As cobalt is substituted for iron in the pyrite, theatrically, it should stay within the pyrrhotite and troilite after decomposition and magnetic separation could be used to create a cobalt concentrate. Testing conditions for thermal decomposition products can be seen in Tables 6.5 and 6.6 below.

Table 6.5: Testing conditions for the thermal decomposition product of the bulk flotation concentrate.

Trial number	Magnetic Field Intensity (Tesla)	Concentrate mass used (g)
1	1.0	18.9
2	0.5	23.0

Table 6.6: Testing conditions for the thermal decomposition product of the differential flotation concentrate.

Trial number	Magnetic Field Intensity (Tesla)	Concnetrate mass used (g)
1	1.0	20.2
2	0.5	20.8

6.2 Wet High Intensity Magnetic Separation Testing Procedures

6.2.1 Deposit Sample Testing Procedure

Deposit samples were crushed using a rod mill to a p80 of 100 microns. 40 g of the crushed sample was then mixed with DI to create a 10% solids solution. The wet high intensity magnetic separator (WHIMS) was set to the appropriate current for the target magnetic field strength. The slurry was poured into the WHIMS. Water was poured through the WHIMS to remove any non-magnetic material stuck inside the matrix. The WHIMS was then turned off. More water was run through the WHIMS to remove the magnetic fraction.

Vacuum filtration was used to separate the samples from the water and were dried in a 100 °C furnace for 4 to 6 hours.

6.2.2 Bulk Flotation Testing Procedure

Testing of the bulk flotation sample followed the same procedure as outlined in section 6.2.1, but the material had a p80 of 75 microns and only 20 g of samples was used due to the limited amount of material available.

6.2.3 Thermal Decomposition Bulk Flotation Product Testing Procedure

Testing of the bulk flotation sample followed the same procedure as outlined in section 6.2.1, but the material had a p80 of 75 microns and only 20 g of samples was used due to the limited amount of material available.

6.2.4 Differential Flotation Product Testing Procedure

Testing of the bulk flotation sample followed the same procedure as outlined in section 6.2.1, but the material had a p80 of 75 microns and only 20 g of samples was used due to the limited amount of material available.

6.2.5 Thermal Decomposition Differential Flotation Product Testing Procedure

Testing of the bulk flotation sample followed the same procedure as outlined in section 6.2.1, but the material had a p80 of 75 microns and only 20 g of samples was used due to the limited amount of material available.

6.3 Preparation of Magnetic Separation Sample for Analysis

All products from magnetic separation testing were analyzed using atomic absorption spectroscopy (AAS). The methods used to prepare the samples for analysis are described in the section below.

6.3.1 AAS Preparation

Given the samples are already aqueous after digestion, the only preparation necessary for analysis is dilution. The dilution is to a concentration that is within the range set by the standards used for calibration for the AAS machine.

Here the elements being analyzed are cobalt, copper, and iron. The range of Co calibration standards is 1 ppm Co to 10 ppm Co, the range for Cu calibration standards is 1 ppm Cu to 10 ppm Cu, and the range for Fe calibration standards is 1 ppm Fe to 100 ppm Fe. While Cu and Co have similar enough concentrations and calibration range that the same dilution can be used, the Fe concentration is much higher and requires its own dilution.

6.3.1.1 Deposit Sample Dilution

Given the cobalt and copper concentration in the deposit sample material is 2500 ppm and 1740 ppm respectively, a 250X dilution of sample containing 2500 ppm Co would report as having 10 ppm Co, within the range set by the calibration standards. The Fe concentration in the deposit sample material is 10.9 wt %, or 109000 ppm. A 1100X dilution of sample containing 109000 ppm Fe would report as having 99 ppm Fe, within the range set by the calibration standards. A 250X dilution with 2% nitric acid

was used for the preparation of samples for Co and Cu AAS analysis and a 1100X dilution with 2% nitric acid was used for the preparation of samples for Fe analysis.

6.3.1.2 Bulk Flotation Concentrate Dilution

Given the cobalt and copper concentration in the bulk flotation concentrate material is 11210 ppm and 9150 ppm respectively, a 1121X dilution of sample containing 11210 ppm Co would report as having 10 ppm Co, with the range set by the calibration standards. The Fe concentration in the deposit sample material is 23.4 wt %, or 234000 ppm. A 2340X dilution of sample containing 234000 ppm Fe would report as having 99 ppm Fe, with the range set by the calibration standards. A 1250X dilution with 2% nitric acid was used for the preparation of samples for Co and Cu AAS analysis and a 2500X dilution with 2% nitric acid was used for the preparation of samples for Fe analysis.

6.3.1.3 Thermal Decomposition Product of Bulk Flotation Dilution

Given the cobalt and copper concentration in the thermal decomposition product of bulk Flotation material is 1.46 wt%, or 14564 ppm, and 9847 ppm respectively, a 1457X dilution of sample containing 14564 ppm Co would report as having 10 ppm Co, with the range set by the calibration standards. A 1500X dilution with 2% nitric acid was used for the preparation of samples for Co and Cu AAS.

6.3.1.4 Differential Flotation Dilution

Given the cobalt and copper concentration in the thermal decomposition product of differential flotation material is 1.59 wt%, or 15870 ppm, and 2269 ppm respectively, a 1587X dilution of sample containing 15780 ppm Co would report as having 10 ppm Co, with the range set by the calibration standards. A 1750X dilution with 2% nitric acid was used for the preparation of samples for Co and Cu AAS analysis.

6.3.1.5 Thermal Decomposition Product of Differential Flotation Dilution

Given the cobalt and copper concentration in the thermal decomposition product of bulk Flotation material is 1.456 wt%, or 14560 ppm, and 9850 ppm respectively, a 1456X dilution of sample containing 14560 ppm Co would report as having 10 ppm Co, with the range set by the calibration standards. Approximately a 1456X dilution with 2% nitric acid was used for the preparation of samples for Co and Cu AAS analysis

6.4 Magnetic Separation AAS Data

Shown below in Table 6.7 through Table 6.11 is the AAS data for the magnetic separation tests detailed in Table 6.2 through Table 6.6.

From the data in Table 6.7, Table 6.8, and Table 6.9, it can be seen that limited cobalt or copper reports to the magnetic fraction. This is to be expected, as the cobalt and copper bearing material do not normally exhibit magnetic properties. Limited iron also reported to the magnetic fraction. This is because much of the iron in the deposit is in the pyrite, which is non-magnetic, as seen Table 6.1. This is also supported by the fact that the cobalt is primarily in pyrite, so a large portion of the iron should report to the same fraction as the cobalt. The cobalt and copper recovery in the deposit sample materials were generally unaffected by changes in the magnetic field strength. Iron recovery did increase with increasing magnetic field strength, most likely due to the presence of iron oxides. This may also be why some cobalt and copper does report to the magnetic fraction, as cobalt was associated with iron oxides in some samples.

Table 6.7: AAS data for deposit sample IC 18-07 magnetic separation tests.

Trial		Element Concentration			Element Recovery (%)		
		Co (ppm)	Fe (wt %)	Cu (ppm)	Co	Cu	Fe
1	Magnetic	5764	19.72	1338	7.99	2.85	7.91
	Non-Magnetic	3104	10.74	2131	92.01	97.15	92.09
2	Magnetic	3510	18.47	1631	6.26	4.11	9.84
	Non-Magnetic	2906	9.36	2107	93.74	95.89	90.16
3	Magnetic	3219	17.43	1586	9.44	6.80	13.70
	Non-Magnetic	2666	9.48	1876	90.56	93.20	86.30
4	Magnetic	2607	16.98	1542	7.81	7.04	16.57
	Non-Magnetic	3663	10.19	2423	92.19	92.96	83.43
5	Magnetic	2547	20.04	1488	9.93	8.60	20.41
	Non-Magnetic	3211	10.86	2197	90.07	91.40	79.59
6	Magnetic	2360	14.89	1558	10.94	10.91	21.56
	Non-Magnetic	3293	9.28	2180	89.06	89.09	78.44
7	Magnetic	2220	13.54	1530	12.48	12.58	24.21
	Non-Magnetic	3365	9.16	2297	87.52	87.42	75.79
8	Magnetic	2067	16.85	1611	11.60	12.95	27.89
	Non-Magnetic	3325	9.2	2285	88.40	87.05	72.11

Table 6.8: AAS data for deposit sample IC 18-09 magnetic separation tests.

Trial		Element Concentration			Element Recovery (%)		
		Co (ppm)	Fe (wt %)	Cu (ppm)	Co	Cu	Fe
1	Magnetic	6248	22.18	1664	7.77	3.29	6.93
	Non-Magnetic	2290	9.21	1513	92.23	96.71	93.07
2	Magnetic	4077	24.09	1171	9.98	4.81	14.87
	Non-Magnetic	2446	9.17	1541	90.02	95.19	85.13
3	Magnetic	3168	19.17	1060	11.06	6.37	17.58
	Non-Magnetic	2462	8.69	1506	88.94	93.63	82.42
4	Magnetic	3260	14.10	1149	13.05	6.91	16.14
	Non-Magnetic	2393	8.07	1704	86.95	93.09	83.86
5	Magnetic	2732	20.24	1095	13.87	8.77	26.17
	Non-Magnetic	2404	8.10	1615	86.13	91.23	73.83
6	Magnetic	2457	15.27	1092	14.35	10.05	27.32
	Non-Magnetic	2430	6.74	1621	85.65	89.95	72.68
7	Magnetic	2701	18.09	1144	14.79	11.50	14.54
	Non-Magnetic	2725	18.62	1542	85.21	88.50	85.46
8	Magnetic	2476	17.57	1260	14.82	12.76	31.05
	Non-Magnetic	2559	7.01	1549	85.18	87.24	68.95

Table 6.9: AAS data for deposit sample IC 18-27 magnetic separation tests.

Trial		Element Concentration			Element Recovery (%)		
		Co (ppm)	Fe (wt %)	Cu (ppm)	Co	Cu	Fe
1	Magnetic	5373	23.05	9815	3.74	1.60	4.65
	Non-Magnetic	3663	12.51	15953	96.26	98.40	95.35
2	Magnetic	4617	17.67	9406	4.40	2.17	4.72
	Non-Magnetic	3436	12.20	14545	95.60	97.83	95.28
3	Magnetic	3316	13.47	8507	6.24	3.82	7.96
	Non-Magnetic	3956	12.38	17003	93.76	96.18	92.04
4	Magnetic	2585	15.91	8462	7.75	5.85	13.51
	Non-Magnetic	3423	11.33	15148	92.25	94.15	86.49
5	Magnetic	2971	16.94	10467	7.84	6.65	13.55
	Non-Magnetic	4106	12.70	17270	92.16	93.35	86.45
6	Magnetic	2299	16.99	8848	8.51	7.75	18.30
	Non-Magnetic	3660	11.23	15598	91.49	92.25	81.70
7	Magnetic	2522	16.38	10689	11.87	11.44	22.93
	Non-Magnetic	3750	11.03	16564	88.13	88.56	77.07
8	Magnetic	2291	18.21	10625	10.51	11.15	24.14
	Non-Magnetic	3808	11.18	16540	89.49	88.85	75.86

Bulk flotation and differential flotation testing, results of which are shown in Tables 6.10 and 6.11, resulted in a more even split in the cobalt and copper recoveries between the magnetic and non-magnetic fractions. At lower magnetic field intensities most of the cobalt and copper reports to the non-magnetic fraction, but at higher intensities it becomes closer to a 50/50 split to each fraction. This could be caused by the reduction in the amount of gangue material, as most of it is removed in flotation. The material tested therefore has a higher concentration of materials that might report to the magnetic fraction.

Table 6.10: AAS data for bulk flotation concentrate magnetic separation tests.

Trial		Element Concentration			Element Recovery (%)		
		Co (wt %)	Cu (wt %)	Fe (wt %)	Co	Cu	Fe
1	Magnetic	1.348	1.073	20.58	19.75	21.80	48.94
	Non-Magnetic	1.380	0.970	21.48	80.25	78.20	51.06
2	Magnetic	1.273	1.284	22.98	27.28	39.20	46.73
	Non-Magnetic	1.468	0.862	26.27	72.72	60.80	51.52
3	Magnetic	1.220	1.326	22.17	41.80	62.93	48.48
	Non-Magnetic	1.477	0.679	23.45	58.20	37.07	51.52
4	Magnetic	1.300	1.167	22.15	49.96	63.93	49.05
	Non-Magnetic	1.444	0.731	23.01	50.04	36.07	50.95

Table 6.11: AAS data for differential flotation concentrate tests.

Trial		Element Concentration (wt%)		Element Recovery (%)	
		Co	Cu	Co	Cu
1	Magnetic	1.48	0.24	48.82	59.61
	Non-Magnetic	1.78	0.19	51.18	40.39
2	Magnetic	1.45	0.25	66.27	74.81
	Non-Magnetic	1.71	0.19	33.73	25.19

Tables 6.12 and 6.13 contain the data for the thermal decomposition tests and show that much of the cobalt reported to the magnetic fraction. This is because during thermal decomposition, the pyrite decomposes into pyrrhotite. One of the three forms of pyrrhotite is magnetic and if the cobalt stays within the pyrrhotite, it will also report to the magnetic fraction. Copper recovery is reduced compared to the cobalt recovery, which is a departure from most of the other experiments done in this report. This could be due to fewer copper bearing minerals being affected during thermal decomposition, which primarily affected sulfide-based minerals. Most of the copper was also removed during flotation in the differential flotation samples, resulting in a much lower copper grade overall. The magnetic field intensity did have an effect on the grade and recovery of cobalt in both the differential flotation and the bulk flotation concentrate tests. Increasing the magnetic field from 0.5 Tesla to 1.0 Tesla resulted in a grade increase of 20.8% in the bulk flotation test magnetic fraction and a grade increase of 47.3% in the differential

floatation test magnetic fraction. The recovery increase was 9.25% in the bulk floatation concentrate and 30.6% in the differential floatation concentrate.

Table 6.12: AAS data for thermal decomposition product of bulk floatation test.

Trial		Element Concentration (wt %)		Element Recovery (%)	
		Co	Cu	Co	Cu
1	Magnetic	2.28	1.27	86.14	63.79
	Non-Magnetic	0.50	0.98	13.86	36.21
2	Magnetic	1.89	1.09	78.84	64.50
	Non-Magnetic	0.91	0.82	21.16	35.50

Table 6.13: AAS data for thermal decomposition of differential floatation tests.

Trial		Element Concentration (wt%)		Element Recovery (%)	
		Co	Cu	Co	Cu
1	Magnetic	3.038	0.316	90.50	76.18
	Non-Magnetic	0.864	0.268	9.50	23.82
2	Magnetic	2.063	0.285	69.32	62.65
	Non-Magnetic	1.228	0.228	30.68	37.35

6.5 Magnetic Separation Washability Curves

Washability curves show how changes in a particular testing variable can affect mineral separation. They are used to determine the ideal conditions for removing a particular mineral or element or causing a separation. While typically used for heavy medium separation and the density of heavy liquid, they can be used with other testing methods and mineral properties. Washability curves were created in all physical beneficiation testing methods to determine the testing conditions that result in the greatest cobalt recovery and grade. Shown below in Figures 6.2 and 6.3 are the washability curves of the cobalt and copper response in the magnetic fraction from the run-of-mine samples.

The mass reported to the magnetic fraction at a consistent rate till the magnetic field intensity reached 0.7 Tesla, where the rate decreased slightly until the maximum field intensity tested was reached. With small amounts of magnetic materials in the deposit based on literature small amounts of material reporting to the magnetic fraction, especially at lower magnetic field intensities, was expected. The cobalt response was minimal at the lower magnetic field intensities, with the lowest magnetic field intensity tested only pulling 7 wt% of the cobalt. The rate of the cumulative cobalt reporting to the magnetic was

consistently increasing with increasing magnetic field intensity until a field intensity of 0.7 Tesla was reached, where then the rate decreased slightly. Approximately 20 wt% of the cobalt reporting to the magnetic fraction at the maximum field intensity tested. Copper exhibited a similar response as the cobalt, with 25 wt% of the copper reporting to the magnetic fraction at the highest magnetic field intensity.

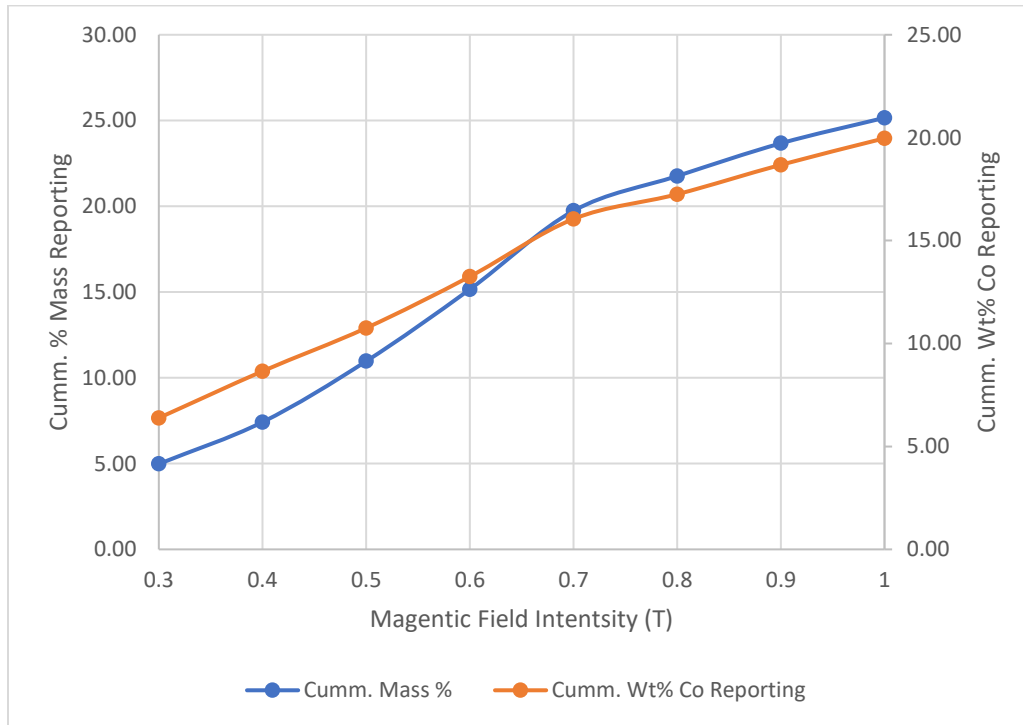


Figure 6.2: WHIMS washability curve of the cobalt response of the magnetic fraction of the deposit sample.

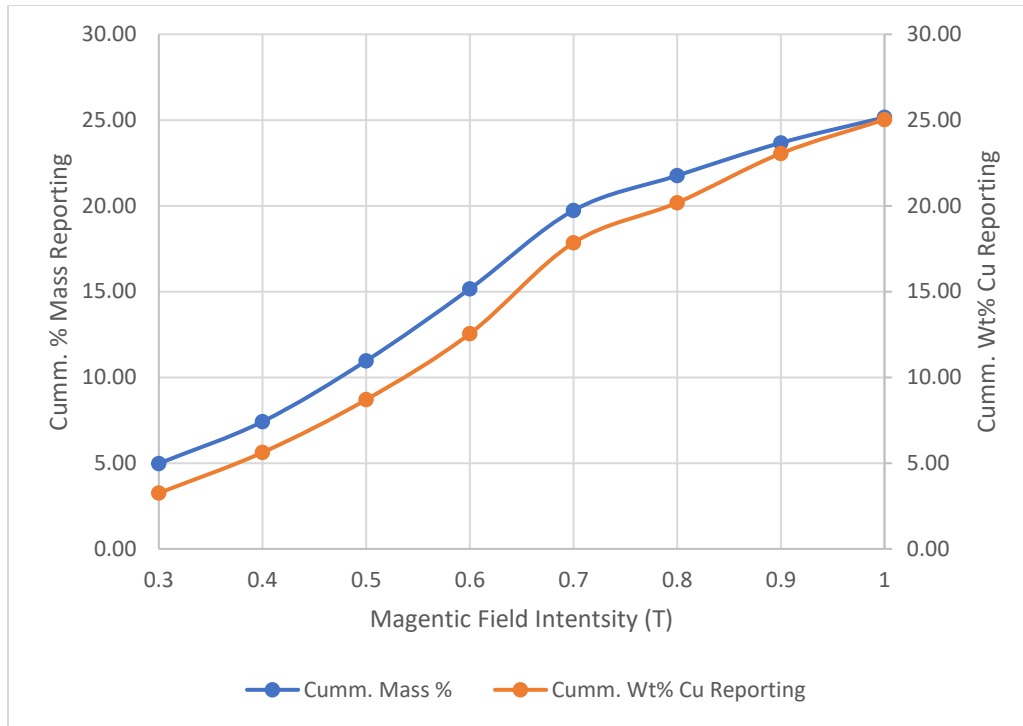


Figure 6.3: WHIMS washability curve of the copper response of the magnetic fraction of the deposit sample.

6.6 Mineralogy of Thermal Decomposition Products

Mineralogy was done on the products of the thermal decomposition of bulk flotation concentrate WHIMS testing. Figures 4.4 and 4.5 below show false color AMICS backscatter images of the magnetic and non-magnetic fraction respectively. The primary cobalt-bearing materials, pyrrhotite and troilite, are indicated blue and purple while quartz and orthoclase, the primary gangue materials are yellow and pink. The majority of the cobalt bearing materials reported to the magnetic fraction. Though only pyrrhotite responds to a magnetic field, since the particles are a mix of pyrrhotite and troilite due to the thermal decomposition not going to completion, the non-magnetic troilite is pulled to the magnetic fraction if there is enough pyrrhotite in the mixed particle. The gangue minerals primarily reported to the non-magnetic fraction. Table 6.14 lists the minerals present by quantity.

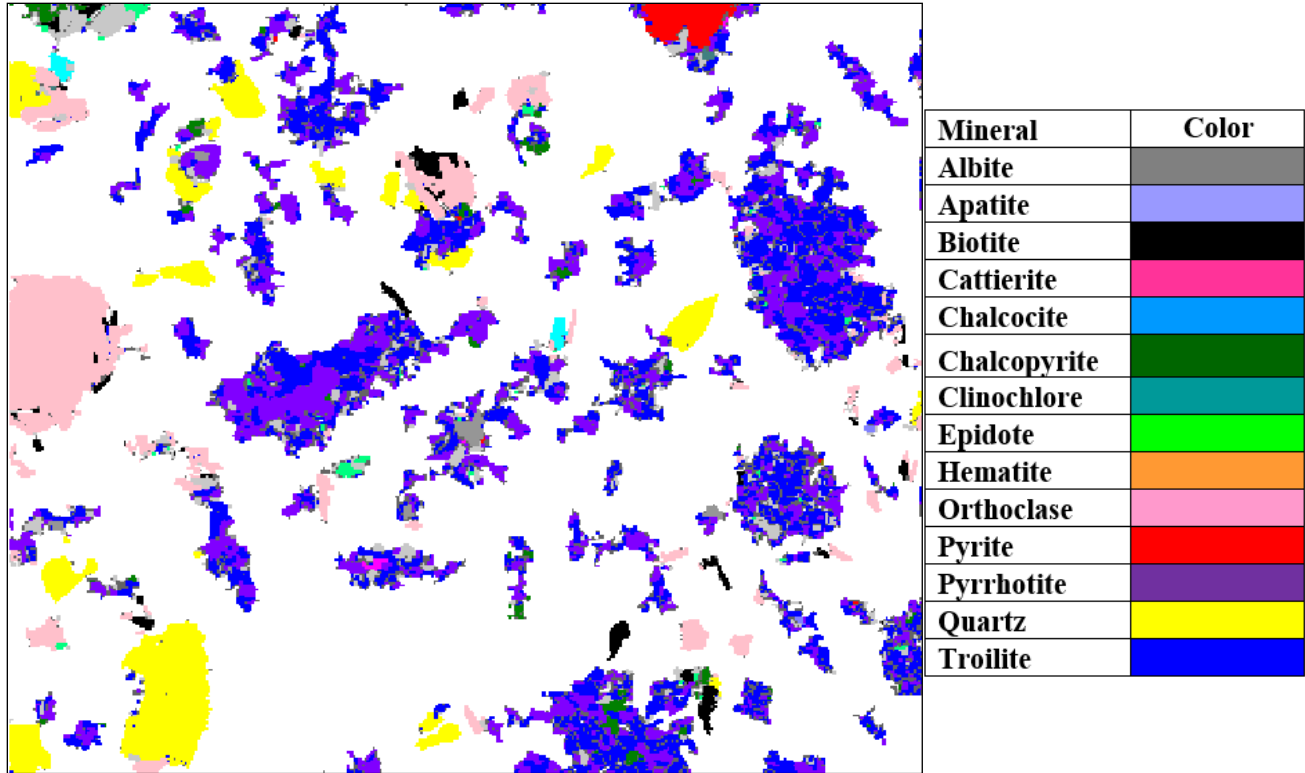


Figure 6.4: Identified image of thermal decomposition product of bulk flotation concentrate magnetic fraction.

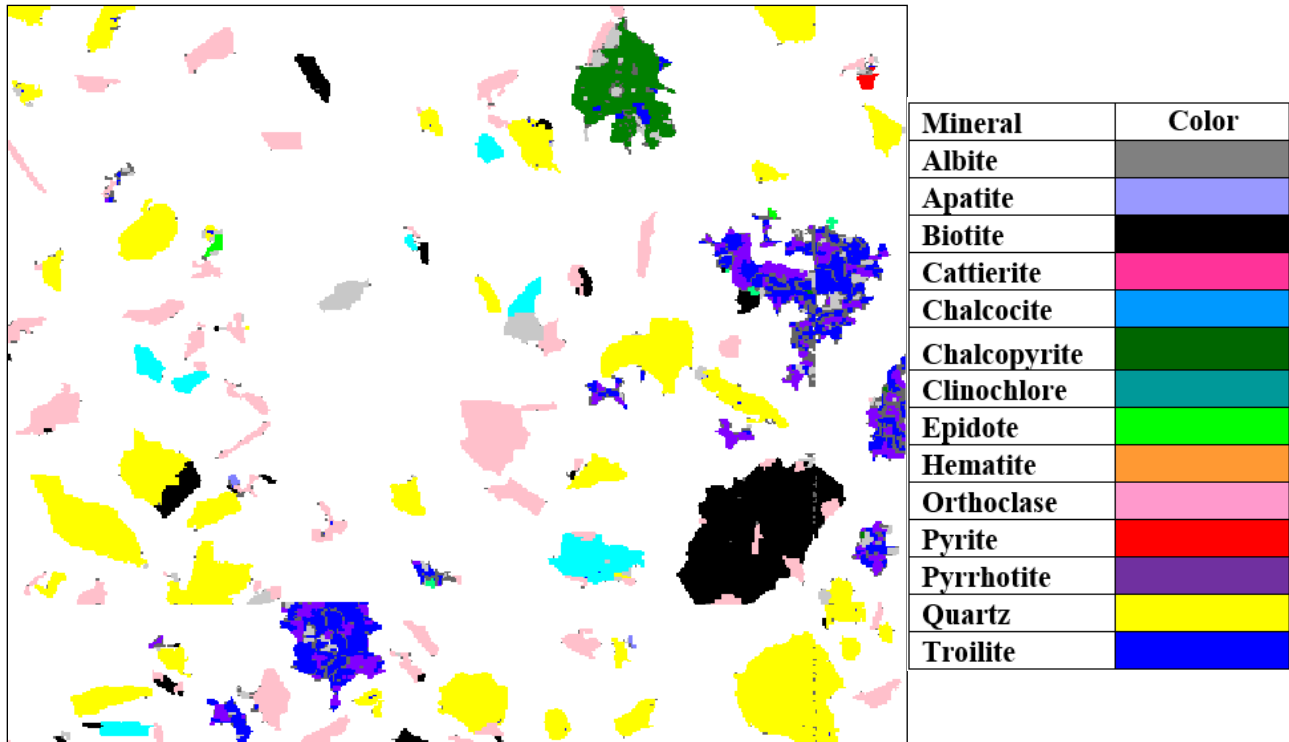


Figure 6.5: Identified image of thermal decomposition product of bulk flotation concentrate non-magnetic fraction.

Table 6.14: Minerals present in magnetic separation thermal decomposition products by quantity.

Mineral	Chemistry	Magnetic Conc.	Magnetic Tails
Albite	NaAlSi ₃ O ₈	0.79	4.38
Apatite	Ca ₅ (PO ₄) ₃ OH	0.02	0.24
Biotite	K(Mg,Fe) ₃ AlSi ₃ O ₁₀ (OH)	3.50	7.57
Cattierite	CoS	0.38	0.06
Chalcocite	Cu ₂ S	0.01	0.07
Chalcopyrite	CuFeS ₂	3.83	6.61
Clinocllore	(Mg,Fe) ₃ AlSi ₄ O ₁₀ (OH) ₆	0.15	0.15
Epidote	Ca ₂ Al ₂ FeSi ₃ O ₁₁ (OH)	0.09	0.20
Hematite	Fe ₂ O ₃	0.02	0.00
Orthoclase	KAlSi ₃ O ₈	7.07	21.04
Pyrite	FeS ₂	4.50	1.02
Pyrrhotite	Fe _(1-x) S _x	33.56	8.76
Quartz	SiO ₂	8.94	38.89
Troilite	FeS	37.14	10.99

6.7 Magnetic Separation Statistical Analysis

Two sets of statistical analyses were performed on the magnetic separation testing data. The first test was on the deposit sample tests to determine if the changes in cobalt and copper grade and recovery over the magnetic field strengths tested were statistically significant. The second analysis was done by comparing the flotation data and the thermal decomposition data of the differential flotation to see if the difference observed in the two tests over the tested magnetic field ranges were statistically significant.

6.7.1 Statistical Analysis on Feed Materials Testing

Statistical analysis testing was done using Excel with a single-factor ANOVA with a confidence interval of 95% to analyze the effect of the magnetic field strength on the target elements grades and recovery. Single-factor ANOVA testing is done on experiments where there are multiple groups with a single independent variable to determine if there is statistical evidence that the means of the groups are significantly different.

As all three samples had similar results, only the data for sample IC 18-07 is shown in this section; the ANOVA tables for samples IC 18-09 and IC 18-27 can be found in Appendix D.

Shown below in Table 6.15 is the ANOVA table for copper grade. As the calculated p-value of 5.19×10^{-6} is far less than 0.05, it can be determined that changing the magnetic field had a statistically

significant effect on the changes in cobalt grade over the course of the testing. The same is also true for the copper recovery for all samples, with the p-value for IC 18-07 being 1.25×10^{-7} , as seen in Table 6.16.

Table 6.15: Magnetic separation feed material cobalt grade ANOVA for sample IC 18-07.

Source	Sum of Squares	df	MS	F	P-value	
Between Groups	36871585	1	36871585	50.66628	5.19E-06	significant
Within Groups	10188280	14	727734.3			
Total	47059865	15				

Table 6.16: Magnetic separation feed material cobalt recovery ANOVA for sample IC 18-07.

Source	Sum of Squares	df	MS	F	P-value	
Between Groups	288.5930548	1	288.5931	121.2172	1.25E-07	significant
Within Groups	28.56951716	12	2.380793			
Total	317.162572	13				

Shown below in Table 6.17 is the ANOVA table for copper grade. As the calculated p-value of 7.84×10^{-17} is far less than 0.05, it can be determined that changing the magnetic field had a statistically significant effect on the changes in cobalt grade over the course of the testing. The same is also true for the copper recovery for all samples, with the p-value for IC 18-07 being 3.15×10^{-17} , as seen in Table 6.18.

Table 6.17: Magnetic separation feed material copper grade ANOVA for sample IC 18-07.

Source	Sum of Squares	df	MS	F	P-value	
Between Groups	9420704.58	1	9420704.58	2225.304	7.84E-17	significant
Within Groups	59268.24454	14	4233.446039			
Total	9479972.825	15				

Table 6.18: Magnetic separation feed material copper recovery ANOVA for sample IC 18-07.

Source	Sum of Squares	df	MS	F	P-value	
Between Groups	28539.14904	1	28539.14904	5256.868	3.15E-17	significant
Within Groups	65.1471115	12	5.428925959			

Total	28604.29615	13
--------------	-------------	----

6.7.2 Statistical Analysis on Flotation and Thermal Decomposition Materials Testing

A statistical analysis was also performed on the flotation material and thermal decomposition results in an attempt to compare the recoveries and to see if the difference was statistically significant. However, due to a lack of material for testing, especially considering the thermal decomposition material, not enough tests were able to be run for any analysis to reach the necessary confidence interval. Therefore, all conclusions made in this section should not be taken as a final answer.

To determine the effect of the magnetic separation on the recovery of each element, a statistical analysis was done using Stat Ease software. This analysis aimed to determine which variables have a statistically significant effect with the confidence interval of 95%. Variables that are determined to not be statistically significant don't necessarily have no effect on recovery, it is just possible that the effect is not large enough to be confirmed with experimental error and noise.

Analysis involves using a half normal plot and a Pareto chart. A half plot shows the probability of a factor's effect being statistically significant relative to the error to determine which factors may be statistically significant. The Pareto chart is then used to confirm the results of the half normal plot. If the t-value in the Pareto chart is above the Bonferroni limit, it is statistically significant. If the t-value is above the t-value limit but below the Bonferroni limit, there is a possibility that it is statistically significant. If it is below the t-value limit, it is not statistically significant. The Bonferroni limit and t-value are determined using Equations 6.1 and 6.2, respectively,

$$P(\cap_{i=1}^g A_i) \geq 1 - \sum_{i=1}^g P[\bar{A}_i] \quad (6.2)$$

Where A_i is the event of interest and \bar{A}_i is the alternate event of interest.

$$t = \frac{\bar{x} - \mu_o}{\frac{s}{\sqrt{n}}} \quad (6.3)$$

Where \bar{x} is the sample mean, μ_o is the population mean, s is the standard deviation, and n is the sample size.

Shown below in Figure 6.6 and Figure 6.7 are the half normal plots showing the standardized effect of each leaching variable and possible interaction for cobalt grade and cobalt recovery. It can be seen that no variables can be considered statistically significant. This is confirmed by the Pareto charts shown in Figure 6.8 and 6.9.

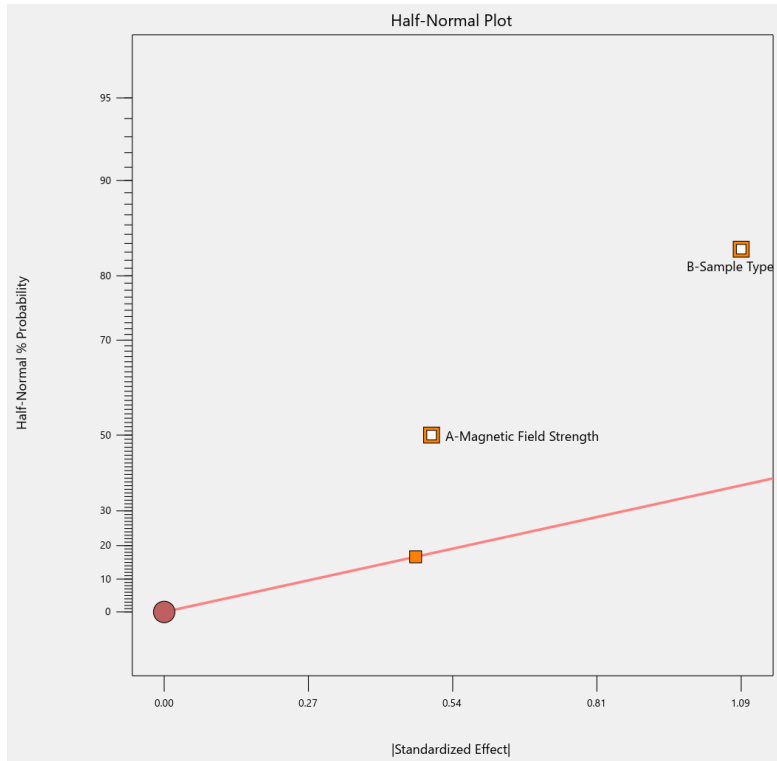


Figure 6.6: Half-normal plot for magnetic separation cobalt grade effects.

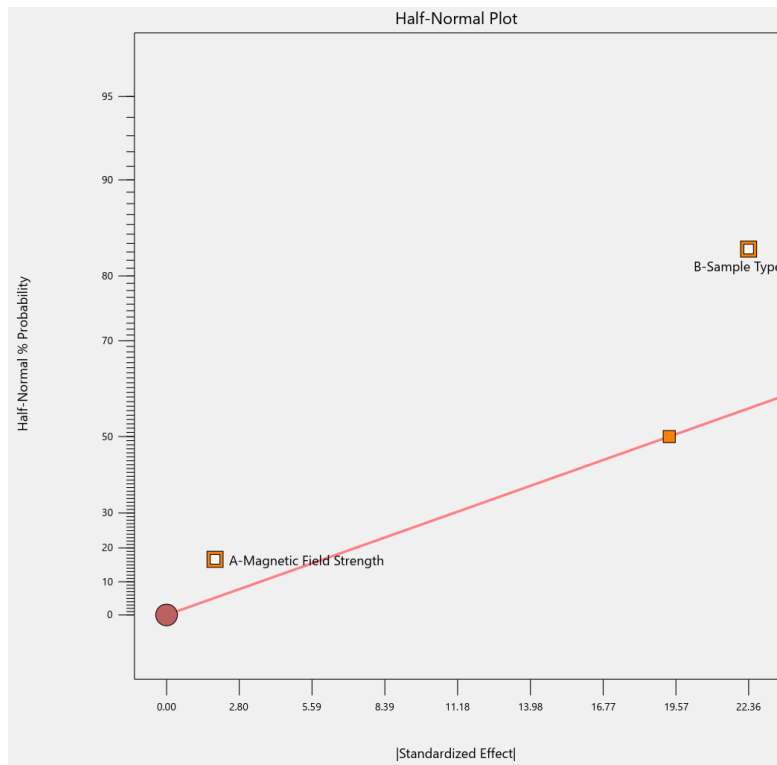


Figure 6.7: Half-normal plot for magnetic separation cobalt recovery effects.

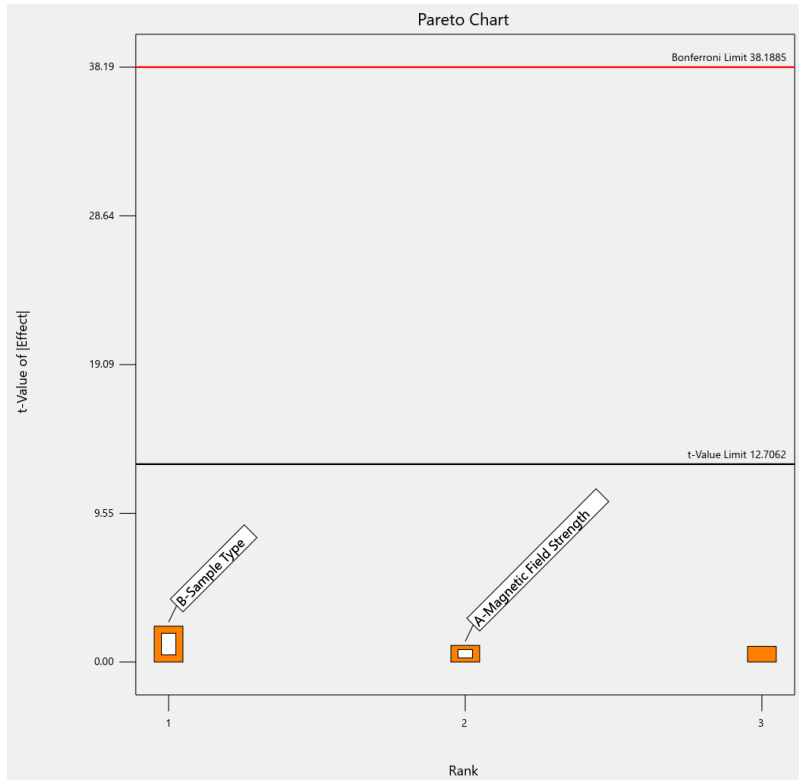


Figure 6.8: Magnetic Separation cobalt grade Pareto chart.

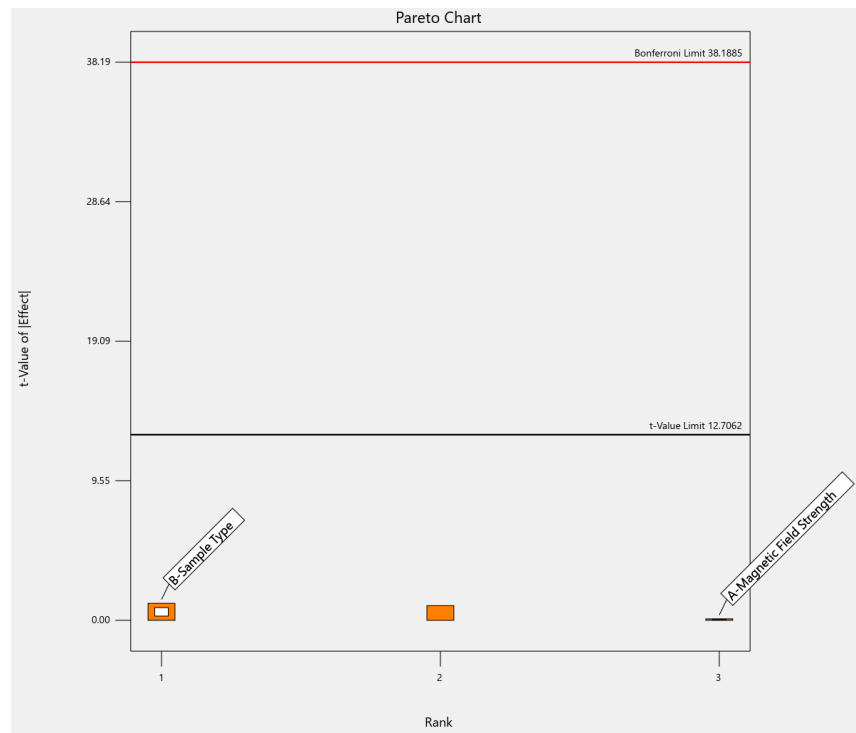


Figure 6.9: Magnetic Separation cobalt recovery Pareto chart.

Shown in Table 6.19 and Table 6.20 are the ANOVA for cobalt grade and recovery using sample material and magnetic field intensity as variables. According to the ANOVA, there are no variables that are statistically significant. The likelihood of the models being incorrect due to noise are 36.77% and 65.23% respectively. The calculated R^2 are 0.8648 and 0.5744.

Table 6.19: Magnetic separation flotation material cobalt grade ANOVA.

Source	Sum of Squares	df	Mean Square	F-value	p-value	
Model	1.433995	2	0.716997	3.197993	0.367707	not significant
A-Magnetic Field Strength	0.253512	1	0.253512	1.13073	0.480458	
B-Sample Type	1.180482	1	1.180482	5.265256	0.261641	
Residual	0.224202	1	0.224202			
Cor Total	1.658197	3				

Table 6.20: Magnetic separation flotation material cobalt recovery ANOVA.

Source	Sum of Squares	df	Mean Square	F-value	p-value	
Model	503.6715	2	251.8357	0.675038	0.652318	not significant
A-Magnetic Field Strength	3.478225	1	3.478225	0.009323	0.93872	
B-Sample Type	500.1932	1	500.1932	1.340752	0.453497	
Residual	373.0692	1	373.0692			
Cor Total	876.7407	3				

Shown below in Figure 6.10 and Figure 6.11 are the half normal plots showing the standardized effect of each leaching variable and possible interaction for copper grade and recovery. It can be seen that the sample type may be considered statistically significant in copper grade. No variables can be considered statistically significant for copper recovery. This is confirmed by the Pareto charts shown in Figure 6.12 and 6.13.

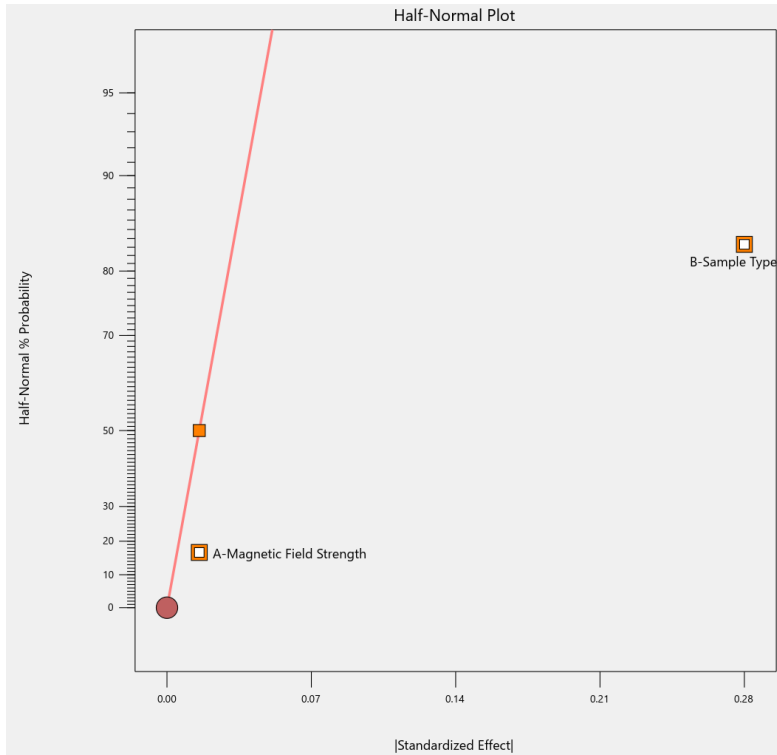


Figure 6.10: Half-normal plot for magnetic separation copper grade effects.

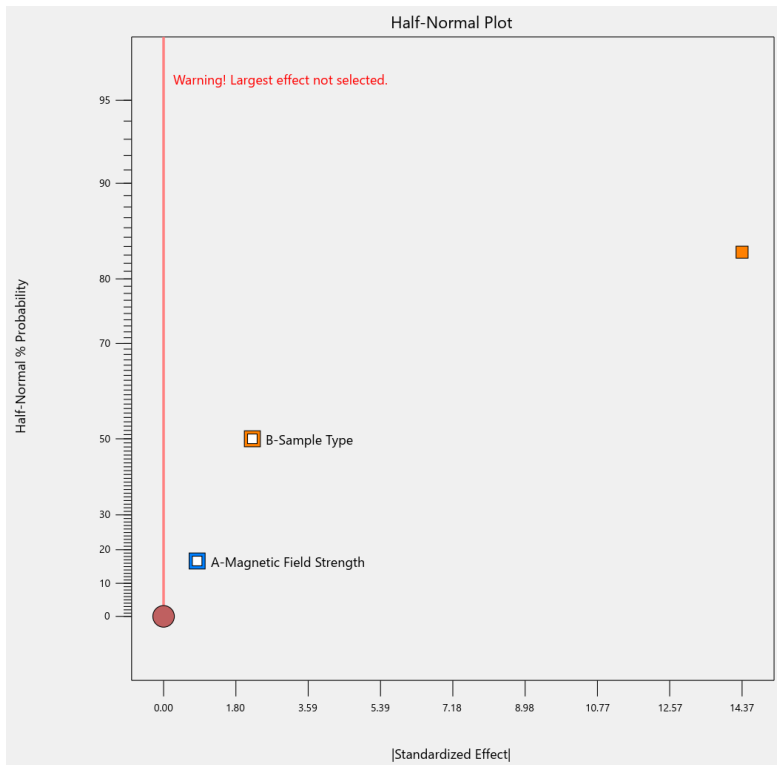


Figure 6.11: Half-normal plot for magnetic separation copper recovery effects.

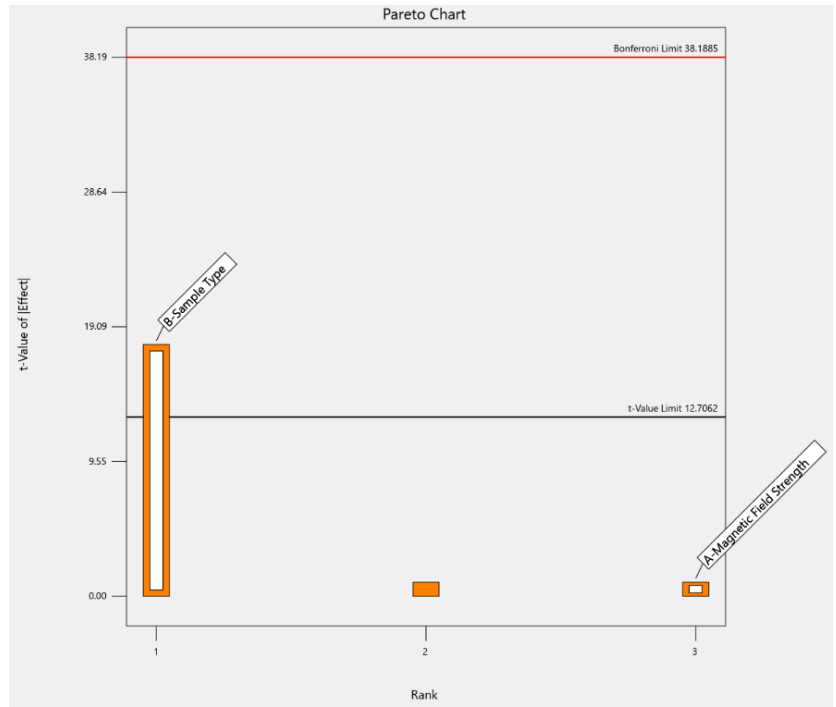


Figure 6.12: Magnetic Separation copper grade Pareto chart.

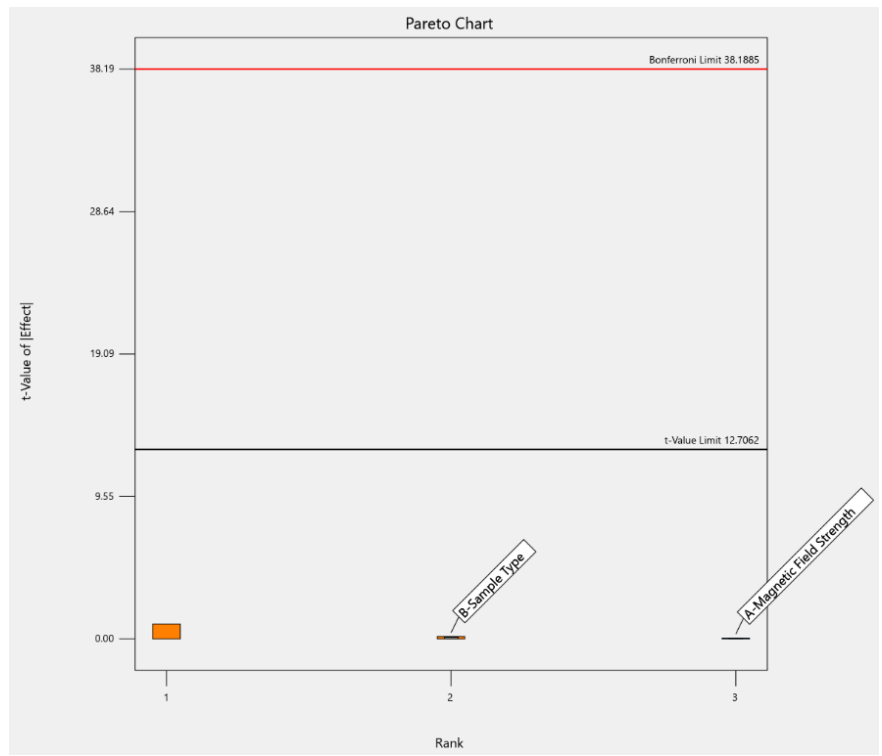


Figure 6.13: Magnetic Separation copper recovery Pareto chart.

Shown in Table 6.21 and Table 6.22 are the ANOVA for cobalt grade and recovery using sample material and magnetic field intensity as variables. According to the ANOVA, the sample type is a variable that is statistically significant in copper grade and there are none in copper recovery. The likelihood of the models being incorrect due to noise are 5.59% and 98.68% respectively. The calculated R^2 are 0.9969 and 0.0262.

Table 6.21: Magnetic separation flotation material copper grade ANOVA.

Source	Sum of Squares	df	Mean Square	F-value	p-value	
Model	0.076693	2	0.038346	159.6098	0.055883	not significant
A-Magnetic Field Strength	0.00024	1	0.00024	1	0.5	
B-Sample Type	0.076452	1	0.076452	318.2196	0.03565	
Residual	0.00024	1	0.00024			
Cor Total	0.076933	3				

Table 6.22: Magnetic separation flotation material copper recovery ANOVA.

Source	Sum of Squares	df	Mean Square	F-value	p-value	
Model	5.55925	2	2.779625	0.01347	0.986796	not significant
A-Magnetic Field Strength	0.697225	1	0.697225	0.003379	0.963037	
B-Sample Type	4.862025	1	4.862025	0.023562	0.903037	
Residual	206.3532	1	206.3532			
Cor Total	211.9125	3				

6.8 Magnetic Separation Discussion

Overall, magnetic separation of samples that have not been chemically altered is ineffective. Magnetic field intensity had little effect on the recoveries and grades, with only a marginal increase in both as the field intensity increased. This increase is mostly caused by the increasing magnetic field strength pulling more paramagnetic materials to the magnetic fraction and small amount of cobalt bearing minerals being contained in these paramagnetic particles. This was the expected response, as according to literature, none of the target minerals should response to a magnetic field.

This is supported by the washability curves created for both the deposit sample and bulk flotation concentrate. The recovery of cobalt was minimal at the lowest magnetic field intensities and only

increased slightly as the magnetic field strength was increased. This increase is again showing that particles that contain mostly paramagnetic minerals contain small amounts of cobalt-bearing minerals, causing the cobalt recovery to increase as they are pulled to the magnetic fraction.

Magnetic separation on the thermal decomposition products, however, was highly effective. The formation of pyrrhotite during thermal decomposition created a magnetic product that could be used to concentrate the cobalt in the magnetic fraction. Mineralogy reports also confirmed the presence of pyrrhotite and showed that the majority of it was well liberated and reported to the magnetic fraction, with the magnetic fraction of the thermal decomposition product being approximately 75% pyrite, pyrrhotite, or troilite. Magnetic field intensity had an effect on the grade and recovery in the thermal decomposition products, with increasing field strength from 0.5 T to 1.0 T increasing the grade and the recovery by 47%.

CHAPTER 7. GRAVITY SEPARATION

7.1 Testing Conditions

The heavy liquid used in all gravity separation tests is sodium polytungstate (SPT), due to it being far less toxic than traditional heavy liquids. Based on the range of the expected specific gravities of the target and gangue material shown in Table 7.1 and the literature available on the functional range of SPT, the specific gravity of the SPT will be approximately 2.8 to 2.9. Shown in Table 7.2 below are the various testing conditions for heavy liquid separation trial with deposit sample IC 18-07. Testing done with all other feed materials were done at 2500 RPM for 90 minutes, with a particle size of 75 microns.

Table 7.1: Specific gravities of target and gangue materials.

Mineral	Specific Gravity
Biotite	2.8
Chalcopyrite	4.19
Chlorite	2.95
Feldspar	2.56
Galena	7.4
Iron Oxides	5.24
Jaipurite	5.45
Kaolinite	2.65
Molybdenite	5.5
Muscovite	2.7
Pyrite	5
Pyrrhotite	4.61
Quartz	2.65

Washability curves were also created for the deposit sample and bulk flotation concentrate. Based on the expected specific gravities of the main minerals in the deposit stated in Table 7.1 above and the range of achievable specific gravities of sodium polytungstate, the tested range of specific gravities will be 2.4 to 3 with 0.5 sg steps. The running time and centrifuge speed for each trial will be constant, at 90 minutes and 2500 revolution per minute (RPM) respectively. To have enough material to run the final tests, the initial tests will be run in duplicate.

Table 7.2: Test conditions for heavy liquid separation trials using deposit sample IC 18-07.

Trial	RPM	Time (minutes)	Particle Size (Microns)
1	2500	15	2000
2	2500	30	250
3	2500	75	75
4	2000	90	75
5	2200	90	75
6	2500	90	75
7	2700	90	75

7.2 Gravity Separation Testing Procedures

Testing procedures for the gravity separation tests are shown below. The procedure for the washability curves is also given below.

7.2.1 Deposit Sample Testing Procedure

The testing procedure for each of the trials in Table 7.2 are as follows:

Prepare the sodium polytungstate (SPT) to the desired specific gravity using DI water.

Six 15 mL vials were filled with approximately 10 mL of SPT and 5 grams of sample with a p80 of 75 microns. The vials were placed into a centrifuge and run for the pre-determined time. The vials were then removed, and the light and heavy fraction were separated.

Samples were separated from the SPT using vacuum filtration. DI was used to wash off any SPT that was still on the samples. Samples were dried in a 100 °C furnace for 16 hours.

7.2.2 Bulk Flotation Testing Procedure

Testing of the bulk flotation sample followed the same procedure as outlined in section 7.2.1, but the material had a p80 of 75 microns due to the previous flotation testing.

7.2.3 Deposit Sample Washability Curve Testing Procedure

The testing procedure to create the washability curve is as follows:

Prepare 12 15mL vials with approximately 10 mL of sodium polytungstate (SPT) with a specific gravity (SG) of 2.4 and 5 grams of sample with a p80 of 75 microns. Remove the vials from the centrifuge and place the remaining 6 vials in, running them for the same time and rpm.

When all vials have completed running, remove the material at the top of vials, the light fraction, and at the bottom, the heavy fraction, into separate beakers. Add DI to each beaker and mix with a stir rod to decrease the SG of the SPT. Using 44 Wattman filter paper, vacuum filtration was used to separate the SPT from each sample. Wash the sample with DI water to ensure all SPT is removed. Place both filtered samples in a furnace for 16 hours at 100 C to dry them.

7.2.4 Bulk Flotation Washability Curve Testing Procedure

Testing to create the washability curve using the bulk flotation concentrate followed the same procedure as outlines in section 5.2.5.

7.3 Preparation of Gravity Separation Sample for Analysis

All products from gravity separation testing were analyzed using atomic absorption spectroscopy (AAS). The methods used to prepare the samples for analysis are described.

7.3.1 Deposit Sample Dilution

Given the cobalt and copper concentration in the deposit sample material is 2500 ppm and 1740 ppm respectively, A 250X dilution of sample containing 2500 ppm Co would report as having 10 ppm Co, with the range set by the calibration standards. The Fe concentration in the deposit material is 10.9 wt %, or 109000 ppm. a 1100X dilution of sample containing 109000 ppm Fe would report as having 99 ppm Fe, with the range set by the calibration standards. A 250X dilution with 2% nitric acid was used for the preparation of samples for Co and Cu AAS analysis and a 1100X dilution with 2% nitric acid was used for the preparation of samples for Fe analysis.

7.3.2 Bulk Flotation Concentrate Dilution

Given the cobalt and copper concentration in the bulk flotation concentrate material is 11210 ppm and 9150 ppm respectively, a 1121X dilution of sample containing 11210 ppm Co would report as having 10 ppm Co, with the range set by the calibration standards. The Fe concentration in the bulk flotation material is 23.4 wt %, or 234000 ppm. A 2340X dilution of sample containing 234000 ppm Fe would report as having 99 ppm Fe, with the range set by the calibration standards. A 1250X dilution with 2% nitric acid was used for the preparation of samples for Co and Cu AAS analysis and a 2500X dilution with 2% nitric acid was used for the preparation of samples for Fe analysis.

7.4 Gravity Separation AAS Data

Shown below in Table 7.3 and Table 7.4 are the AAS data for the gravity separation tests outlined in Table 7.2.

As shown by the results of the particle size testing in Table 7.3, recovery increased as particle size decreased. This is due to the target minerals being more liberated, and it being less likely that the composition of the particles causing minerals to report to the incorrect fraction. The copper and cobalt grade in the sink fraction remained generally unchanged throughout all testing. This could be caused by the large difference in specific gravities between the target materials and the gangue materials, making it difficult for them to report to the incorrect fraction unless a particle has poor liberation. Recovery in the sink fraction was lower in the 2000-micron test compared to the other two. This could be due to insufficient liberation of the cobalt and copper bearing materials at the larger particle size to the other tests or particles becoming surrounded by ones of the opposite fraction and getting trapped, resulting in minerals reporting to the incorrect fraction.

Table 7.3: AAS data for gravity separation particle size testing.

Particle Size (micron)	Mass % Reporting	Element Concentration			Element Recovery (%)			
		Co (ppm)	Cu (ppm)	Fe (Wt %)	Co	Cu	Fe	
2000	Float	63.27%	649	540	5.92	13.75	18.00	34.39
	Sink	36.73%	7015	4239	19.45	86.25	82.00	65.61
250	Float	65.78%	145	153	2.39	3.79	5.09	18.05
	Sink	34.22%	7050	5491	20.85	96.21	94.91	81.95
75	Float	46.10%	115	134	2.11	1.63	2.89	9.00
	Sink	53.90%	5917	3863	18.23	98.37	97.11	91.00

In the RPM testing, Table 7.4, there were minimal trends for either grade or recovery. All tests resulted in sufficient force to push the sink fraction to the bottom of the vial in the tested running time.

Table 7.4: AAS data for gravity separation RPM testing.

RPM	Mass % Reporting	Element Concentration			Element Recovery (%)			
		Co (ppm)	Cu (ppm)	Fe (Wt %)	Co	Cu	Fe	
2200	Float	60.54%	304	291	0.06	6.81	9.37	21.75
	Sink	39.46%	6393	4323	17.88	93.19	90.63	78.25
2500	Float	46.10%	115	134	0.03	1.63	2.89	9.00
	Sink	53.90%	5917	3863	18.23	98.37	97.11	91.00
2700	Float	57.83%	255	236	0.04	5.61	7.42	19.51
	Sink	42.17%	5878	4038	16.71	94.39	92.58	80.49

7.5 Heavy Liquid Separation Washability Curves

Shown below in Figure 7.1 and Figure 7.2 are the washability curves of the cobalt response created using the deposit sample and the bulk flotation concentrate.

Both curves show a similar response, though the deposit sample has a more extreme response due to the additional gangue material in the tested material. There are two large jumps in the rate of material reporting to the float fraction. The first occurs around a specific gravity of 2.6. This is where nearly all of the gangue material should report to the float fraction when looking at their specific gravities in Table 7.1. The other jump is at a specific gravity of approximately 2.9. This is immediately after the heavy gangue material should be reporting to the float fraction. The percentage of the cobalt report starts to greatly increase after a specific gravity of 2.8. There are no cobalt-bearing minerals near this specific gravity, so it is expected that particles with partially made up of cobalt but primarily made up of gangue material start to float.

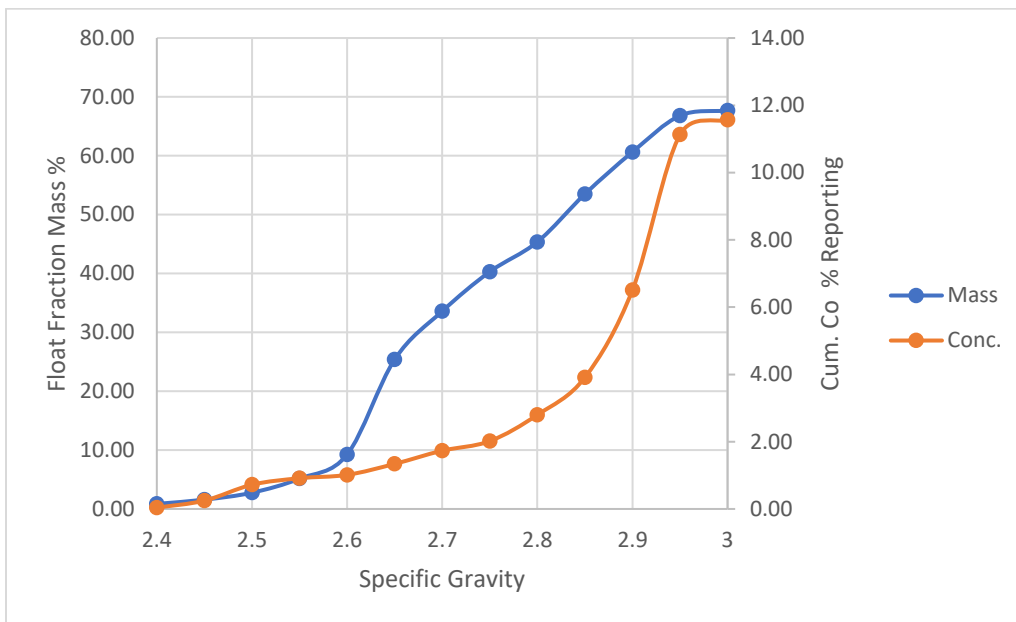


Figure 7.1: Washability curve of the cobalt response of the deposit sample.

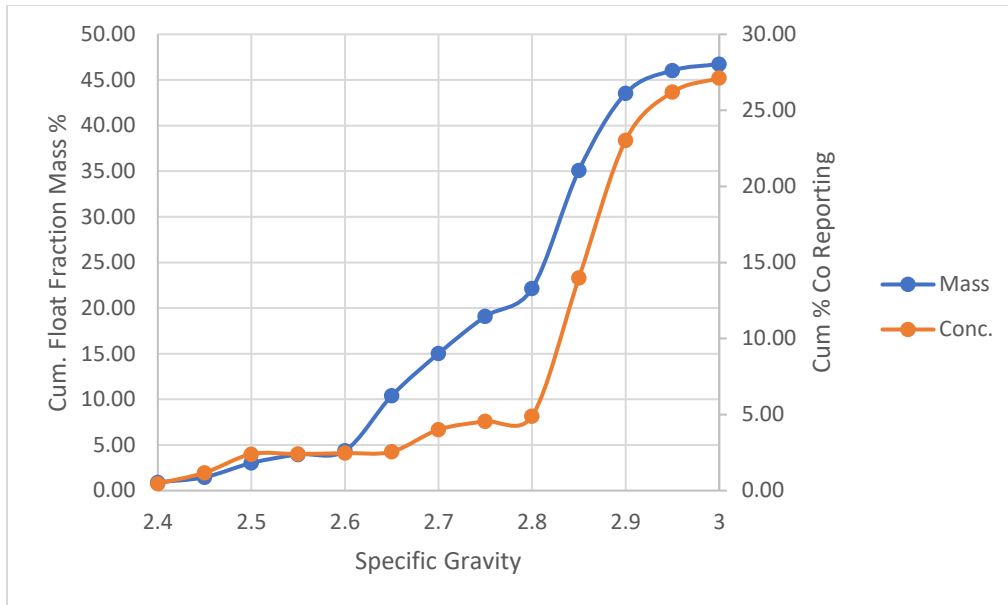


Figure 7.2: Washability curve of the cobalt response of the bulk flotation concentrate.

Shown below in Figure 7.3 and Figure 7.4 are the washability curves of the copper response created using the deposit sample and the bulk flotation concentrate.

Both curves show a similar response to the corresponding cobalt curves, with slight differences. This is most likely due to cobalt and copper being in similar minerals. In the run-of-mine fraction, there are two large changes in the rate of mass reporting to the float fraction, with the first being at 2.6 sg and the second being at 2.9. These are where the light and heavy gangue are supposed to report to the float fraction respectively. The percentage of the copper reporting to the float fraction starts to greatly increase after a specific gravity of 2.8. There are no cobalt-bearing minerals near this specific gravity, so it is expected that particles with partially made up of cobalt, but primarily made up of gangue material start to float.

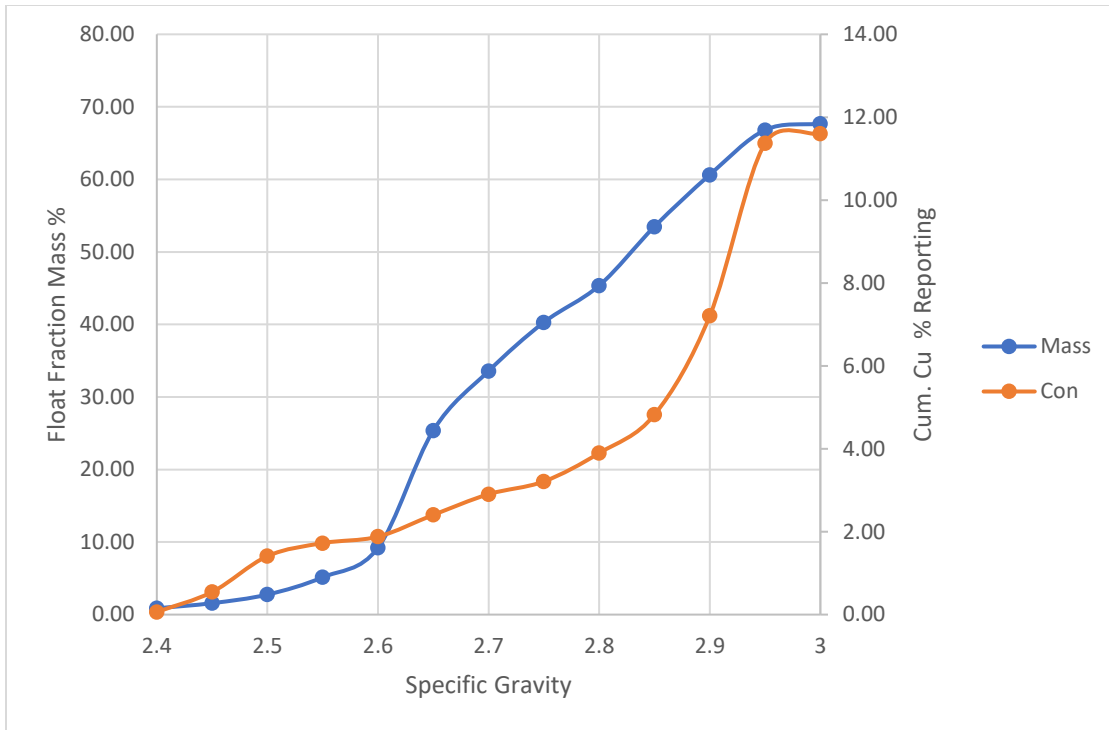


Figure 7.3: Washability curve of the copper response of the deposit sample.

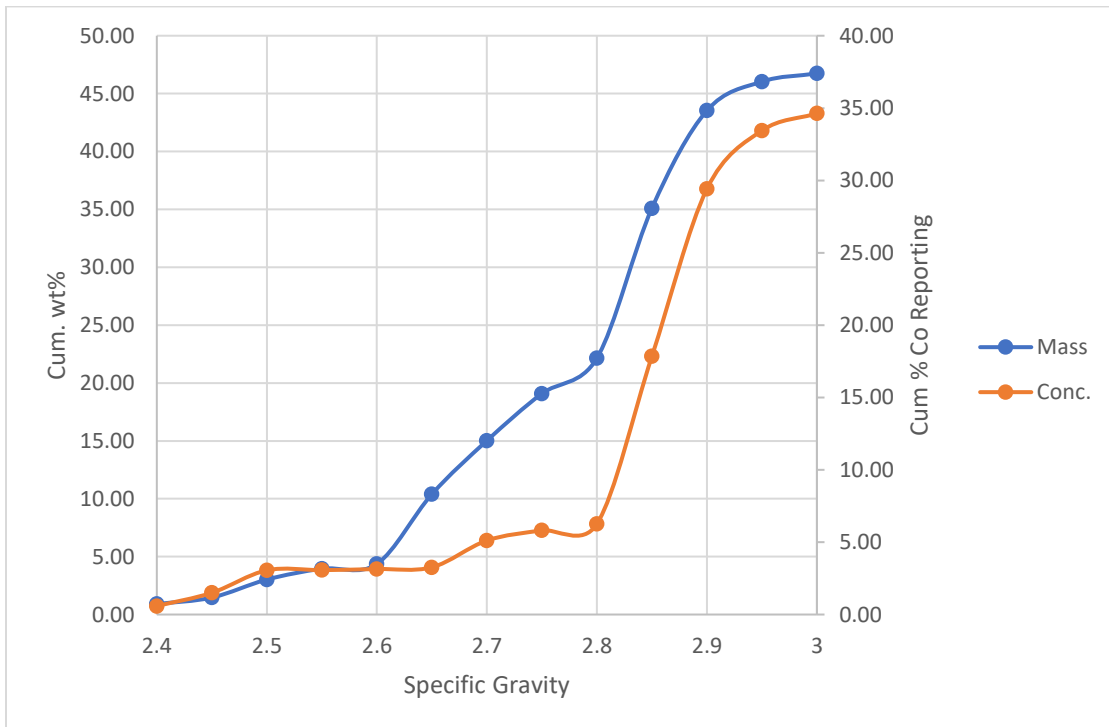


Figure 7.4: Washability curve of the copper response of the bulk flotation concentrate.

7.6 Gravity Separation Statistical Analysis

Two sets of statistical analysis testing were done on the gravity separation testing done, one on the RPM testing and one on the particle size testing. The method use is detailed in Section 6.7.1.

Statistical analysis was not done on the washability curve testing data, as the testing conditions for each repetition of the test were not the same, meaning that they cannot be compared.

7.6.1 Statistical Analysis on RPM Testing

Shown below in Table 7.5 is the ANOVA table for cobalt grade. As the calculated p-value of 0.000953 is far less than 0.05, it can be determined that changing the magnetic field had a statistically significant effect on the changes in cobalt grade over the course of the testing. The same is also true for the copper recovery for all samples, with the p-value for IC 18-07 being 0.001592, as seen in Table 7.6.

Table 7.5: AAS data for gravity separation RPM testing.

Source	Sum of Squares	df	MS	F	P-value	
Between Groups	10873506.3	1	10873506	1047.518725	0.000953	significant
Within Groups	20760.5	2	10380.25			
Total	10894266.8	3				

Table 7.6: RPM testing feed material cobalt recovery ANOVA.

Source	Sum of Squares	df	MS	F	P-value	
Between Groups	6268113	1	6268113.104	626.5632	0.001592	significant
Within Groups	20007.92	2	10003.9601			
Total	6288121	3				

Shown below in Table 7.7 is the ANOVA table for copper grade. As the calculated p-value of 0.009542 is far less than 0.05, it can be determined that changing the magnetic field had a statistically significant effect on the changes in copper grade over the course of the testing. The same is also true for the copper recovery for all samples, with the p-value for IC 18-07 being 0.00159, as seen in Table 7.8.

Table 7.7: RPM testing feed material copper grade ANOVA.

Source	Sum of Squares	df	MS	F	P-value	
Between Groups	1824023.67	1	1824024	103.2978565	0.009542	significant
Within Groups	35315.8086	2	17657.9			
Total	1859339.48	3				

Table 7.8: RPM testing feed material copper recovery ANOVA.

Source	Sum of Squares	df	MS	F	P-value	
Between Groups	6275801	1	6275801	627.2572749	0.00159	significant
Within Groups	20010.29	2	10005.15			
Total	6295811	3				

7.6.2 Statistical Analysis on Particle Size Testing

Shown below in Table 7.9 is the ANOVA table for copper grade. As the calculated p-value of 0.00811 is less than 0.05, it can be determined that changing the magnetic field had a statistically significant effect on the changes in cobalt grade over the course of the testing. With cobalt recovery however, seen in Table 7.10, the p-value of 0.533814 is greater than 0.05, meaning that the RPM is not a statistically significant factor in the overall recovery.

Table 7.9: RPM testing feed material cobalt grade ANOVA.

Source	Sum of Squares	df	MS	F	P-value	
Between Groups	39954944.5	1	39954944	121.8012572	0.00811	significant
Within Groups	656067.85	2	328033.9			
Total	40611012.3	3				

Table 7.10: RPM testing feed material cobalt recovery ANOVA.

Source	Sum of Squares	df	MS	F	P-value	
Between Groups	4252.568	1	4252.568	0.555352803	0.533814	not significant
Within Groups	15314.83	2	7657.416			
Total	19567.4	3				

Shown below in Table 7.11 is the ANOVA table for copper grade. As the calculated p-value of 0.031333 is less than 0.05, it can be determined that changing the magnetic field had a statistically significant effect on the changes in copper grade over the course of the testing. With copper recovery however, seen in Table 7.12, the p-value of 0.526725 is greater than 0.05, meaning that the RPM is not a statistically significant factor in the overall recovery.

Table 7.11: RPM testing feed material copper grade ANOVA.

Source	Sum of Squares	df	MS	F	P-value	
Between Groups	20378926	1	20378926	30.42350648	0.031333	significant
Within Groups	1339682.92	2	669841.5			
Total	21718608.9	3				

Table 7.12: RPM testing feed material copper recovery ANOVA.

Source	Sum of Squares	df	MS	F	P-value	
Between Groups	4420.518	1	4420.518	0.577282471	0.526725	not significant
Within Groups	15314.92	2	7657.462			
Total	19735.44	3				

7.7 Gravity Separation Discussion

Overall, gravity separation appears to be effective at removing the cobalt and copper-bearing minerals from the gangue material in the deposit sample and the bulk flotation concentrate. Given sufficient liberation, the particle size and speed of the centrifuge seem to have a minimal effect on the

grade or recovery of the float and sink fraction. That said, it does not appear to be effective at separating the cobalt-bearing from other potentially valuable elements, mainly copper. This may be explained by the fact that cobalt and copper are often hosted in the same minerals and this testing does not contain a chemical change that would cause them to separate.

Testing done to produce washability curves in the deposit sample and bulk flotation concentrate showed some general trends in the behavior of the material tested. The ideal SPT SG to use seems to be 2.8, as it maximizes the amount of gangue material that reports to the float fraction while minimizing the amount of cobalt and copper. The curves also show that much of the gangue material was removed in the bulk flotation, as only approximately 45% of the mass reported to the float fraction compared to nearly 70% in the deposit sample curve. Less cobalt and copper also reported to the float fraction in the bulk flotation concentrate curve compared to the run-of-mine test, most likely due to the lack of primarily gangue material particles that contained small amounts of the target elements that could report to the float fraction.

CHAPTER 8. ELECTROSTATIC SEPARATION

8.1 Testing Conditions

Electrostatic separation was done in a high-tension roll separator. The purpose of this was to see if the conductivity of the materials in the deposit could be used to create a separation between the cobalt and other minerals. Material is fed into a hopper at the top of the machine and falls onto a roll in a thin layer, where it is exposed to two electrodes. The first electrode is a wire, which primary function is to pin non-conductive material to the roll. The second electrode is a plate, which pulls the conductive material off the roll. The material then falls into bins under the roll based on its response to the electrodes, with the more conductive material falling into the bins farther from the roll.



Figure 8.1: High-tension roll separator.

The expected electrostatic response of the primary target and gangue minerals are shown in Table 8.1. Testing the high-tension separation roll was done on two samples, deposit sample and a bulk flotation concentrate. Testing conditions for each trial can be found in Table 8.2. Trial 5 was the only test done with the bulk flotation concentrate due to a lack of material.

Table 8.1: Expected electrical conductivities of target and gangue materials.

Mineral	Electrical Conductivity
Biotite	Non-Conductive
Chalcopyrite	Semiconductor
Chlorite	Non-Conductive
Feldspar	Non-Conductive
Galena	Semiconductor
Iron Oxides	Non-Conductive
Jaipurite	Semiconductor
Kaolinite	Non-Conductive
Molybdenite	Conductive
Muscovite	Non-Conductive
Pyrite	Conductive
Pyrrhotite	Conductive
Quartz	Non-Conductive

Table 8.2: Test conditions for electrostatic separation trials.

Trial	Voltage (kV)	Ore mass (g)	Particle Size (Microns)
1	15	237.2	175
2	20	253.9	175
3	25	270.5	175
4	29	238.8	175
5	29	93.3	75

8.2 Electrostatic Separation Testing Procedures

8.2.1 Deposit Sample Testing Procedure

The testing procedure for each of the trials shown in Table 8.2 is as follow:

The electrostatic separator was set to the desired test settings and allowed to heat up for an hour. The rollers were turned on and the temperature was allowed to stabilize at 100 °C. Three hundred grams

of the sample was poured into the hopper at the top of the machine. Once all the material went through the machine, turn off the electrode. Each fraction is removed and massed.

8.2.2 Bulk Flotation Testing Procedure

Testing of the bulk flotation sample followed the same procedure as outlined in section 8.2.1, but with 100g of sample that had a p80 of 75 microns.

8.3 Preparation of Electrostatic Separation Sample for Analysis

All products from electrostatic separation testing were analyzed using atomic absorption spectroscopy (AAS). The methods used to prepare the samples for analysis are described.

8.3.1 Deposit Sample Dilution

Given the cobalt and copper concentration in the deposit sample material is 2500 ppm and 1740 ppm respectively, A 250X dilution of sample containing 2500 ppm Co would report as having 10 ppm Co, with the range set by the calibration standards. The Fe concentration in the deposit sample material is 10.9 wt %, or 109000 ppm. A 1100X dilution of sample containing 109000 ppm Fe would report as having 99 ppm Fe, with the range set by the calibration standards. A 250X dilution with 2% nitric acid was used for the preparation of samples for Co and Cu AAS analysis and a 1100X dilution with 2% nitric acid was used for the preparation of samples for Fe analysis.

8.3.2 Bulk Flotation Concentrate Dilution

Given the cobalt and copper concentration in the bulk flotation concentrate material is 11210 ppm and 9150 ppm respectively, a 1121X dilution of sample containing 11210 ppm Co would report as having 10 ppm Co, with the range set by the calibration standards. The Fe concentration in the bulk flotation material is 23.4 wt %, or 234000 ppm. A 2340X dilution of sample containing 234000 ppm Fe would report as having 99 ppm Fe, with the range set by the calibration standards. A 1250X dilution with 2% nitric acid was used for the preparation of samples for Co and Cu AAS analysis and a 2500X dilution with 2% nitric acid was used for the preparation of samples for Fe analysis.

8.4 Electrostatic AAS Data

Shown in Table 8.3 below is the AAS data for the product generated from the trials shown in Table 8.2. It should be noted that trial 5 used the bulk flotation concentrate as the tested material, which has a much higher grade in all elements and less gangue material. Splits labeled concentrate and tails in this section were made by combining smaller splits created during testing, the data for which can be found in Appendix F. The combinations were the same for all tests.

From the data in Table 8.3, there is a large difference in the grade of all elements between the concentrate and the tails. This is expected, as the conductivities for the target minerals are conductors while the gangue materials are primary insulators, as seen in Table 8.1 above. This is also why the recoveries generally are also very high in the concentrate. The grade increases as the voltage of the tests increases. This is because more gangue material is being rejected to the tailings and the mass percent reporting to the concentrate is lower.

Trial 5, the trial run with the bulk flotation concentrate, has higher grades and lower recoveries than the deposit sample tests. This is because much of the grade concentration in the previous test had come from removing gangue material, which in the bulk flotation concentrate had already been removed during the flotation.

Table 8.3: AAS data output for electrostatic separation.

Trial	Mass % Reporting	Element Concentrations			Element Recovery (%)			
		Co (ppm)	Cu (ppm)	Fe (wt%)	Co	Cu	Fe	
1	Conc.	95.4%	3674	2497	20.26	99.15	97.89	97.14
	Tails	4.6%	648	1109	12.27	0.85	2.11	2.86
2	Conc.	79.2%	4344	2855	16.81	95.83	94.68	98.74
	Tails	20.8%	1044	1216	12.45	4.17	5.32	1.26
3	Conc.	52.1%	6017	3548	16.38	96.89	95.31	94.67
	Tails	47.9%	1572	1510	9.60	3.11	4.69	5.33
4	Conc.	45.5%	6280	3876	20.69	97.10	95.92	94.23
	Tails	54.5%	1623	1459	13.24	2.90	4.08	5.77
5	Conc.	63.7%	13903	10601	N/A	76.09	74.25	N/A
	Tails	36.3%	8166	6441	N/A	23.91	25.75	N/A

8.5 Electrostatic Washability Curve

Shown below in Figures 8.2 and 8.3 are the washability curves of the cobalt and copper response in the tailings, the non-conductive fraction, from the deposit samples.

Both elements show similar trends, with an increasing amount of cobalt and copper reporting to the tailings as the voltage increases, though copper has a higher percentage of materials reporting to tailings, most likely due to the presence of more conductive copper-bearing materials. The amount of material reporting to the tailings increased as the voltage increased, as less conductive materials were pulled to the tailings. Cobalt minimally reported to the tailings at the lowest two voltages tested, with both

being below 2 wt%. The amount of cobalt reporting increased sharply after that, with the highest voltage having just under 10 wt% cobalt reporting to the tailings. Copper had a similar response, with less than 6 wt% of the copper reporting in the first two fractions but increasing to 16 wt% of the copper by the final test.

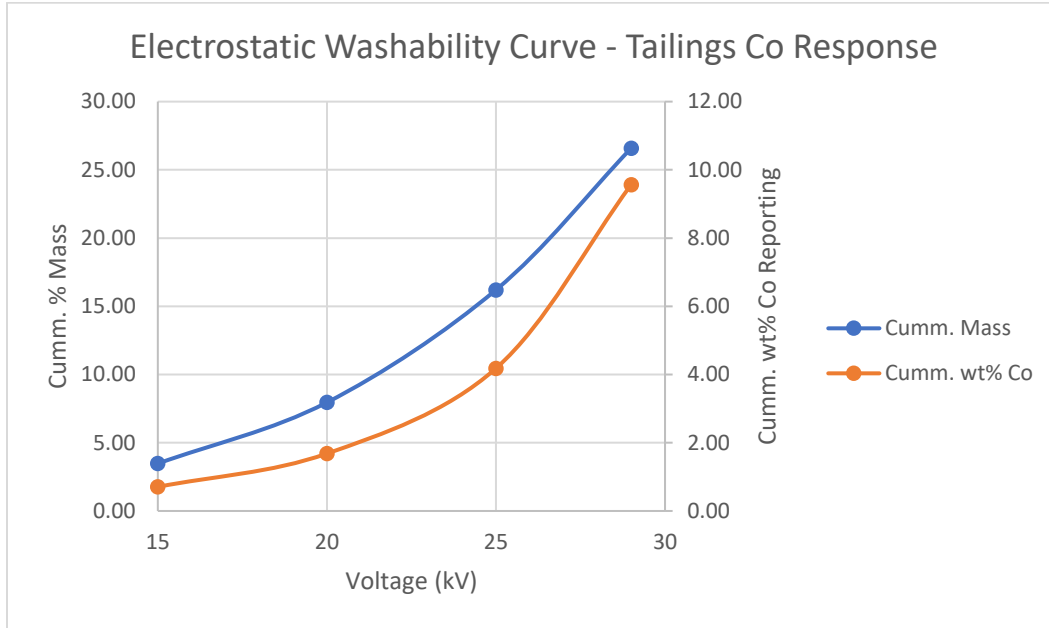


Figure 8.2: Electrostatic washability curve of the cobalt response of the deposit sample.

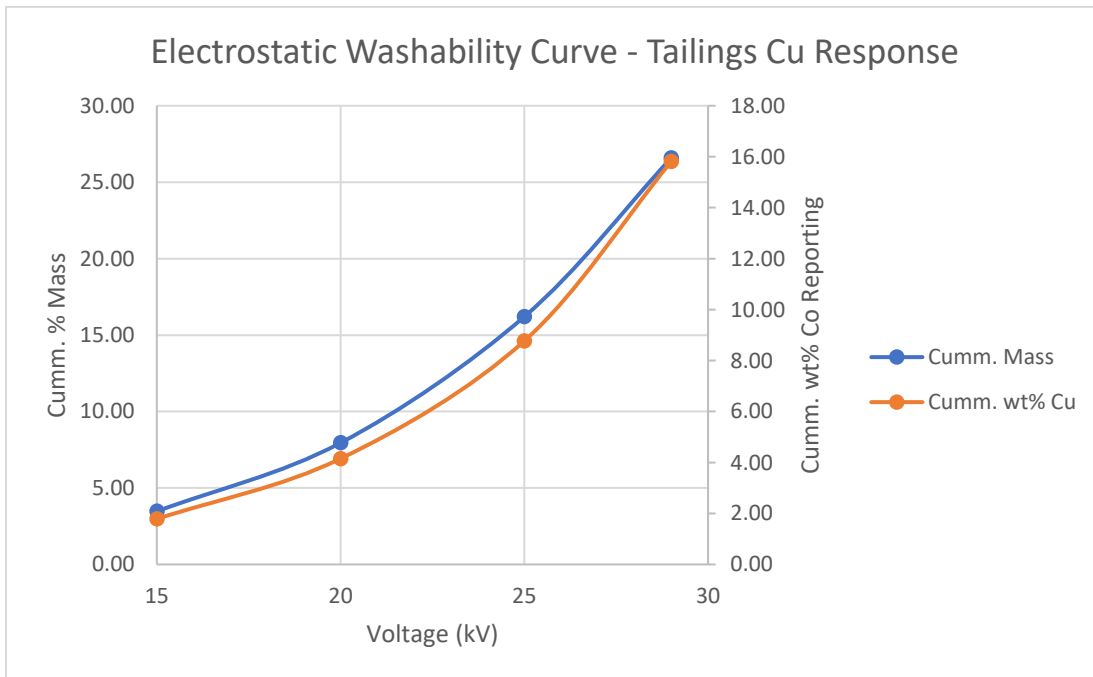


Figure 8.3: Electrostatic washability curve of the copper response of the tailings in the deposit sample.

8.6 Electrostatic Statistical Analysis

Statistical analysis for the electrostatic separation testing was done on the feed material and looked at the test voltage and splitter position using two-factor ANOVA tests. Statistical analysis done with splitter position was done using data from individual splitter positions instead of the concentrate and tails grouping and can be seen in Appendix F. The methodology used is detailed in Section 6.7.1.

Shown below in Table 8.4 is the ANOVA table for cobalt grade. It shows that the differences in the cobalt grade from changes in the testing voltage and splitter position are statistically significant, as the p-values are 0.02375 and 0.00011 respectively. The same is not true for cobalt recovery, as the p-values, shown in Table 8.5, were calculated to be 0.99999 and 0.18822, both much larger than the 0.05 threshold.

Table 8.4: Electrostatic separation testing feed material cobalt grade ANOVA.

Source	Sum of Squares	df	MS	F	P-value	
Voltage	13549814.75	3	4516605	5.175171	0.023753843	significant
Splitter Poistion	65221914.75	3	21740638	24.91064	0.000108107	significant
Error	7854706.25	9	872745.1			
Total	86626435.75	15				

Table 8.5: Electrostatic separation testing feed material cobalt recovery ANOVA.

Source	Sum of Squares	df	MS	F	P-value	
Voltage	0.036869	3	0.01229	1.79E-05	0.999999887	not significant
Splitter Position	4070.753	3	1356.918	1.97582	0.188223075	not significant
Error	6180.857	9	686.7619			
Total	10251.65	15				

Shown below in Table 8.6 is the ANOVA table for copper grade. It shows that the differences in the cobalt grade from changes in the splitter position is statistically significant, as the p-values was 0.000851. The changes in copper grade caused by the testing voltage were not statistically significant, with a p-value of 0.18172. The same applies to the changes in copper recovery for both splitter position and voltage, with p-values of .23062 and 1 respectively, both well above 0.05.

Table 8.6: Electrostatic separation testing feed material copper grade ANOVA.

Source	Sum of Squares	df	MS	F	P-value	
Splitter Position	15598817.13	3	5199606	14.53083	0.000850966	significant
Voltage	2168190.268	3	722730.1	2.019743	0.181716148	not significant
Error	3220494.945	9	357832.8			
Total	20987502.34	15				

Table 8.7: Electrostatic separation testing feed material copper recovery ANOVA.

Source	Sum of Squares	df	MS	F	P-value	
Splitter Position	3769.825	3	1256.608	1.727655	0.23062108	not significant
Voltage	1.88E-05	3	6.25E-06	8.59E-09	1	not significant
Error	6546.142	9	727.3491			
Total	10315.97	15				

8.7 Electrostatic Separation Discussion

Overall, electrostatic separation of the deposit sample and bulk flotation material was effective at removing the target materials from the gangue materials. The grades of all elements tested generally increased as the voltage increased, while the recoveries decreased slightly. Cobalt and copper grades and recoveries were very similar throughout the tests, indicating that the cobalt and copper-bearing minerals behaved very similarly to each other. This means that this separation method would not be suitable for creating a separation between the cobalt and the copper.

The cobalt recovery was more effective in the deposit sample than the bulk flotation concentrate. The largest deposit sample grade increase was 151% while the largest in the bulk flotation concentrate was 24%. This large difference may be due to the presence of more gangue material in the deposit sample. More gangue material means that there is more material overall to remove, therefore increasing the grade of the cobalt and copper by subtraction. Since most of the gangue materials were removed during the creation of the bulk flotation material, the amount of cobalt and copper reporting to the tailings was more obvious. The particle size may have influenced the recoveries as well. Due to the requirement for flotation, the particle size of the bulk flotation test was less than half of that of the run-of-mine tests. This may have resulted in material getting trapped in the machine during testing, as the particles lacked the mass necessary to overcome the electromagnetic forces to fall to the bottom of the machine.

The washability curves created also support some of these observations. Cobalt and copper had nearly identical curves, though copper had slightly higher recoveries at higher voltages. This supports that creating a split between the cobalt and cobalt using this method would be very difficult. The recovery of the elements tested and the mass reporting to the tailings increased with increasing voltage without signs of slowing or decreasing, so achieving higher grades and recoveries could be possible at higher voltages than the ones tested here. However, this would be difficult to do without causing arcing, which would interfere with the grade and recoveries, as arcing causes momentary dips in the magnetic field strength.

CHAPTER 9. SULFURIC ACID LEACHING

9.1 Pourbiax Diagrams

A Pourbiax diagram, as known as an Eh-pH diagram, is a diagram that shows the regions of electro-potential and acidity/alkalinity where particular phases are thermodynamically stable. These diagrams provide the ability to predict what conditions are likely to cause a soluble or aqueous phase to form, therefore, they are useful in predicting which leaching conditions are likely to cause a given substance to transfer to the aqueous phase during leaching and what conditions may result in any desired separations. These diagrams do not account for kinetics and only indicate the equilibrium state of a given system. They do not indicate the potential to form any metastable phases or the time necessary for equilibrium to occur. Other variables that affect a Pourbiax diagram are temperature, pressure, and concentrations of the involved species. These variables are generally kept at 25 °C, atmospheric pressure, and molarities of around 10^{-6} .

The stability of water is an important factor in many industrial processes and often provides the practical upper and lower bounds for many process variables. On the Pourbaix diagram in this paper, the upper and lower bounds of water stability are indicated by dashed lines, with the upper limit represented by Equation 9.1 and the lower limit represented by Equation 9.2.



9.1.1 Iron Pourbaix Diagram

Shown below in Figure 9.1 is an Eh-pH diagram for iron at 1 atm and 30 C. It can be seen that in strongly reducing conditions, metallic iron is the dominant phase across the entire pH range. In slightly reducing conditions, troilite and pyrite are the dominant phases, especially as acidity increases. In oxidizing conditions, iron hydroxides are the dominant phases.

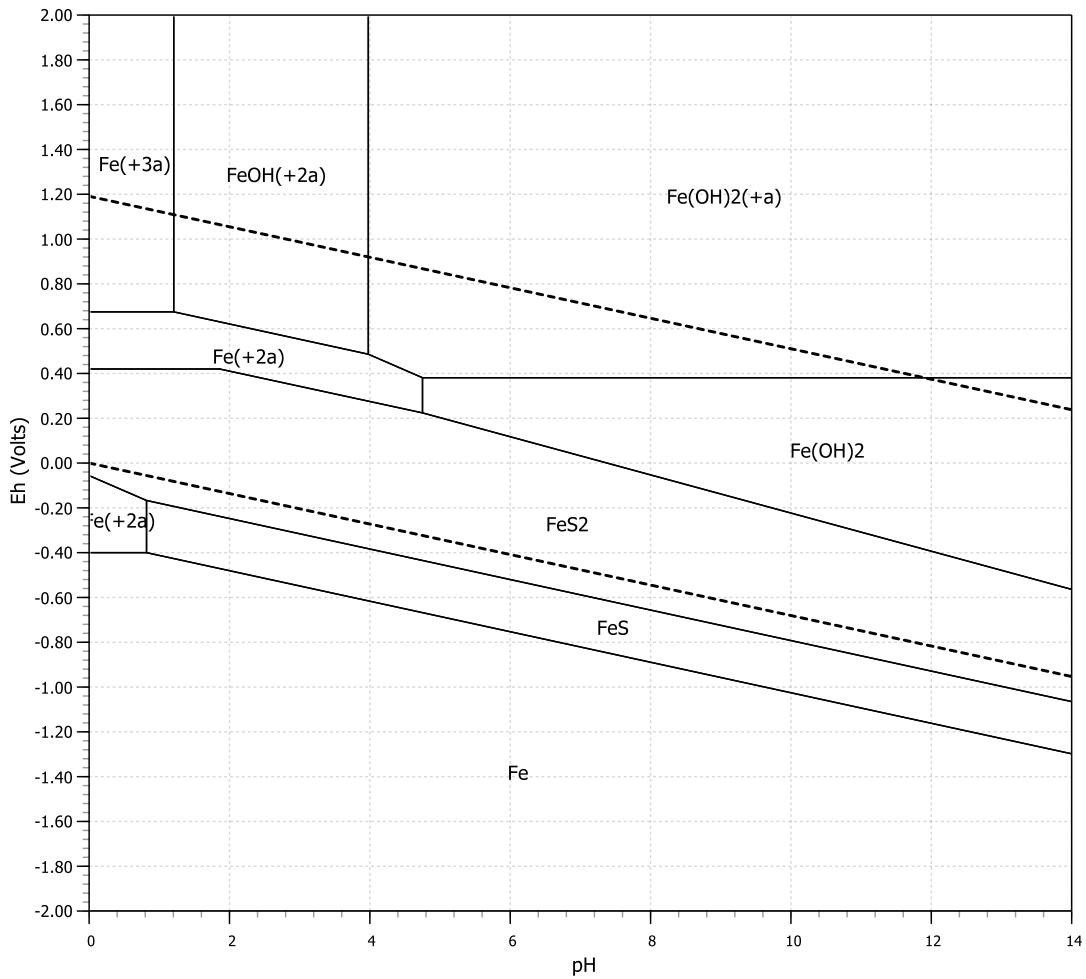


Figure 9.1: Iron Eh-pH diagram.

9.1.2 Sulfur Pourbaix Diagram

As the Fe-S-O-H Pourbaix diagram focuses on iron-based minerals, a Pourbaix diagram that focused on sulfur minerals in the system was examined and can be seen in Figure 9.2. In reducing conditions, hydrogen sulfide gas is the dominant phase across the entire pH range. Pyrite and pyrrhotite again are the dominant phases in slightly reducing and oxidizing conditions, with Fe(OH)_2^+ being dominant in most oxidating conditions, especially with increasing acidity.

As hydrogen sulfide is a toxic gas and its formation should be avoided, additional steps need to be taken. In this experiment, steps will be taken to ensure that the leaching environment stays in an oxidative state to limit its formation.

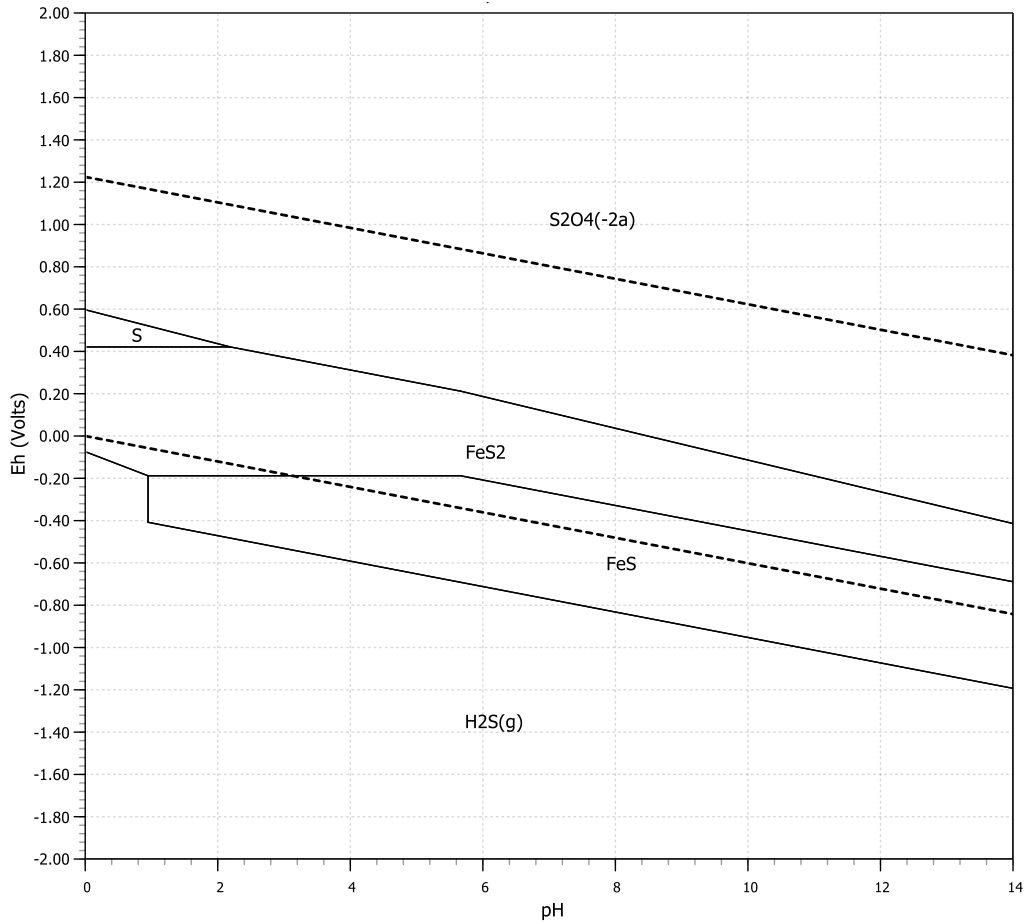


Figure 9.2: Sulfur Eh-pH diagram.

9.2 Leaching Testing Conditions

The range of sulfuric acid concentrations used would be 10 % to 30 % H₂SO₄. Leaching times would be between 1 hour and 3 hours. Due to material limitations, each trial was run with either 1 gram or 1.5 grams of thermal decomposition magnetic fraction concentrate. Based off methods found in literature, leach temperatures were between 30 °C and 70 °C. Shown in Table 9.1 below are the various test conditions for each acid leach trial. The specific conditions for each trial were generated using Stat-Ease.

Table 9.1: Test conditions for leaching trials.

Trial	Time (Hr)	Temperature C	Acid %	Oxide %	Concentrate Mass (g)
1	1	30	10	0	1.5
2	3	30	10	0	1
3	1	70	10	0	1
4	3	70	10	0	1.5
5	1	30	30	0	1
6	3	30	30	0	1.5
7	1	70	30	0	1.5
8	3	70	30	0	1
9	1	30	10	5	1
10	3	30	10	5	1.5
11	1	70	10	5	1.5
12	3	70	10	5	1
13	1	30	30	5	1.5
14	3	30	30	5	1
15	1	70	30	5	1
16	3	70	30	5	1.5

9.3 Leaching Testing Procedure

The testing procedure for each of the trials shown in Table 9.1 is as follow:

A 100 mL of DI water and concentrated sulfuric acid is prepared to the appropriate sulfuric acid concentration is achieved. This solution was placed in a 400 mL beaker with a magnetic stir rod and placed on a hot plate. The appropriate amount of sodium peroxide is then slowly added to the beaker. The beaker is agitated by the stir bar at 200 rpm and is heated until the solution is at the appropriate leaching temperature. The temperature of the hot plate was automatically controlled by a thermocouple placed in the solution. A sample with approximately the indicated mass for the trial of the cobalt concentrate is placed in the beaker. At this time the leaching time starts. Once the leaching time is reached, the beaker is removed from the hot plate and the remaining solids are filtered out. Once all the solids have been removed, the leachate is stored, and the residue is allowed to dry and then stored.

9.4 Leaching AAS Data

Shown below in Table 9.2 is the AAS data for the leachate generated from the trials. From the data, it can be seen that the grades in the leachates are fairly low. Low grades are expected, as the addition of the additional material to a fraction that does not contain any of the target minerals lowers the grade, in this case, sulfuric acid. Masses of the leachates also vary greatly from trial to trial, making comparison difficult.

In this case, recovery is a better measure of success than grade. From the data in Table 9.2, it can be seen that the recoveries for all elements are extremely low. The highest recovery for all elements was trial 12, with 11.94%, 10.4%, and 12.70% for cobalt, copper, and iron respectively. Trials 1 through 8 overall had lower recoveries than Trials 9 through 16, which corresponds with the trials that do not and do have sodium peroxide. Trials with longer times and higher acid content also generally had higher recoveries.

Table 9.2: AAS data for sulfuric acid leach test leachates.

Run	Cobalt Grade (ppm)	Cobalt Recovery (%)	Copper Grade (ppm)	Copper Recovery (%)	Iron Grade (ppm)	Iron Recovery (%)
1	0.00	0.00	0.00	0.00	0.00	0.00
2	0.44	0.21	0.54	0.66	0.00	0.00
3	1.04	0.46	1.84	2.14	34	0.90
4	2.57	0.97	4.06	3.73	123	2.73
5	1.24	0.70	0.34	0.53	27	0.93
6	0.08	0.04	0.00	0.00	33	0.77
7	1.71	0.74	1.82	2.03	78	2.11
8	1.70	1.08	1.30	1.80	54	2.06
9	3.74	1.79	2.33	2.72	67	1.89
10	14.84	6.16	6.66	6.70	217	5.37
11	25.69	8.29	7.45	5.75	467	9.21
12	26.39	11.94	9.31	10.40	454	12.70
13	8.08	3.17	5.80	5.56	262	5.76
14	10.95	6.33	6.47	9.88	189	6.51
15	17.60	9.84	8.13	9.99	323	10.57
16	29.09	11.30	11.71	10.35	526	12.35

9.5 Leaching Statistical Analysis

A statistical analysis using Stat Ease software was conducted on the leachate recoveries. The methodology is detailed in Section 6.7.2.

9.5.1 Analysis of Cobalt Recovery

Shown below in Figure 9.3 is a half normal plot showing the standardized effect of each leaching variable and possible interaction. It can be seen that only the amount of Na_2O_2 is a significantly variable, with temperature possibly being statistically significant. This is confirmed by the Pareto chart shown in Figure 9.4.

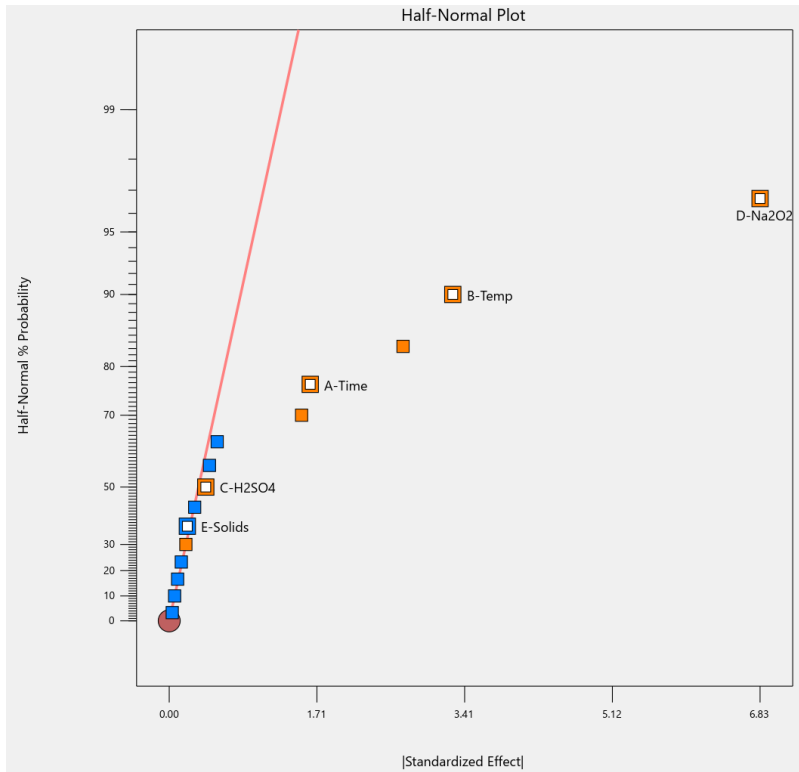


Figure 9.3: Half-normal plot for sulfuric acid cobalt effects.

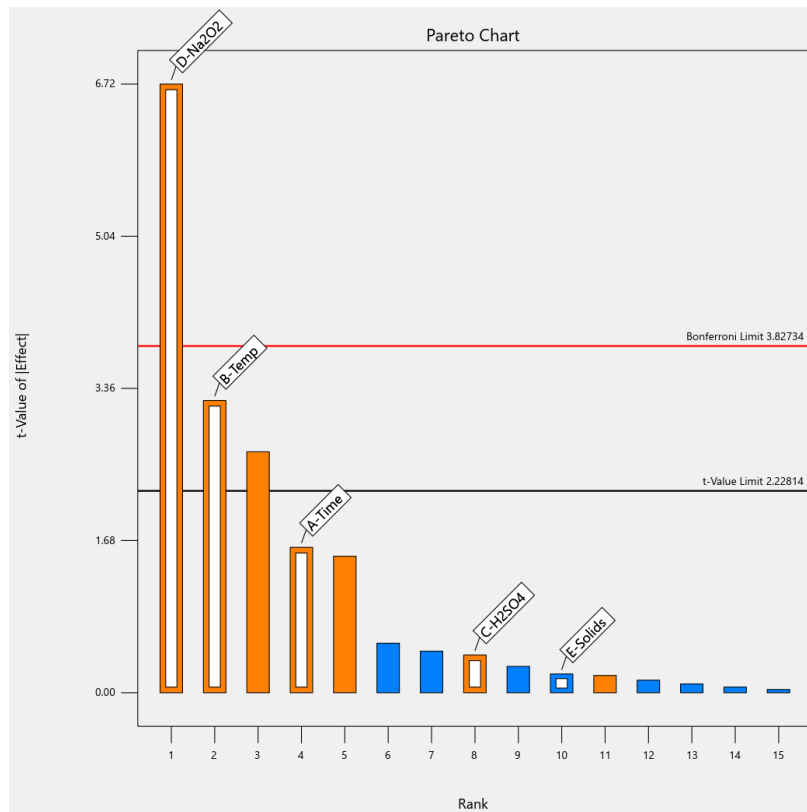


Figure 9.4: Sulfuric acid cobalt Pareto chart.

Shown in Table 9.3 is the ANOVA for cobalt recovery using temperature, time, mass, acid amount, and Na₂O₂ amount as variables. According to the ANOVA, the Na₂O₂ amount and temperature are the variables that are statistically significant. The likelihood of the model being incorrect due to noise is 0.06%. The calculated R² is 0.8536.

Table 9.3: Sulfuric acid cobalt recovery ANOVA.

Source	Sum of Squares	df	Mean Square	F-value	p-value	
Model	240.9451	5	48.18902	11.66581	0.000648	significant
A-Time	10.6276	1	10.6276	2.572777	0.139798	
B-Temp	42.96803	1	42.96803	10.40189	0.009095	
C-H2SO4	0.714025	1	0.714025	0.172854	0.686369	
D-Na2O2	186.459	1	186.459	45.13883	5.24E-05	
E-Solids	0.1764	1	0.1764	0.042704	0.840431	
Residual	41.3079	10	4.13079			
Cor Total	282.253	15				

9.5.2 Analysis of Copper Recovery

Shown below in Figure 9.5 is a half normal plot showing the standardized effect of each leaching variable and possible interaction. It can be seen that only the amount of Na₂O₂ is a significantly variable, with temperature and time possibly being statistically significant. This is confirmed by the Pareto chart shown in Figure 9.6.

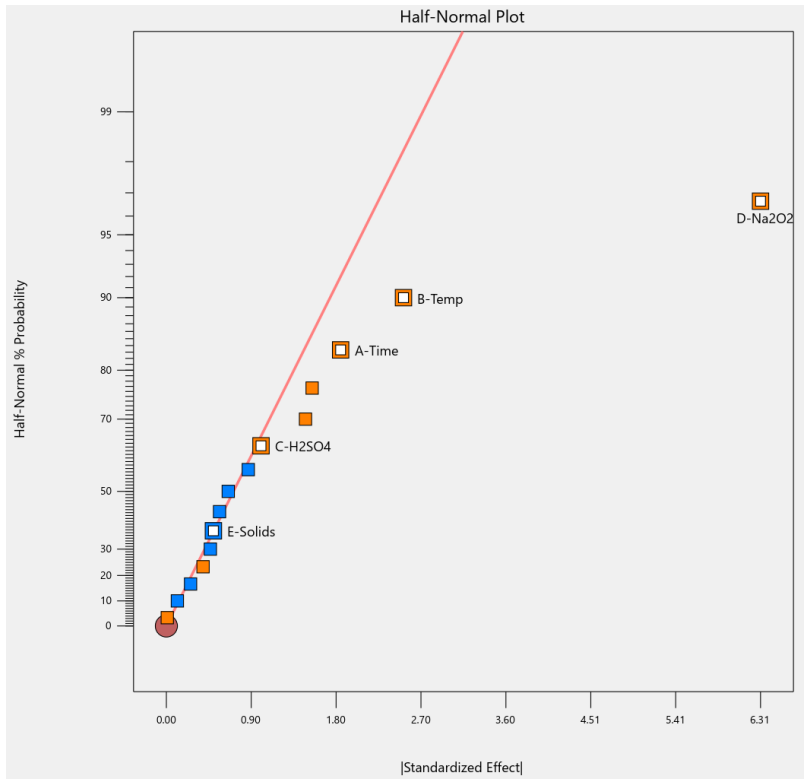


Figure 9.5: Half-normal plot for sulfuric acid copper effects.

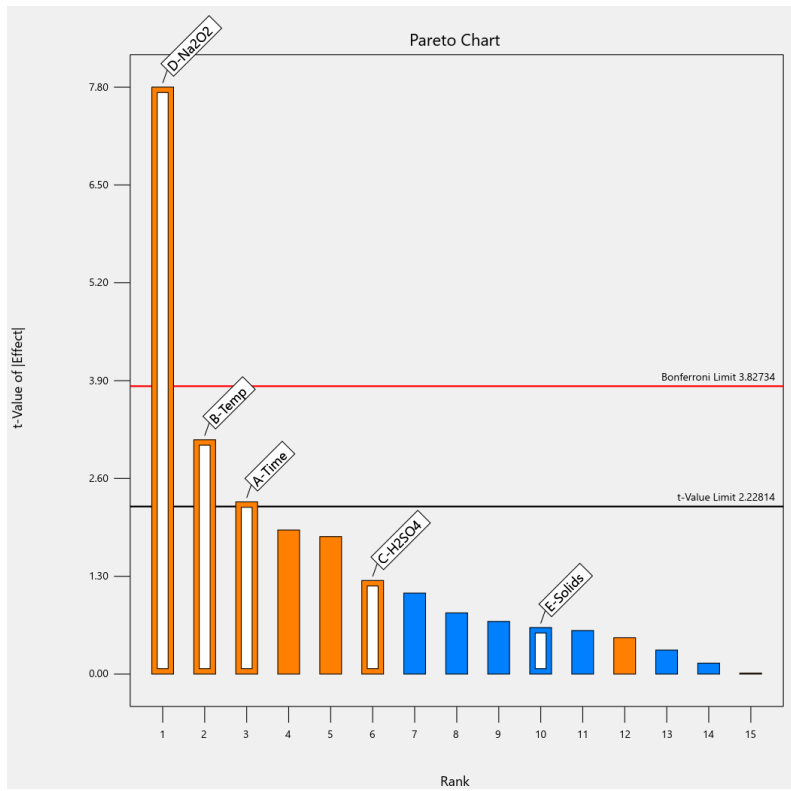


Figure 9.6: Sulfuric acid copper Pareto chart.

Shown in Table 9.4 is the ANOVA for copper recovery using temperature, time, mass, acid amount, and Na₂O₂ amount as variables. According to the ANOVA, Na₂O₂ amount, time, and temperature are the variables that are statistically significant. The likelihood of the model being incorrect due to noise is 0.02%. The calculated R² is 0.8860.

Table 9.4: Sulfuric acid copper recovery ANOVA.

Source	Sum of Squares	df	Mean Square	F-value	p-value	
Model	203.2196	5	40.64391	15.54364	1.94E-04	significant
A-Time	13.69	1	13.69	5.235532	0.045157	
B-Temp	25.35123	1	25.351225	9.69519	0.010991	
C-H2SO4	4.0401	1	4.0401	1.545075	0.242219	
D-Na2O2	159.1382	1	159.138225	60.85999	1.47E-05	
E-Solids	1	1	1	0.382435	0.550128	
Residual	26.14825	10	2.614825			
Cor Total	229.3678	15				

9.5.3 Analysis of Iron Recovery

Shown below in Figure 9.7 is a half normal plot showing the standardized effect of each leaching variable and possible interaction. It can be seen that there are no statistically significant variables. This is confirmed by the Pareto chart shown in Figure 9.8.

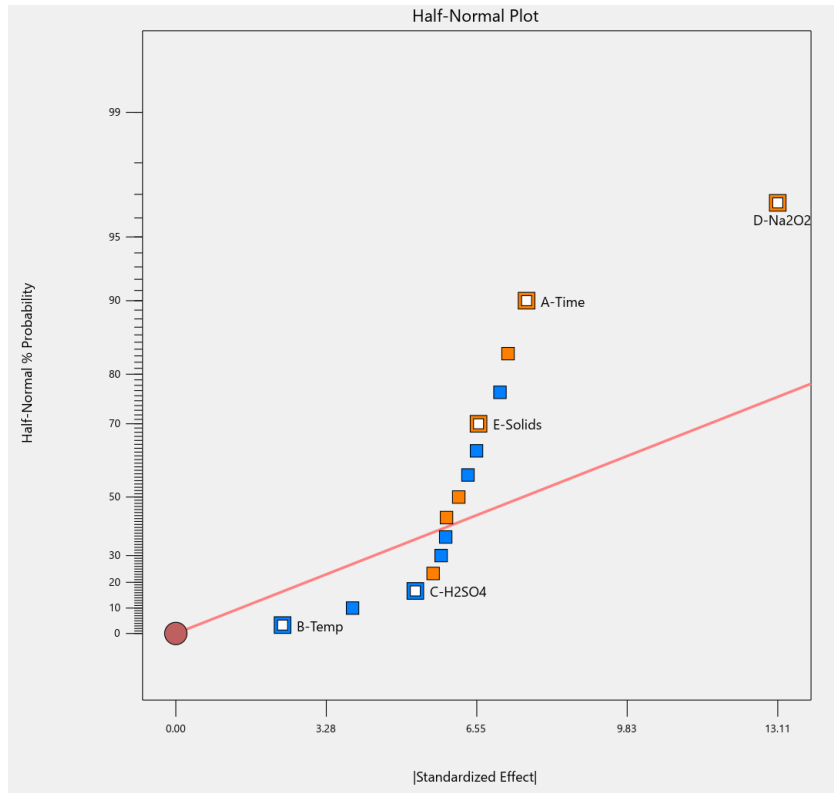


Figure 9.7: Half-normal plot for sulfuric acid iron effects.

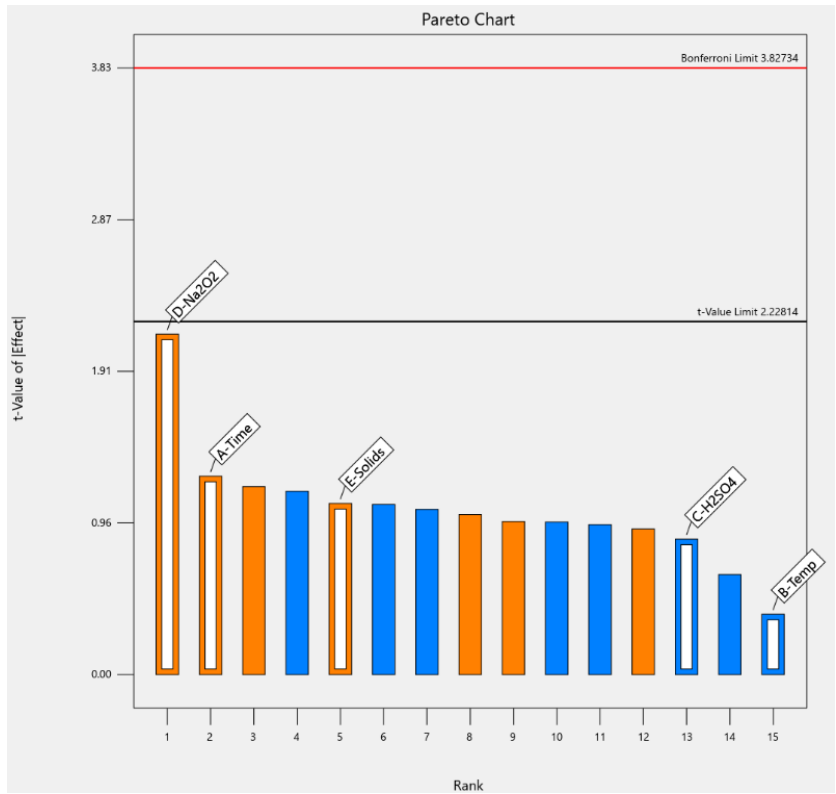


Figure 9.8: Sulfuric acid iron Pareto chart.

Shown in Table 9.5 is the ANOVA for iron recovery using temperature, time, mass, acid amount, and Na₂O₂ amount as variables. According to the ANOVA, there are no variables that are statistically significant. The likelihood of the model being incorrect due to noise is 23.51%. The calculated R² is 0.4512.

Table 9.5: Sulfuric acid iron recovery ANOVA.

Source	Sum of Squares	df	Mean Square	F-value	p-value	
Model	1225.061	5	245.012115	1.644539	2.35E-01	not significant
A-Time	233.4784	1	233.4784	1.567124	0.239114	
B-Temp	21.6225	1	21.6225	0.145132	0.7112	
C-H2SO4	108.8892	1	108.889225	0.730872	0.412614	
D-Na2O2	687.2262	1	687.226225	4.612712	5.73E-02	
E-Solids	173.8442	1	173.844225	1.166855	0.305412	
Residual	1489.853	10	148.98528			
Cor Total	2714.913	15				

9.6 Leaching Discussion

Overall, sulfuric acid leaching does not satisfactorily transfer the target elements into solution. According to literature through there have been several successful attempts to leach pyrite and pyrrhotite using sulfuric acid. One possible reason for this is that the sodium peroxide is being completely consumed before the end of the test, resulting in the targeted elements not fully dissolving.

The recovery of each target element was impacted differently by each variable tested. Sodium peroxide was the most common factor that impacted recovery, having a statistically significant impact on cobalt and copper recovery. Temperature only had a confirmed significant impact on copper recovery, with only a possible impact on cobalt recovery. The concentration of sulfuric acid had no effect on the recovery of any element, suggesting that there is excess acid in all tests and that is not a limiting factor. Time also has no effect on element recovery, though this may be because all that sodium peroxide is consumed before the tests are completed, meaning that leaching stopped before the end of test.

Generally, it seems that elemental recovery can be optimized by changing sodium peroxide amount and temperature. This makes sense as sodium peroxide makes the leaching environment oxidative, making leaching more likely to occur and higher temperature allows for improved kinetics.

CHAPTER 10. ECONOMIC ANALYSIS

Based on testing done, any of the beneficiation methods tested expect leaching could be used to increase the cobalt grade, given the correct feed material is used. This is further discussed in Chapter 11. In order to determine the practicality of each method, a basic economic model was generated for each method. It should be noted that a number of assumptions had to be made in order to create each model. These assumptions may not be completely accurate and could affect the output of the models. This analysis contains both individual process analysis and an overall flowsheet analysis, which was created as a whole project collaboration. The individual process analyses are labeled as value generated rather than profit or loss as these models only focus on the physical beneficiation, not the complete process which would have additional costs associated with other processing stages. The whole process analysis is also in value created, even though some salable products are created.

10.1 Model Assumptions

With all economic models, a number of assumptions are necessary. These assumptions may not be completely accurate but are close enough that they provide a reasonable approximation. The most significant is that market prices will not change, which is more than likely untrue. This assumption is due to the prediction of future market trends and prices being beyond the scope of this research. It is also assumed that many of the model inputs are accurate and not subject to change, given that several inputs change based off of market prices, this assumption is more than likely incorrect. Again, the prediction of future market trends and prices is beyond the scope of this research.

A large portion of model inputs are assumed based on available sources and knowledge. A non-exhaustive list of such inputs follows:

10.1.1 Operation Assumptions

This model assumes that, per year, Iron Creek produces 340 days of the 365, based on industry standards for industrial production facilities. It accounts for any downtime that may occur due to repair and maintenance operations, equipment upgrades, and other unforeseen circumstances, as well as holiday closures. It is also assumed that the plant is operating 24 hours a day.

10.1.2 Elemental Value Assumptions

The value of each element is assumed based on the 36-month average price at the time of writing due to the volatility of cobalt prices in 2023. Both cobalt and copper are used in calculating the expected profits in the gravity and electrostatic separation models, but only cobalt is used in the magnetic separation model. This is because of the theoretical location of each process in the processing flowsheet. Gravity and Electrostatic would be before the differential flotation that would remove the copper, while the magnetic separation would be after, and copper is not expected to be recoverable in the cobalt

refining. Shown in Table 10.1 are the model values used for the price of each target element in the concentrates used in testing.

Table 10.1: Pricing data for each element.

Element	Price (\$/tonne)
Cobalt	\$ 49,993.00
Copper	\$ 8,690.00

10.1.3 Assumptions for Testing Conditions

The model testing conditions follow the recommendations in sections 11.2, 11.3, and 11.4. For magnetic separation processing, the magnetic field strength will be 1 Tesla. For gravity separation processing, sodium polytungstate will be used with a specific gravity of 2.85. For electrostatic separation processing, a voltage of 29 kV will be used. The particle size of the material across all processes will be approximately 75 microns.

10.1.4 Consumable Operating Cost Assumptions

Shown in Table 10.2 are the assumed costs for process consumables based on available pricing information from the stated sources.

Table 10.2: Consumables pricing.

Item	Cost	Amount	Unit	Source
Water	\$5	1000	Gallons	
Electricity	\$0.621	1	kWh	Electricity Local
Sodium Polytungstate	\$288	1	lb	Geo Liquids

10.1.5 Employee Number, Wage, and Salary Assumptions

Shown in Table 7.3 are the assumed salaries and number of employees needed for each separation process, based on available data, industry standards, and process considerations. Both the high and low number of employees are given, with the average being used for the model calculations.

Table 10.3: Employee type, number, and wage information [57, 58, 59].

Position	Salary		Number		Annual Pay	
	Low	High	Low	High	Low	high
General	\$39,648	\$46,668	1	2	\$39,648	\$93,336
Operator						
Operations	\$66,100	\$92,800	1	2	\$66,100	\$185,600
Supervisor						
Metallurgical	\$62,725	\$73,219	1	2	\$62,725	\$146,438
Engineer						

10.1.6 Model Discount Rate

The discount rate (i^*) used for the net present value (NPV) and time value of money calculations will be 15%. This rate is the industry standard discount rate for possible operations with lots of variability still present in the operation planning [60].

10.1.7 Model Timeline

There is no estimated start date for the mining operation at Iron Creek, as site evaluations are ongoing. Therefore, for this analysis, initial model capital expenditure (CAPEX) will be assumed to occur in the year 2023, with the actual processing of material starting in 2024 and running until 2033, based on the indicated mineral resources at Iron Creek as of 2023 and expected processing capacity.

10.2 Model Capital Expenditures (CAPEX)

The larger portion of CAPEX would be the cost of the necessary separation equipment. As each process requires significantly different equipment, each process needs a unique CAPEX. Electra has no equipment on site that could be used for these processes, so new equipment will have to be purchased for each one.

10.2.1 Gravity Separation CAPEX

The CAPEX for the gravity separation process can be seen in Table 10.4. All values are conservative estimated. Equipment cost also included the necessary machines to regenerate the sodium polytungstate. The estimated CAPEX of the magnetic separation process is \$2.755 million USD.

Table 10.4: Gravity Separation CAPEX.

Expense	Factor	Cost
Major Equipment	---	\$ 450,600.00
Minor Equipment	0.9	\$ 405,540.00
Construction	0.65	\$ 556,491.00
Contingency	0.3	\$ 423,789.30
Installation Labor	0.5	\$ 918,210.15
Total		\$ 2,754,630.45

10.2.2 Electrostatic Separation CAPEX

The CAPEX for the magnetic separation process can be seen in Table 10.5. All values are conservative estimated. The estimated CAPEX of the magnetic separation process is \$4.433 million USD.

Table 10.5: Electrostatic separation CAPEX.

Expense	Factor	Cost
Major Equipment	---	\$ 725,200.00
Minor Equipment	0.9	\$ 652,680.00
Construction	0.65	\$ 895,622.00
Contingency	0.3	\$ 682,050.60
Installation Labor	0.5	\$ 1,477,776.30
Total		\$ 4,433,328.90

10.3 Model Recoveries of Separation Methods

The recoveries used in the models are based on testing results discussed in previous sections. They are shown in Table 10.6 and Table 10.7 below. The gravity and electrostatic separation process models were run using flotation concentrate as the feed material while the magnetic separation process was run using a thermal decomposition concentrate. The models were calculated assuming 2000 tonnes of material were processed per day, meaning that gravity and electrostatic separation models assumed 333 tonnes of concentrate were processed a day, while the magnetic separation model assumed 273 tonnes per day. The flowsheet and mass balance calculations used to determine this can be seen in Appendix J.

Table 10.6: Gravity separation value per tonne.

Metal	Price (\$/t)	Grade (%)	Payable Metal %	Value/tonne (\$)	Payable Value/tonne (\$)
Cobalt	49,993	1.97	95	\$984.8621	\$935.619
Copper	8,690	3.15	98	\$273.735	\$268.2603

Table 10.7: Electrostatic separation value per tonne.

Metal	Price (\$/t)	Grade (%)	Payable Metal %	Value/tonne (\$)	Payable Value/tonne (\$)
Cobalt	49,993	2.23	95	\$1,114.8439	\$1,059.10
Copper	8,690	1.31	98	\$113.839	\$111.56

10.4 Gravity Separation Model Output

The model for the gravity separation process can be seen in Table 10.8 below with the costs, profits, and returns for each year. The return in the first year of the model is negative, as all the capital needed to run the operation has been purchased but no production has begun. Each year after generates approximately \$46.9 million USD in value. This means that the payback period for the initial capital is less than a month. Based on the annual overall values generated over the model time frame, the model NPV is approximately \$532 million USD, with an internal rate of return (IRR) of 4445%. With the NPV of the model being greater than zero, it can be assumed that the model indicates that this gravity separation process is likely to have economic potential.

Table 10.8: Gravity separation model output, USD per annum.

Year	Costs	Profits	Return	Cash Flow
2023	\$ (2,754,630.45)	\$ -	\$ (2,754,630.45)	\$ (2,754,630.45)
2024	\$ (344,130.67)	\$ 122,795,688.09	\$ 122,451,557.42	\$ 119,696,926.97
2025	\$ (344,130.67)	\$ 122,795,688.09	\$ 122,451,557.42	\$ 242,148,484.38
2026	\$ (344,130.67)	\$ 122,795,688.09	\$ 122,451,557.42	\$ 364,600,041.80
2027	\$ (344,130.67)	\$ 122,795,688.09	\$ 122,451,557.42	\$ 487,051,599.21
2028	\$ (344,130.67)	\$ 122,795,688.09	\$ 122,451,557.42	\$ 609,503,156.63
2029	\$ (344,130.67)	\$ 122,795,688.09	\$ 122,451,557.42	\$ 731,954,714.05
2030	\$ (344,130.67)	\$ 122,795,688.09	\$ 122,451,557.42	\$ 854,406,271.46
2031	\$ (344,130.67)	\$ 122,795,688.09	\$ 122,451,557.42	\$ 976,857,828.88
2032	\$ (344,130.67)	\$ 122,795,688.09	\$ 122,451,557.42	\$ 1,099,309,386.29
2033	\$ (344,130.67)	\$ 122,795,688.09	\$ 122,451,557.42	\$ 1,221,760,943.71
			NPV=	\$ 532,001,220.95

10.5 Electrostatic Separation Model Output

The model for the magnetic separation process can be seen in Table 10.9 below with the costs, profits, and returns for each year. The return in the first year of the model is negative, as all the capital needed to run the operation has been purchased but no production has begun. Each year after generates approximately \$54.1 million USD in value. This means that the payback period for the initial capital is less than a month. Based on the annual overall values generated over the model time frame, the model

NPV is approximately \$231 million USD, with an internal rate of return (IRR) of 1212%. With the NPV of the model being greater than zero and the IRR larger than the model discount rate, it can be assumed that the model indicates that this electrostatic separation process is likely to have economic potential.

Table 10.4: Electrostatic separation model output, USD per annum.

Year	Costs	Profits	Return	Cash Flow
2023	\$ (4,433,328.90)	\$ -	\$ (4,433,328.90)	\$ (4,433,328.90)
2024	\$ (347,088.67)	\$ 54,057,398.30	\$ 53,710,309.63	\$ 49,276,980.73
2025	\$ (347,088.67)	\$ 54,057,398.30	\$ 53,710,309.63	\$ 102,987,290.36
2026	\$ (347,088.67)	\$ 54,057,398.30	\$ 53,710,309.63	\$ 156,697,599.99
2027	\$ (347,088.67)	\$ 54,057,398.30	\$ 53,710,309.63	\$ 210,407,909.62
2028	\$ (347,088.67)	\$ 54,057,398.30	\$ 53,710,309.63	\$ 264,118,219.25
2029	\$ (347,088.67)	\$ 54,057,398.30	\$ 53,710,309.63	\$ 317,828,528.88
2030	\$ (347,088.67)	\$ 54,057,398.30	\$ 53,710,309.63	\$ 371,538,838.51
2031	\$ (347,088.67)	\$ 54,057,398.30	\$ 53,710,309.63	\$ 425,249,148.14
2032	\$ (347,088.67)	\$ 54,057,398.30	\$ 53,710,309.63	\$ 478,959,457.78
2033	\$ (347,088.67)	\$ 54,057,398.30	\$ 53,710,309.63	\$ 532,669,767.41
			NPV=	\$ 230,544,598.23

10.6 Model Sensitivity Analysis

In order to determine how the models would react to changes in the costs or revenue, a sensitivity analysis was conducted. Capital costs (CAPEX), operating costs (OPEX), and cobalt price were examined with percent changes ranging from a 75% decrease to a 75% increase with a 15% discount rate. Changes to the discount rate were also examined, with it ranging from 5% to 25% with all costs and revenue the same as in the sections above.

10.6.1 Gravity Separation Sensitivity Analysis

Figures 10.1 and 10.2 show the sensitivity analysis for the gravity separation model. The process has a positive NPV for all scenarios and discount rates tested. The analysis looks similar to the one for magnetic separation as the CAPEX, OPEX, and revenue are similar between the two. Changing the discount rate does have some differences compared to the magnetic separation due to the CAPEX being slightly less. As NPV is heavily affected by the first few years of the model, with cashflows having less of an impact the further in the future they are, the lower initial cost results in a higher NPV, especially in the first four years of the model.

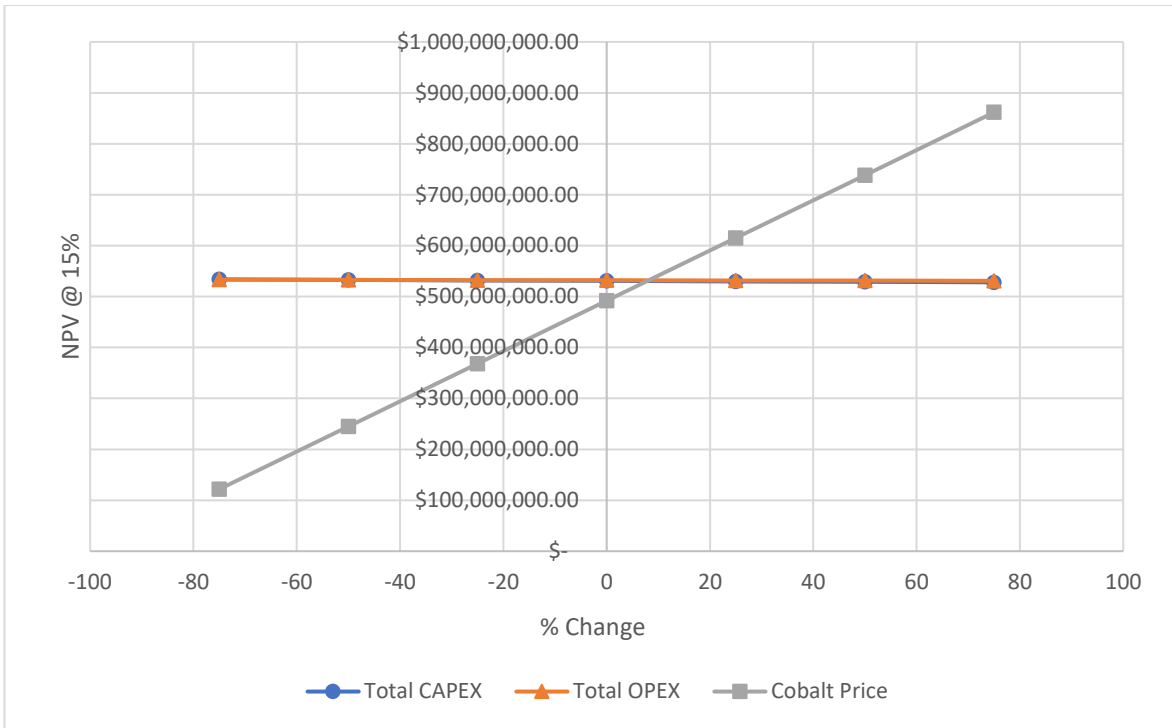


Figure 10.1: Sensitivity analysis for gravity separation model.

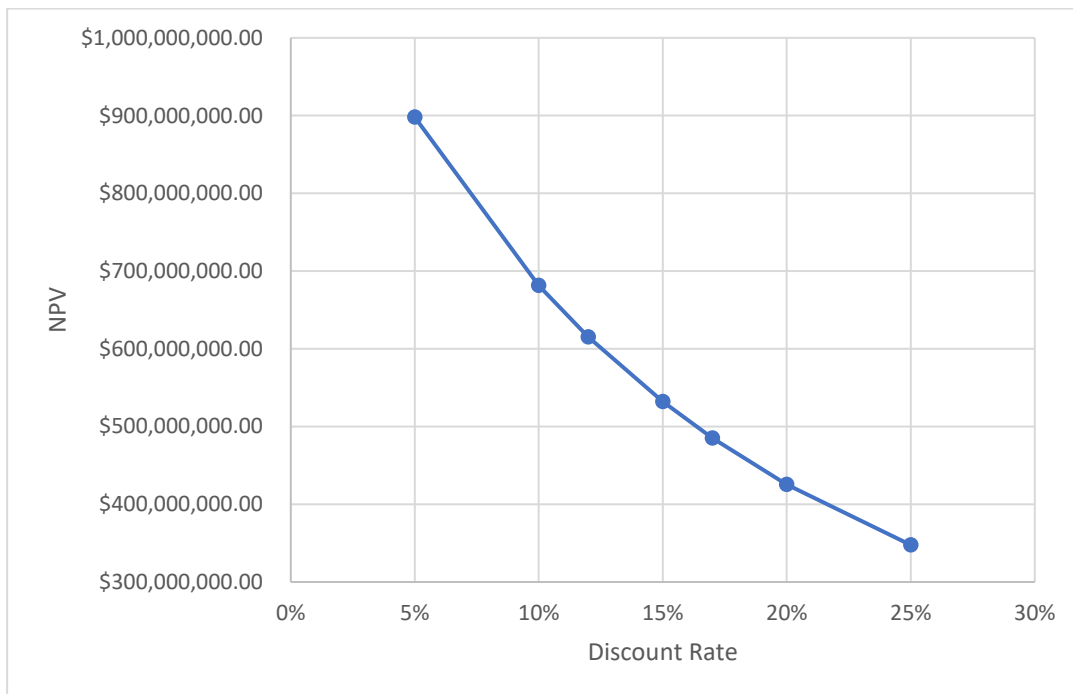


Figure 10.2: Effect of discount rate on NPV for gravity separation model.

10.6.2 Electrostatic Separation Sensitivity Analysis

Figures 10.3 and 10.4 show the sensitivity analysis for the electrostatic separation model. The process has a positive NPV for all scenarios and discount rates tested. As this model has lower CAPEX and OPEX than the other two models created, these have even less of an impact on the NPV. The NPV is still positive for all scenarios despite this. When changing the discount rate, all rates returned a positive NPV, with a maximum NPV of approximately \$390 million.

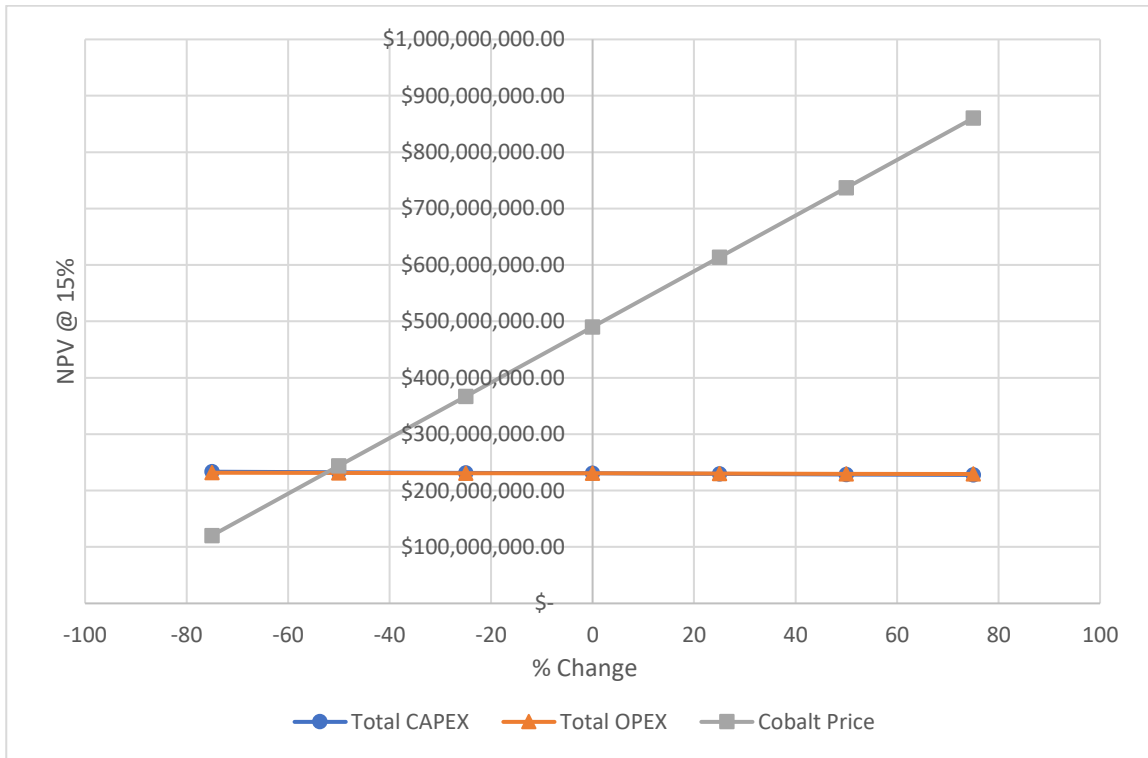


Figure 10.3: Sensitivity analysis for electrostatic separation model.

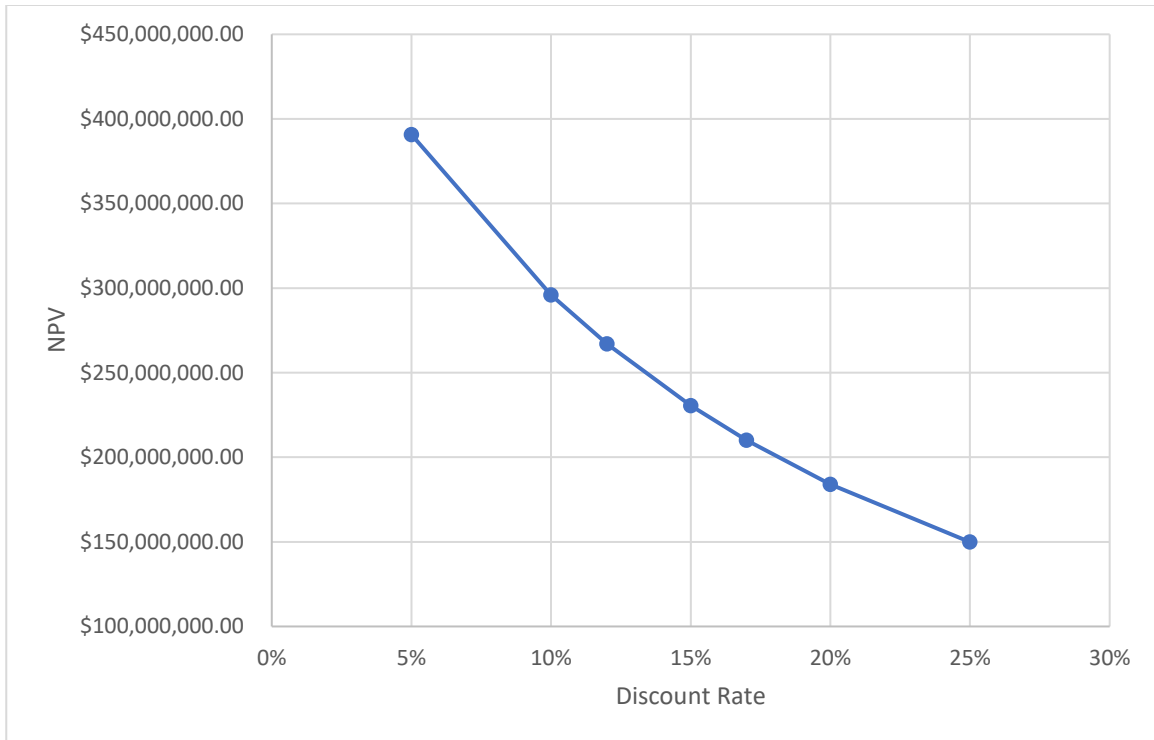


Figure 10.4: Effect of discount rate on NPV for electrostatic separation model.

10.7 Combined Economic Model

One of the goals of this project is to examine the overall economic viability for the entire process, starting with mining the material to shipping the produced concentrate to Temiskaming Shores for processing, i.e. mining, crushing, sortation, flotation, roasting, and magnetic separation as depicted in Figure 11.2. Evaluation of the whole flowsheet required the combination of three areas of research. The combined flowsheet comprises three research tasks, completed by three Luis Aguayo Torrez, Emma Bishop, and Mason Brevig. This section is a combination of all sections of research and was produced as a collaborative effort between all members of the project.

10.7.1 Combined Model Assumptions

The mining costs were estimated using Mining Cost Service (A.K.A. CostMine), as the mining operation was outside the scope of this study. It was assumed that 2000 tonnes were mined per day, with the initial cobalt and copper grades as extracted from Electra's latest technical report as part of an estimation of indicated deposit resources. This model was created with the operation running 340 days a year, 24 hours a day. For product transportation, it was assumed that the cobalt concentrate was to be sent to Temiskaming Shores, Ontario, Canada via truck and rail, while the copper concentrate was sent to the closest copper smelter, Kennocott, by truck. It was also assumed in the transportation cost that only

current infrastructure and routes would be used. This model used the industry standard discount rate for early project development, 15%, and assumed a mine life of 10 years.

10.7.2 Combined Model Output

Table 10.10 shows the capital costs for mining and all major unit operations in the process. Table 10.11 shows the yearly operating costs for mining and all major unit operations in the process along with transportation and smelter costs. Each category includes the labor, water, electricity, and other expendables needed for the process; a more detailed breakdown can be seen in Appendix J. Copper smelting costs are included here as the copper concentrate produced would be processed by a different company.

Table 10.10: Capital costs for the combined project economics.

Capital Costs	
Category	Cost (US\$)
Underground Mining	(76,543,100)
Processing	
Sortation	(850,000)
Flotation (Crushing and Grinding Included)	(41,550,700)
Thermal Decomposition	(17,811,125)
Magnetic Separation	(5,221,326)
Total	(141,976,251)

Table 10.11: Yearly operating costs for the combined project economics.

Yearly Operating Costs	
Category	Cost (US\$)
Underground Mining	(38,212,720)
Sortation	(311,556)
Flotation	(12,143,373)
Thermal Decomposition	(2,493,682)
Magnetic Separation	(383,230)
Cobalt Transportation	(11,520,920)
Copper Transportation	(105,954)
Cobalt Smelting Treatment	(14,527,240)
Cobalt Smelting Refining	(12,746)
Copper Smelting Treatment	(210,240)
Copper Smelting Refining	(3,119)
Total	(79,884,667)

The total capital cost is approximately \$US 142 MM, with approximately \$US 65 MM employing the processing methods studied in this research. Mining operating costs of US\$ 38 MM are included here as established by CostMine, while it is noted that the yearly operating cost for processing is approximately US\$ 42 MM.

Table 10.12 below shows the value of each targeted element in the concentrates produced. The price per tonne for each element is an average of the past 36-months, as prices have changed significantly over this time, especially for cobalt. Table 10.13 details the overall project cash flow.

Table 10.12: Element value for the combined economics.

Metal	Price (US\$/t)	Grade (%)	Payable Metal %	Value/tonne (US\$)	Payable Value/tonne (US\$)
Cobalt	49,993	3.50	95.0	1749.76	1662.27
Copper	8,690	6.10	98.0	530.09	519.49
Sulfur	121	NA	100.0	121.00	121.00

Table 10.13: Overall project cashflow.

Category	Cost (\$)
Capital Cost	(141,976,251)
Yearly Operating Cost	(79,884,667)
Revenue	115,181,157
CFD Yearly	35,296,490.

This model is calculated to have a yearly operating cost of approximately \$US 80 MM with a revenue of \$US 115 MM, resulting in a yearly cashflow of approximately \$US 35 MM.

Shown below in Table 10.14 shows the cumulative cash flow for the overall project.

Table 10.14: Cashflow diagram for the combined project economics.

Time (years)	Yearly Cashflow (USD)	Cumulative Cashflow (USD)
0	\$ (141,976,251.80)	\$ (141,976,251.80)
1	\$ 35,296,490.10	\$ (106,679,761.70)
2	\$ 35,296,490.10	\$ (71,383,271.60)
3	\$ 35,296,490.10	\$ (36,086,781.51)
4	\$ 35,296,490.10	\$ (790,291.41)
5	\$ 35,296,490.10	\$ 34,506,198.69
6	\$ 35,296,490.10	\$ 69,802,688.79
7	\$ 35,296,490.10	\$ 105,099,178.89
8	\$ 35,296,490.10	\$ 140,395,668.98
9	\$ 35,296,490.10	\$ 175,692,159.08
10	\$ 35,296,490.10	\$ 210,988,649.18

The NPV for the project was calculated to be \$US 35.2 MM, with an IRR of 21.2%. This indicates that the project is economically feasible and that it should be pursued as long as there are no other alternatives with a higher NPV. The payback period would be 1,469 days, or 4.03 years. This is an acceptable payback period, as it is less than the project length, though a shorter period is always preferred.

10.7.3 Sensitivity Analysis

A sensitivity analysis of the combined economic model was conducted to assess the potential risks associated with the implementation of the proposed circuit. The CAPEX, OPEX, cobalt price, copper price, and sulfur price were modified by $\pm 75%$ of the actual value calculated and its effects on the NPV are shown in Figure 10.5.

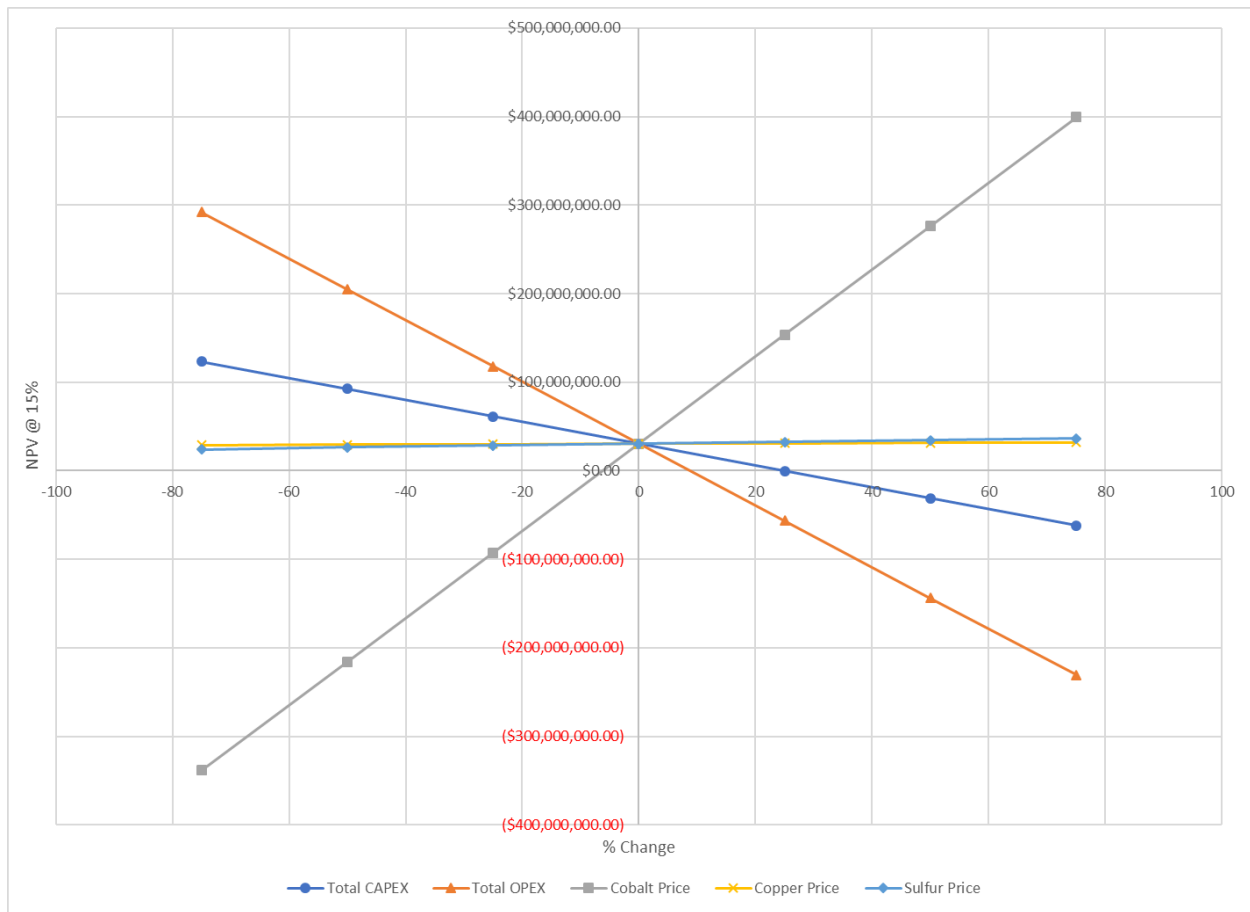


Figure 10.5: Sensitivity analysis for the combined economic model.

The cobalt price and the OPEX have the largest impacts on the model's economics, with the copper and sulfur prices having a minimal impact. Most of the tested values returned a positive NPV, but certain CAPEX, OPEX, and cobalt price scenarios returned negative NPVs, meaning that increasing the CAPEX and OPEX or decreasing the cobalt price would make the model uneconomical.

10.9 Model Comparisons and Conclusions

By comparing the annual value generated during the production years, the NPV, and the IRR of all three models, it can be concluded that while both models examined are likely to be economically favorable, the gravity separation process has the superior economics. This is most likely due to the grade of the cobalt in the feed material used in the gravity separation process model being higher, which was due to its location in the process flowsheet. The IRR of the magnetic separation process is also much higher than the electrostatic separation process, meaning that it is a more desirable investment to make.

It should be noted that these models do not consider the costs associated with processing and recovering the copper and cobalt before or after these processes take place. These models only look at the potential economic impact of these steps in isolation and the required processes needed to actually create a final product will most likely have an impact on the overall economics.

The combined economic model shows that the overall model is also economically feasible, with an NPV of \$US 35.2 MM and an IRR of 21.2%. These are less than the individual processes, as there are more processes involved and the revenue does not change compared to the individual process model.

CHAPTER 11. CONCLUSIONS

Most of the physical beneficiation methods tested to concentrate cobalt-bearing minerals were successful. The exception to this was most of the magnetic separation tests, primarily the testing that did not use a thermal decomposition product as the feed material.

Testing showed that gravity and electrostatic separation methods were able to remove the gangue materials from the targeted materials but were not able to create a separation between the cobalt-bearing materials and the copper- and iron-bearing minerals, with maximum grade increases of 132% and 151%, respectively, and recoveries for both being greater than 80% in testing with the deposit samples. This can be partially attributed to the fact that the cobalt contained within pyrite, so iron will always concentrate with the cobalt to some degree. The iron- and copper-bearing minerals also have similar properties to the cobalt-bearing materials, so they will often end up in the same fraction. This was supported by statistical analysis, as ANOVA testing done on various testing conditions showed that factors such as the particle size and RPM in the heavy liquid separation test and the voltage used in the electrostatic separation testing are able to produce a statistically significant separation between the target materials and the waste rock.

The effectiveness of the magnetic separation testing depended on the tested material. The deposit sample and all flotation materials had minimal reactions to the magnetic fields tested, with the maximum recoveries for cobalt and copper being in the range of 10-15%. Increases in grade and recovery occurred in the non-magnetic fraction, though it was due to minor amounts of iron-based minerals being pulled to the magnetic fraction. It was shown through statistical analysis that this increase was significant though, and not just due to minor variations in the feed material sample used. The flotation concentrates tested also had a similar reaction as the feed material, with only small increases in grade taking place with poor recovery.

Magnetic separation testing done with thermal decomposition products had an extremely positive reaction to the magnetic field, resulting in cobalt grade increases up to 60% and recoveries greater than 90%. Experiments at higher field intensities during testing lead to greater grades and recoveries, however, statistical analysis of the test results comparing feed material and magnetic field intensity found that there was no statistical significance in the test results for nearly all results. This may have been due to not enough tests being performed due to a lack of material to create a large enough test set, possibly altering the results.

Sulfuric acid leaching testing done on the thermal decomposition product of magnetic separation testing showed was not successful. Recoveries for all tested elements were very poor, with less than 10%

of the target elements reporting to the leachate in most tests. Testing did confirm that an oxidizer is needed for leaching of the target elements to occur and that leaching is more effective if the temperature of the leaching environment is elevated.

Though the magnetic, gravity, and electrostatic separation methods tested were shown to be effective, the economic analysis showed that all of them are unlikely to be economically viable. All the economic models performed had negative NPVs, though all the IRR were higher than the discount rate used. A possible solution to this is the price of cobalt. The price of cobalt has dropped significantly in the past year and as a result, some cobalt operations have had to shut down. Economics analysis ran with 2022 cobalt prices returned a positive NPV. While the price of cobalt cannot be controlled, even a small rise could make the processes economically viable.

11.1 Proposed Flowsheets

This project was 1/3 of a larger project that looked at possible ways to combine flotation, thermal decomposition, and various physical beneficiation methods together to create an economical flowsheet. The first theoretical flowsheet produced that could be used to concentrate cobalt at the Iron Creek deposit is shown in Figure 8.1 below. The various physical separation methods could be used in multiple ways and combinations but the most promising appears to be magnetic separation. The material would be processed by XRD sortation, a rougher flotation, differential flotation, and then thermal decomposition before being subjected to a form of magnetic separation to remove pyrrhotite, and with it the cobalt.

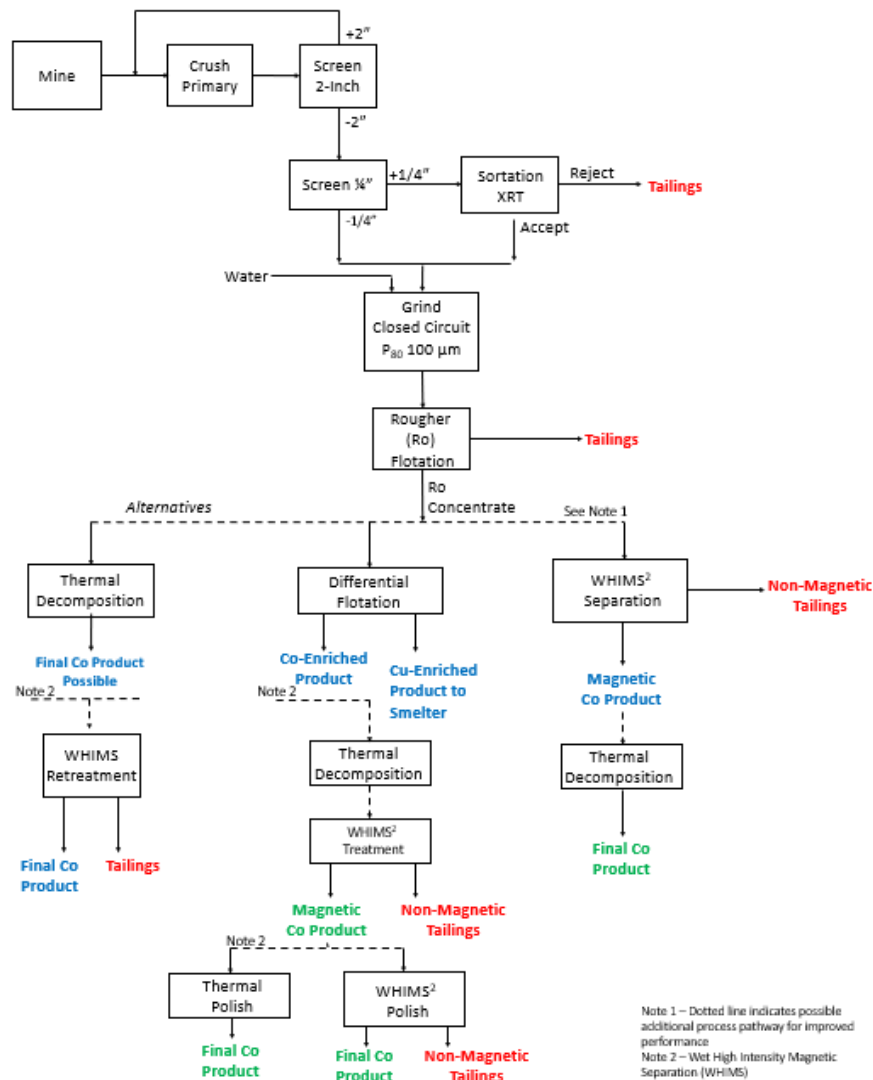


Figure 11.1: First possible proposed flowsheet for the concentration of cobalt at the Iron Creek Deposit.

Figure 11.2 shows the refined proposed flowsheet for the Iron Creek deposit. It was determined that thermal decomposition had to occur before the magnetic separation for a significant separation to take place, so the branch without thermal decomposition was removed. Any polish steps after the magnetic separation were also removed. Sulfur dust was added as a product of thermal decomposition, as it was determined that it could be used later in the process to create acid or sold as a by-product. A version of the refined flowsheet with mass balances can be found in Appendix K.

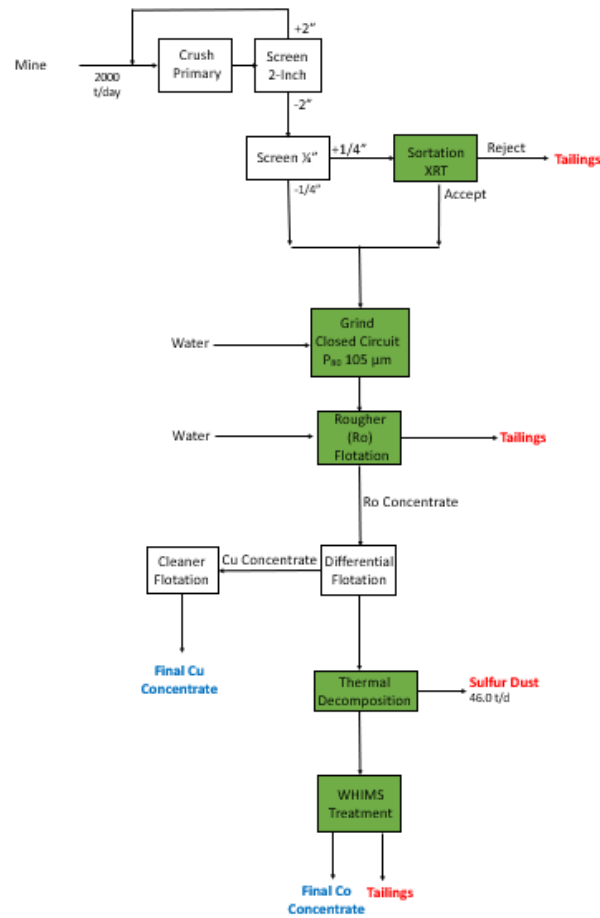


Figure 11.2: Proposed flowsheet for the concentration of cobalt at the Iron Creek Deposit.

11.2 Further Work

While the testing done in this study shows promising results, further testing is needed to confirm and expand on these findings.

11.2.1 Magnetic Separation Further Work

Based on testing results, the future testing conditions for magnetic separation could include testing cobalt concentration and recovery at higher magnetic field intensities. Testing done in this report was limited to a maximum of 1.0 Tesla due to machine limitations. Trends in the testing showed the recovery and grade were increasing with increasing magnetic field intensities up to the maximum achievable intensity by the machine, and further testing could be done to determine if this trend continues or if it tapers off at higher intensities.

Examining the effects of different matrices is also recommended. The shape of the matrix changes how the material moves through the WHIMS and the chance that the material reports to the correct fraction. Most testing in this report was done on the type of matrix depending on the particle size

of the material being tested; expanded metal mesh for deposit sample testing and fine metal mesh for flotation and thermal decomposition products. Testing different matrices could affect the amount of reporting material and reveal if the matrix is being overloaded in any way, causing material to be trapped.

11.2.2 Gravity Separation Further Work

Based on the testing results, it is recommended to test other heavy liquids. Sodium polytungstate is one of the least dangerous and toxic heavy liquids, making it ideal for testing in a laboratory setting. However, it has a limited and low specific gravity range and is difficult to process. Testing with other heavy liquids could show what the deposit sample behavior is at higher specific gravities and result in more effective or useful separation. Potential heavy liquids that could be tested are bromoform and tetrabromoethane, as they are the most common in coal separation, which often involves pyrite.

Additional gravity separation testing could be looked at other gravity separation testing techniques. This report only looked at heavy liquid separation, as it is a suitable indicator of the response, but there are several other gravity separation techniques. Some techniques to look into would be a Falcon concentrator and a spiral concentrator, as they are already used in pyrite separation, mainly from coal, and bench scale testing is common.

11.2.3 Electrostatic Separation Further Work

Based on testing results, future testing could include changing more parameters in the test than just the voltage. The machine used in testing was limited to only altering the voltage, but other possible changes could include feed roll speed, temperature of the hopper or roll, and the location of the splitters. Changing roll speeds would affect how long the materials are exposed to the magnetic field, possibly allowing for more or less material to send to the concentrate. Changing the temperature of the hopper or roll would change the temperature of the materials being tested, altering the conductivity of the material. Changing the location of the splitters would change the cut of the concentrate, affecting both possible grade and recovery of the concentrate. It should be noted that changing the splitter location would have an inverse effect, increasing either the grade or recovery while decreasing the other.

11.2.4 Leaching Further Work

Some interesting further testing would be to examine the Eh during the leaching process more closely. It was assumed during testing that the lack of leaching was due to all the sodium peroxide being consumed before the cobalt could be completely leached. Monitoring the Eh would be able to confirm this and show the rate the sodium peroxide is being consumed. Testing different amounts and types of oxidizers would also be informative to see how the leaching process is affected.

Additional further testing could include testing the leaching with different acids or adjusting the pH of the leaching environment. Sulfuric acid was used during testing as that is what is expected to be

used by Electra at their processing plant, but leaching can be done with different acids. Pressure acid leaching could also be considered, as it can speed up the leaching process. Changing the pH of the leaching system could also yield some interesting results. Looking at the Eh-pH diagrams in Section 9.1, increasing the pH reduces the Eh of the system needed to create some of the targeted products. This could help with the issue of all the oxidizer being consumed before the leaching is complete.

REFERENCES

- [1] J. Burton, "U.S. Geological Survey Releases 2022 List of Critical Minerals," United States Geological Survey, 2022.
- [2] "Final List of Critical Minerals 2022," IEA, 2022. [Online]. Available: <https://www.iea.org/policies/15271-final-list-of-critical-minerals-2022>. [Accessed 3 February 2023].
- [3] "Cobalt," Royal Society of Chemistry, [Online]. Available: <https://www.rsc.org/periodic-table/element/27/cobalt>. [Accessed 12 10 2022].
- [4] F. W. Schwartz, S. Lee and T. H. Darrah, "A Review of the Scope of Artisanal and Small-Scale Mining Worldwide, Poverty, and the Associated Health Impacts," *GeoHealth*, vol. 5, no. 1, 2021.
- [5] A. L. Gulley, E. A. McCullough and K. B. Shedd, "China's Domestic and Foreign Influence in the Global Cobalt Supply Chain," *Resources Policy*, vol. 62, pp. 317-323, 2019.
- [6] "Sao Miguel Paulista Refinery," Jervois, 2023. [Online]. Available: <https://jervoisglobal.com/projects/sao-miguel-paulista-refinery/>. [Accessed 21 2 2023].
- [7] Y. Kim, W. M. Seong and A. Manthiram, "Cobalt-free, High-nickel Layered Oxide Cathodes for Lithium-ion Batteries: Progress, Challenges, and Perspectives," *Energy Storage Materials*, vol. 34, pp. 250-259, 2021.
- [8] M. Li and J. Lu, "Cobalt in Lithium-ion Batteries," *Science*, vol. 367, no. 6841, pp. 979-980, 2020.
- [9] A. A. Bookstrom, "The Idaho Cobalt Belt," *Northwest Geology*, vol. 42, pp. 149-162, 2013.
- [10] J. L. Nold, "The Idaho Cobalt Belt, Northwestern United States — A Metamorphosed Proterozoic Exhalative Ore District," *Mineralium Deposita*, vol. 25, no. 3, pp. 163-168, 1990.
- [11] "Blackbird MRDS," USGS, [Online]. Available: https://mrdata.usgs.gov/mrds/show-mrds.php?dep_id=10144621. [Accessed 21 2 2023].
- [12] "Idaho Cobalt Project," Mining Technology, 24 September 2018. [Online]. Available: <https://www.mining-technology.com/projects/idaho-cobalt-project/>. [Accessed 21 2 2023].
- [13] Q. Dehaine, L. T. Tijsseling, H. J. Glass, T. Tormanen and A. R. Butcher, "Geometallurgy of cobalt ores: A review," *Minerals Engineering*, 2021.
- [14] "The Element Cobalt," JLab Science Education, [Online]. Available: <https://education.jlab.org/itselemental/ele027.html>. [Accessed 21 February 2023].
- [15] "Cobalt," Britannica, 15 February 2023. [Online]. Available: <https://www.britannica.com/science/cobalt-chemical-element>. [Accessed 21 February 2023].
- [16] "Technical Data for Cobalt," periodictable.com, [Online]. Available: <https://periodictable.com/Elements/027/data.html>. [Accessed 21 February 2023].

- [17] "Cobalt – Strength – Hardness – Elasticity – Crystal Structure," material-properties.org, [Online]. Available: <https://material-properties.org/cobalt-mechanical-properties-strength-hardness-crystal-structure/>. [Accessed 21 February 2023].
- [18] "Cobalt (Co) – Properties, Applications," azom.com, 12 July 2013. [Online]. Available: <https://www.azom.com/article.aspx?ArticleID=9077>. [Accessed 21 February 2023].
- [19] "Curie Point," Britannica, 7 March 2016. [Online]. Available: <https://www.britannica.com/science/Curie-point>. [Accessed 21 February 2023].
- [20] "Cobalt," British Geological Survey, 2008. [Online]. Available: www.MineralsUK.com. [Accessed 21 February 2023].
- [21] S. A. Nelson, "Mineral Chemistry," Tulane University, 30 September 2013. [Online]. Available: https://www2.tulane.edu/~sanelson/eens211/mineral_chemistry.htm#:~:text=The%20size%20of%20the%20ions,to%20fit%20into%20the%20site.. [Accessed 26 July 2023].
- [22] USGS, "Cobalt Data Sheet - Mineral Commodity Summaries 2020," 2020.
- [23] A. Kracke, "Superalloys, The Most Successful Alloy System Of Modern Times - Past, Present, and Future," in *The Minerals, Metals & Materials Society*, 2010.
- [24] B. Ohl, F. Xue, P. T. Jacques, D.-W. Chung and F. Reyes, "Cobalt-based Superalloys," *Dunand Research Group*.
- [25] S. Wang, "Cobalt—Its Recovery, Recycling, and Application," *JOM*, no. 58, pp. 47-50, 2006.
- [26] USGS, "Mineral Commodity Summaries 2022 - Cobalt," USGS, 2022.
- [27] U. G. Survey, "Mineral Commodity Summaries: Cobalt," U.S. Geological Survey, 2020.
- [28] "Leading Countries Based on Annual Cobalt Refinery Capacity as of 2019," 23 September 2022. [Online]. Available: <https://www.statista.com/statistics/339798/annual-cobalt-refinery-capacity-by-country/>.
- [29] P. A. Lusty and B. J. Murton, "Deep-Ocean Mineral Deposits: Metal Resources and Windows into Earth Processes," *Elements*, vol. 14, no. 5, pp. 301-306, 2018.
- [30] Sudiby, A. S. Handoko, A. Junaedi, U. Herlina, S. Sumardi, F. R. Mufakhir, F. Nurjaman, Y. I. Supriyatna, L. Hermida and D. Fatmawati, "Separation of Cobalt from Slag of Nickel Pig Iron Using," *AIP Conference Proceedings*, vol. 2382, no. 1, 2021.
- [31] Sudiby, L. Hermida, S. F. Isfrianti, A. Junaedi, A. S. Handoko, U. Herlina, F. R. Mufakhir, S. Sumardi, Y. I. Supriyatna and F. Nurjaman, "Cobalt Recovery from the Slag of Nickel Pig Iron using," *AIP Conference Proceedings*, vol. 2381, no. 1, 2021.
- [32] K. G. Fisher, "Cobalt Processing Developments," in *6th Southern African Base Metals Conference*, 2011.

- [33] "Magnetic Dipole," *Encyclopedia Britannica*, 04 August 2022. [Online]. Available: <https://www.britannica.com/science/magnetic-dipole>. [Accessed 4 June 2023].
- [34] W. J. Bronkala, "Magnetic Separation," in *Ullmann's Encyclopedia of Industrial Chemistry*, vol. 22, 2000, pp. 133-144.
- [35] "Ferromagnetic vs Paramagnetic vs Diamagnetic: What's the Difference?," *OneMonroe Engineering*, 23 February 2022. [Online]. Available: <https://monroeengineering.com/blog/ferromagnetic-vs-paramagnetic-vs-diamagnetic-whats-the-difference/#:~:text=Ferromagnetic%20materials%20are%20strongly%20attracted,repel%20both%20poles%20of%20magnets.> . [Accessed 22 February 2023].
- [36] R. E. Hucko and K. J. Miller, "A Technical Performance Comparison of Coal-Pyrite Flotation and High-Gradient Magnetic Separation," in *AIME Annual Meeting*, Chicago, 1981.
- [37] F. Ye, J. Liu, T. Xiong and M. Xie, "Arsenopyrite Removal from Pyrite Concentrate using Pulsating High Gradient," *Physics*, vol. 10, pp. 822-826, 2018.
- [38] R. Liu, N. Jing, Y. Song, Q. Zhai, Z. Mao, Y. Zhou and W. Sun, "Recovery of Valuable Elements from Pyrite Pyrolysis Slag using Magnetic Separation-Flotation Technique," *Separation and Purification Technology*, vol. 299, pp. 1-9, 2022.
- [39] T. Uslu, U. Atalay and A. Arol, "Effect of Microwave Heating on Magnetic Separation of Pyrite," *Colloids and Surfaces A: Physicochem. Eng. Aspects*, vol. 225, pp. 161-167, 2003.
- [40] N. Can and B. I., "Effects of Microwave Treatment on the Flotation and Magnetic Separation Properties of Pyrite, Chalcopyrite, Galena, and Sphalerite," *Minerals & Metallurgical Processing*, vol. 24, no. 3, pp. 185-192, 2007.
- [41] "Specific Gravity," *Britannica*, 1 November 2022. [Online]. Available: <https://www.britannica.com/science/specific-gravity>. [Accessed 22 February 2023].
- [42] R. O. Burt, "Gravity Concentration," in *Ullmann's Encyclopedia of Industrial Chemistry*, vol. 17, 2000, pp. 167-174.
- [43] R. O. Burt, "Dense-Medium Separation," in *Ullmann's Encyclopedia of Industrial Chemistry*, vol. 11, 2000, pp. 87-93.
- [44] A. A. Terchick, "Comparison of Concentrating Tables, Hydroclones, and Heavy-Medium Units for Achieving Maximum Sulfur Reduction on 1/4-Inch by 28-Mesh Coal," in *Coal Preparation Section, Society of Mining Engineers of AIME*, New York, 1971.
- [45] "Removing Sulfur From Coal by a Combination of Gravity and Flotation Methods," *Mining Engineering*, pp. 1221-1224, 1982.
- [46] "About Conductivity," *University of Cambridge*, [Online]. Available: <https://www.lehigh.edu/~amb4/wbi/kwardlow/conductivity.htm#:~:text=Conductivity,electric%20current%20or%20thermal%20energy..> [Accessed 22 February 2023].

- [47] M. Dotterl, U. Wachsmuth, L. Waldmann, Flachberger, M. Mirkowska, L. Brands, P.-M. Beier and I. Stahl, "Electrostatic Separation," in *Ullmann's Encyclopedia of Industrial Chemistry*, 2016, pp. 1-35.
- [48] "Work Function," Chemeurope.com, [Online]. Available: https://www.chemeurope.com/en/encyclopedia/Work_function.html. [Accessed 23 June 2023].
- [49] D. Inculet, R. Quigley and I. Inulet, "Electrostatic Separation of Sulphides from Quartz: A Potential Method for Mineral Beneficiation," *Journal of Electrostatics*, vol. 34, no. 1, pp. 17-25, 1995.
- [50] F. Abrahamsson, "Leaching of Pyrrhotite from Nickel Concentrate," 2017.
- [51] J. Makinen, G. Pietek, Miettinen, Ville, M. Khoshkhoo, J.-E. Sundkvist and P. Kinnunen, "Removal of Pyrrhotite from High-Sulphur Tailings Utilising Non-Oxidative H₂SO₄ Leaching," *Minerals*, vol. 12, no. 12, 2022.
- [52] T. A. Chepushtanova, K. K. Mamyrbayeva and V. A. . Luganov, "Mechanism of Nonoxidizing and Oxidative Pyrrhotite Leaching," *Minerals and Metallurgical Processing*, vol. 29, no. 3, pp. 159-164, 2012.
- [53] M. M. Antonijevid, M. Dimitrijevid and Z. Jankovic, "Leaching of Pyrite with Hydrogen Peroxide in Sulphuric Acid," *Hydrometallurgy*, no. 46, pp. 71-83, 1997.
- [54] "The Iron Creek Cobalt-Copper Project," Electra Battery Minerals, [Online]. Available: <https://electrabmc.com/our-business/iron-creek/>. [Accessed 21 2 2023].
- [55] "Experimental Characterization of Chalcopyrite Ball Mill Grinding Process in Batch and Continuous Flow Processing Modes to Reduce Energy Consumption," *Journal of Materials Research and Technology*, no. 15, pp. 5428-5444, 2021.
- [56] "Table of Bond Work Index by Minerals," 911 Metallurgist, 19 June 2015. [Online]. Available: <https://www.911metallurgist.com/blog/table-of-bond-work-index-by-minerals>. [Accessed 7 July 2023].
- [57] "Miner Operator Salary in Idaho," Salary.com, [Online]. Available: <https://www.salary.com/research/salary/hiring/miner-operator-salary/id?pay=month#sa-section-hps>. [Accessed 25 July 2023].
- [58] "Mining Manager Salary in Idaho," Salary.com, [Online]. Available: <https://www.salary.com/research/salary/alternate/mining-manager-salary/id>. [Accessed 25 July 2023].
- [59] "Metallurgical Engineer I Salary in Boise, Idaho," Salary.com, [Online]. Available: <https://www.salary.com/research/salary/benchmark/metallurgical-engineer-i-salary/boise-id>. [Accessed 25 July 2023].
- [60] "Statement on Longer-Run Goals and Monetary Policy Strategy," 31 January 2023. [Online]. Available: https://www.federalreserve.gov/monetarypolicy/files/fomc_longerrungoals.pdf. [Accessed 25 July 2023].

[61] A. F. B. K. J. Miller, "Electrophoretic-Specific Gravity," United States Department of the Interior, 1970.

APPENDICES

APPENDIX A. Elemental Characterization

Table A.1: Full elemental analytical report for Run-of-Mine samples

	Client Sample ID:		IC-18-07	IC-18-09	IC-18-27
ATOMIC NUMBER	ELEMENT NAME	ELEMENT SYMBOL	Conc µg/g	Conc µg/g	Conc µg/g
1	Hydrogen	H	NA	NA	NA
2	Helium	He	NA	NA	NA
3	Lithium	Li	21	15	18
4	Beryllium	Be	1	1	< 1
5	Boron	B	NA	NA	NA
6	Carbon	C	NA	NA	NA
7	Nitrogen	N	NA	NA	NA
8	Oxygen	O	NA	NA	NA
9	Fluorine	F	NA	NA	NA
10	Neon	Ne	NA	NA	NA
11	Sodium	Na	3500	10300	1270
12	Magnesium	Mg	8720	9310	8630
13	Aluminum	Al	57500	59100	50200
14	Silicon	Si	NA	NA	NA
15	Phosphorus	P	400	400	700
16	Sulfur	S	61600	52100	93400
17	Chlorine	Cl	NA	NA	NA
18	Argon	Ar	NA	NA	NA
19	Potassium	K	37000	23200	30500
20	Calcium	Ca	1260	1420	956
21	Scandium	Sc	10	14	15
22	Titanium	Ti	2730	2820	2400
23	Vanadium	V	39	41	15
24	Chromium	Cr	312	336	384
25	Manganese	Mn	388	433	433
26	Iron	Fe	100000	94600	123000
27	Cobalt	Co	2685	2083	3404
28	Nickel	Ni	< 1	< 1	< 1
29	Copper	Cu	2476	1248	13987
30	Zinc	Zn	53	36	112
31	Gallium	Ga	29	28	29
32	Germanium	Ge	< 1	< 1	< 1
33	Arsenic	As	323	292	499
34	Selenium	Se	24	20	40
35	Bromine	Br	NA	NA	NA
36	Krypton	Kr	NA	NA	NA
37	Rubidium	Rb	116	94	80
38	Strontium	Sr	29	48	16

Table A.1 Continued

39	Yttrium	Y	12	17	10
40	Zirconium	Zr	117	94	86
41	Niobium	Nb	11	11	8
42	Molybdenum	Mo	24	15	23
43	Technetium	Tc	NA	NA	NA
44	Ruthenium	Ru	< 1	< 1	< 1
45	Rhodium	Rh	< 1	< 1	< 1
46	Palladium	Pd	< 1	< 1	< 1
47	Silver	Ag	< 1	< 1	6
48	Cadmium	Cd	1	< 1	< 1
49	Indium	In	< 1	< 1	1
50	Tin	Sn	< 1	< 1	< 1
51	Antimony	Sb	< 1	< 1	< 1
52	Tellurium	Te	NA	NA	NA
53	Iodine	I	NA	NA	NA
54	Xenon	Xe	NA	NA	NA
55	Cesium	Cs	NA	NA	NA
56	Barium	Ba	1506	605	1394
57	Lanthanum	La	35	46	48
58	Cerium	Ce	123	126	154
59	Praseodymium	Pr	9	11	13
60	Neodymium	Nd	33	40	42
61	Promethium	Pm	NA	NA	NA
62	Samarium	Sm	7	8	9
63	Europium	Eu	1	1	2
64	Gadolinium	Gd	6	7	7
65	Terbium	Tb	< 1	< 1	< 1
66	Dysprosium	Dy	3	4	3
67	Holmium	Ho	< 1	< 1	< 1
68	Erbium	Er	1	2	< 1
69	Thulium	Tm	< 1	< 1	< 1
70	Ytterbium	Yb	2	2	1
71	Lutetium	Lu	< 1	< 1	< 1
72	Hafnium	Hf	NA	NA	NA
73	Tantalum	Ta	NA	NA	NA
74	Tungsten	W	NA	NA	NA
75	Rhenium	Re	NA	NA	NA
76	Osmium	Os	NA	NA	NA
77	Iridium	Ir	< 1	< 1	< 1
78	Platinum	Pt	< 1	< 1	< 1
79	Gold	Au	< 1	< 1	< 1
80	Mercury	Hg	NA	NA	NA
81	Thallium	Tl	< 1	< 1	< 1
82	Lead	Pb	27	13	40
83	Bismuth	Bi	12	10	17
90	Thorium	Th	3	2	< 1
92	Uranium	U	7	5	5

APPENDIX B. Bond Work Index G_{pr} , F_{80} , P_{80} Data

Table B.1. G_{pr} data sample for IC 18-07

Cycle #	New Feed (g)	Undersized in Feed	Mat'l to be ground	Revolutions (calculated)	Revolutions (Whole #)	Product Produced	Net Undersized	Grams/rev
1	1388.4	224.9	171.8	100	100	567.3	342.4	3.424
2	574.4	93.1	303.6	88.68	89	307.8	277.7	3.132
3	378.3	61.3	335.4	107.09	107	396.6	335.3	3.134
4	405.6	65.7	331.0	105.61	106	390.9	325.2	3.068
5	400.5	64.9	33.18	108.15	108	395.5	330.6	3.061
6	403.8	65.4	331.3	108.22	108	409.9	344.5	3.19
7	420.2	68.1	328.6	103.01	103	392.1	324.0	3.146
8	400.5	64.9	331.8	105.47	105	380.9	316.0	3.01
9	387.7	62.8	333.9	110.92	111	405.7	342.9	3.089
10	413.9	67.1	329.6	106.71	107	414	346.9	3.243
11	422.9	68.5	328.2	101.2	101	375.4	306.9	3.039
12	382.9	62	334.7	110.12	110	404.1	342.1	3.11
13	411.7	66.7	330.0	106.11	106	389.3	322.6	3.034

Table B.2. G_{pr} data sample for IC 18-09

Cycle #	New Feed (g)	Undersized in Feed	Mat'l to be ground	Revolutions (calculated)	Revolutions (Whole #)	Product Produced	Net Undersized	Grams/rev
1	1272.6	133.5	230.1	100	100	328.6	195.1	1.95
2	333.8	35.0	328.6	168.505	168	373.8	338.8	2.011
3	378.5	39.7	323.9	161.06	161	262.6	322.9	2.006
4	371.1	38.9	324.7	161.85	162	369	330.1	2.037
5	376.4	39.5	324.1	159.11	159	365.8	326.3	2.052
6	373.3	39.2	324.4	158.11	158	343.8	304.6	1.928
7	351.5	36.9	326.7	169.46	169	384.3	347.4	2.056
8	393.5	41.3	322.3	156.77	157	360.2	318.9	2.031
9	367.4	38.5	325.1	160.05	160	367.8	329.3	2.058

Table B.3. G_{pr} data sample for IC 18-27

Cycle #	New Feed (g)	Undersized in Feed	Mat'l to be ground	Revolutions (calculated)	Revolutions (Whole #)	Product Produced	Net Undersized	Grams/rev
1	1443.7	233.9	178.6	100	100	484.7	250.8	2.508
2	493.8	80.0	332.5	132.57	133	434.3	354.3	2.673
3	441.5	71.5	341.0	127.56	128	463	391.5	3.058
4	472.8	76.6	335.9	109.84	110	358.4	281.8	2.562
5	368.6	59.7	352.8	137.69	138	426.9	367.2	2.661
6	433	70.0	342.3	128.65	129	425.6	355.5	2.755
7	432.4	70.1	342.4	124.30	124	408.8	338.8	2.732

Table B.4. F₈₀ data for sample IC 18-07

Size (tyler mesh)	Size (microns)	Mass (g)	% retained	Cum. % retained	Cum. % passing
6	3360	0.4	0.13	0.13	99.86
8	2830	60.7	19.98	20.11	79.89
10	1680	68.1	22.42	42.53	57.47
12	1410	29.3	9.64	52.17	47.83
16	1000	33.4	10.99	63.17	36.83
20	841	11.5	3.79	66.95	33.05
Pan	0	100.4	33.05	100	0.00

Table B.5. F₈₀ data for sample IC 18-09

Size (tyler mesh)	Size (microns)	Mass (g)	% retained	Cum. % retained	Cum. % passing
6	3360	1.7	0.76	0.76	99.24
8	2830	60.4	27.11	27.87	72.13
10	1680	45.3	20.33	48.20	51.80
12	1410	16.7	7.50	55.70	44.30
16	1000	21.7	9.74	65.44	34.56
20	841	7.7	3.46	68.90	31.10
Pan	0	69.3	31.10	100	0.00

Table B.6. F₈₀ data for sample IC 18-27

Size (tyler mesh)	Size (microns)	Mass (g)	% retained	Cum. % retained	Cum. % passing
6	3360	0.25	0.25	99.75	0.25
8	2830	26.66	26.91	73.09	26.66
10	1680	23.90	50.80	49.20	23.90
12	1410	8.24	59.04	40.96	8.24
16	1000	9.81	68.85	31.15	9.81
20	841	3.17	72.02	27.98	3.17
Pan	0	27.98	100.00	0.00	27.98

Table B.7 P₈₀ for sample IC 18-07

Size (tyler mesh)	Size (microns)	Mass (g)	% retained	Cum. % retained	Cum. % passing
100	149	0.0	0	0	0
115	125	9.7	9.70	5.66	5.66
150	105	11.2	11.20	6.54	12.20
200	74	22.2	22.20	12.96	25.16
270	53	19.1	19.10	11.15	36.31
400	37	20.5	20.50	11.97	48.27
Pan	0	98.3112	98.31	57.39	100.00

Table B.8 P₈₀ for sample IC 18-09

Size (tyler mesh)	Size (microns)	mass (g)	% retained	Cum. % retained	Cum. % passing
100	149	0.00	0.00	0.00	100.00
115	125	14.40	9.05	9.05	90.95
150	105	14.90	9.36	18.40	81.60
200	74	25.10	15.77	34.17	65.83
270	53	19.50	12.25	46.42	53.58
400	37	19.60	12.31	58.73	41.27
Pan	0	80.10	50.31	100.00	0.00

Table B.9 P₈₀ for sample IC 18-09

Size (tyler mesh)	Size(microns)	mass (g)	% retained	Cum. % retained	Cum. % passing
100	149	0.00	0.00	0.00	100.00
115	125	11.9	6.57	6.57	93.43
150	105	14.3	7.90	14.48	85.52
200	74	27.7	15.30	29.78	70.22
270	53	24.2	13.37	43.15	56.85
400	37	24.5	13.54	56.69	43.31
Pan	0	90.293	49.89	100.00	0.00

APPENDIX C. Additional Magnetic Separation Washability Curves

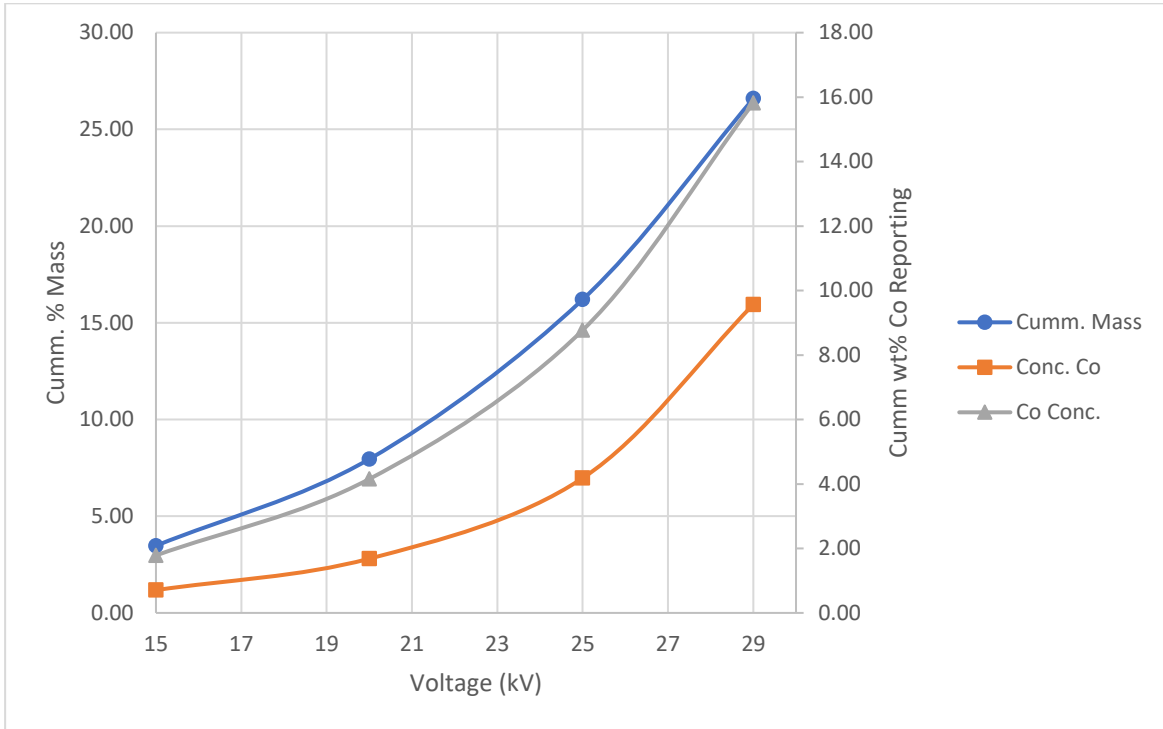


Figure C.1: Feed Material Tailings Fraction Elemental Concentration Response

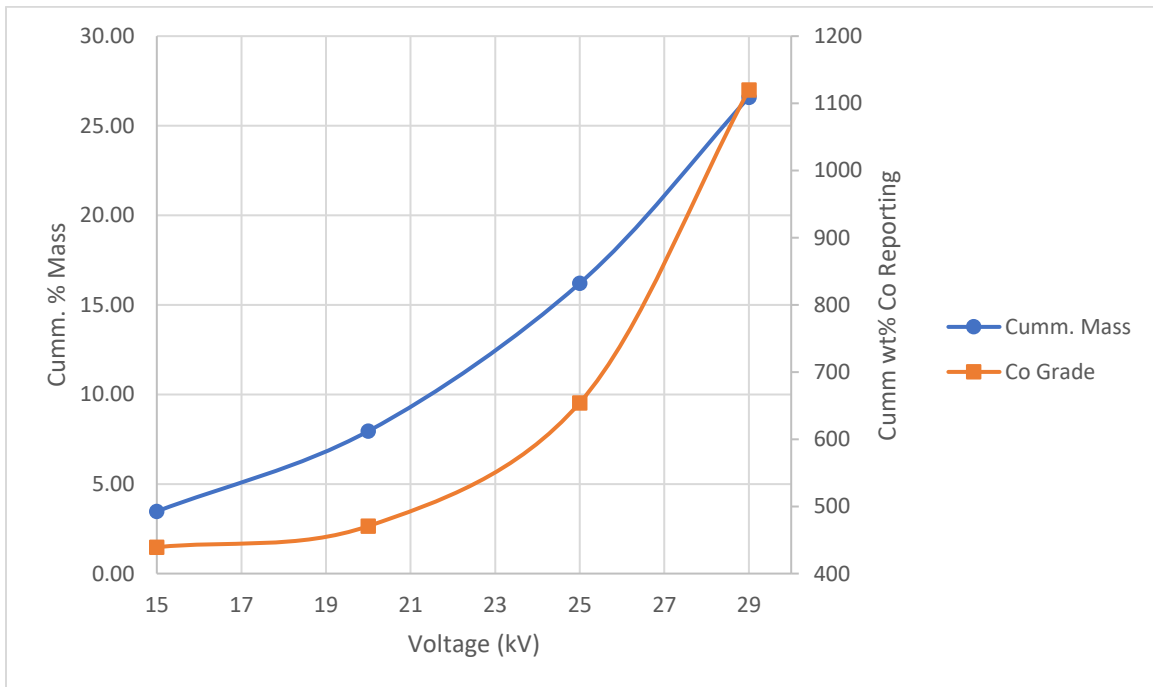


Figure C.2: Feed Material Cobalt Grade by Step

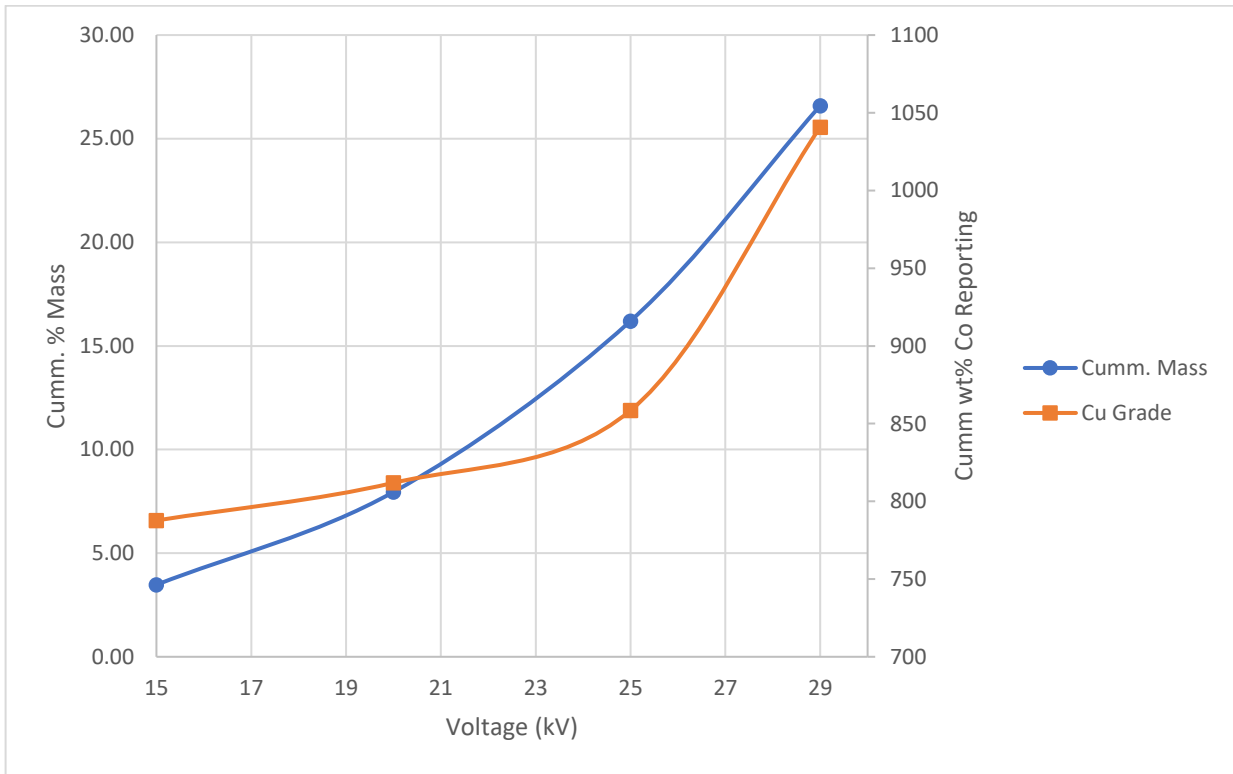


Figure C.3: Feed Material Cu Grade by Step

APPENDIX D. Additional Magnetic Separation Statistical Analysis Data

Table D.1: Magnetic separation feed material cobalt grade ANOVA for sample IC 18-09.

Source	Sum of Squares	df	MS	F	P-value	
Between Groups	45944080.72	1	45944081	56.82482	2.72E-06	significant
Within Groups	11319299.65	14	808521.4			
Total	57263380.37	15				

Table D.2: Magnetic separation feed material cobalt grade ANOVA for sample IC 18-27.

Source	Sum of Squares	df	MS	F	P-value	
Between Groups	42147650	1	42147650	63.7579	1.4E-06	significant
Within Groups	9254807	14	661057.7			
Total	51402457	15				

Table D.3: Magnetic separation feed material copper grade ANOVA for sample IC 18-09.

Source	Sum of Squares	df	MS	F	P-value	
Between Groups	9898545.817	1	9898546	4352.149	7.31E-19	significant
Within Groups	31841.66131	14	2274.404			
Total	9930387.479	15				

Table D.4: Magnetic separation feed material copper grade ANOVA for sample IC 18-27.

Source	Sum of Squares	df	MS	F	P-value	
Between Groups	1.03E+09	1	1.03E+09	2338.616	5.55E-17	significant
Within Groups	6189291	14	442092.2			
Total	1.04E+09	15				

Table D.5: Magnetic separation feed material cobalt recovery ANOVA for sample IC 18-09.

Source	Sum of Squares	df	MS	F	P-value	
Between Groups	540.9636146	1	540.9636	292.966	8.52E-10	significant
Within Groups	22.15807638	12	1.846506			
Total	563.121691	13				

Table D.6: Magnetic separation feed material cobalt recovery ANOVA for sample IC 18-27.

Source	Sum of Squares	df	MS	F	P-value	
Between Groups	194.7626	1	194.7626	61.83345	4.48E-06	significant
Within Groups	37.79751	12	3.149793			
Total	232.5601	13				

Table D.7: Magnetic separation feed material copper recovery ANOVA for sample IC 18-09.

Source	Sum of Squares	df	MS	F	P-value	
Between Groups	33337.14249	1	33337.14	6111.339	6.83E-20	significant
Within Groups	76.3695178	14	5.454966			
Total	33413.51201	15				

Table D.8: Magnetic separation feed material copper recovery ANOVA for sample IC 18-27.

Source	Sum of Squares	df	MS	F	P-value	
Between Groups	34630.71	1	34630.71	4943.754	3E-19	significant
Within Groups	98.0692	14	7.004943			
Total	34728.78	15				

APPENDIX E. Additional Gravity Separation Washability Curves

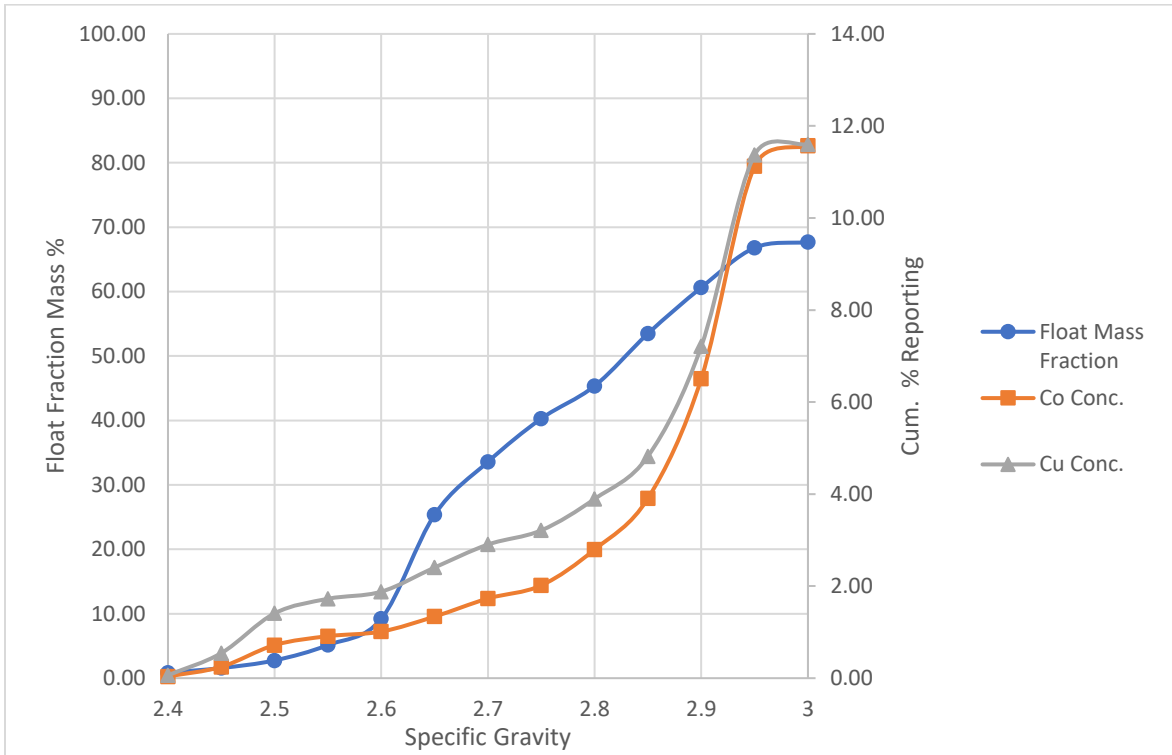


Figure E.1: Feed Material Float Fraction Elemental Concentration Response.

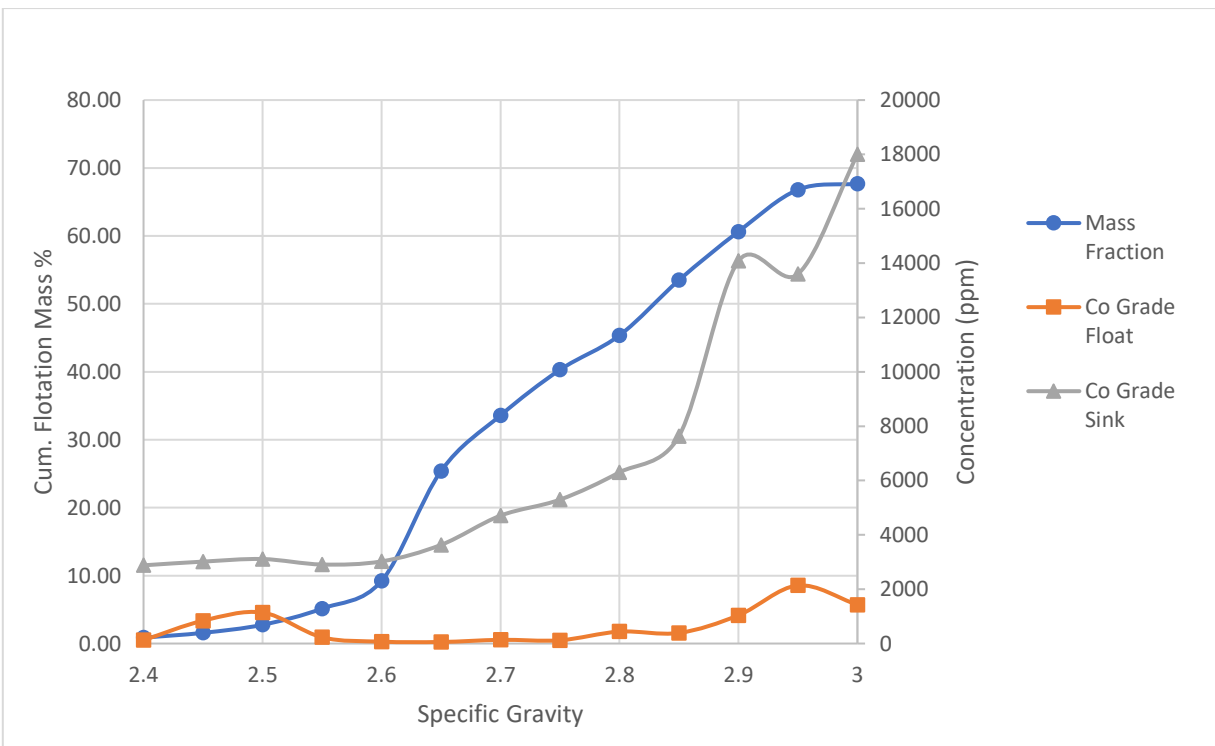


Figure E.2: Feed Material Cobalt Grade by Step.

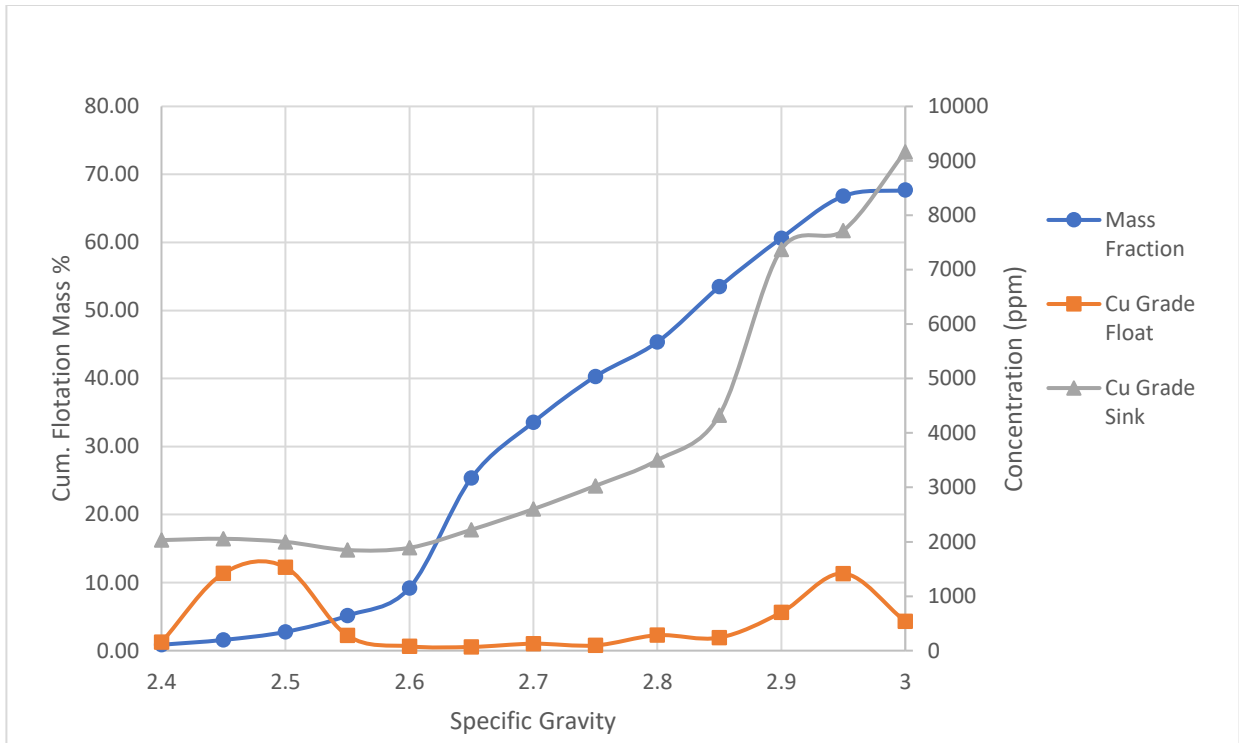


Figure E.3: Feed Material Cu Grade by Step.

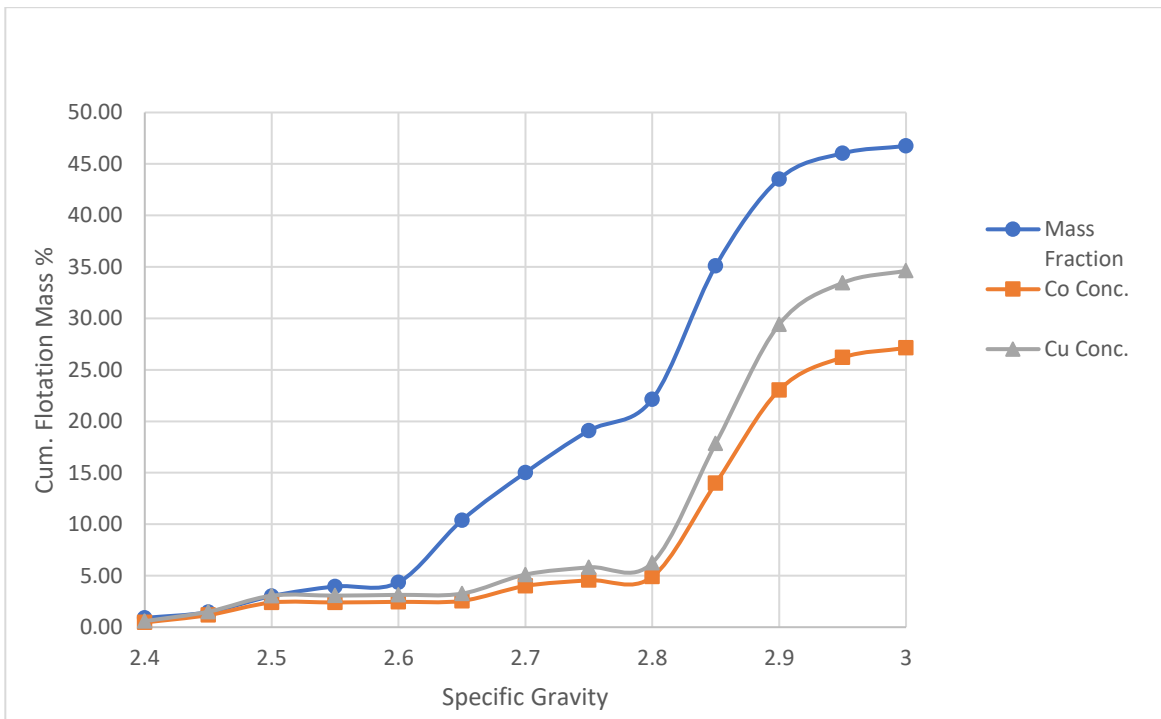


Figure E.4: Bulk Flotation Material Float Fraction Elemental Concentration Response.

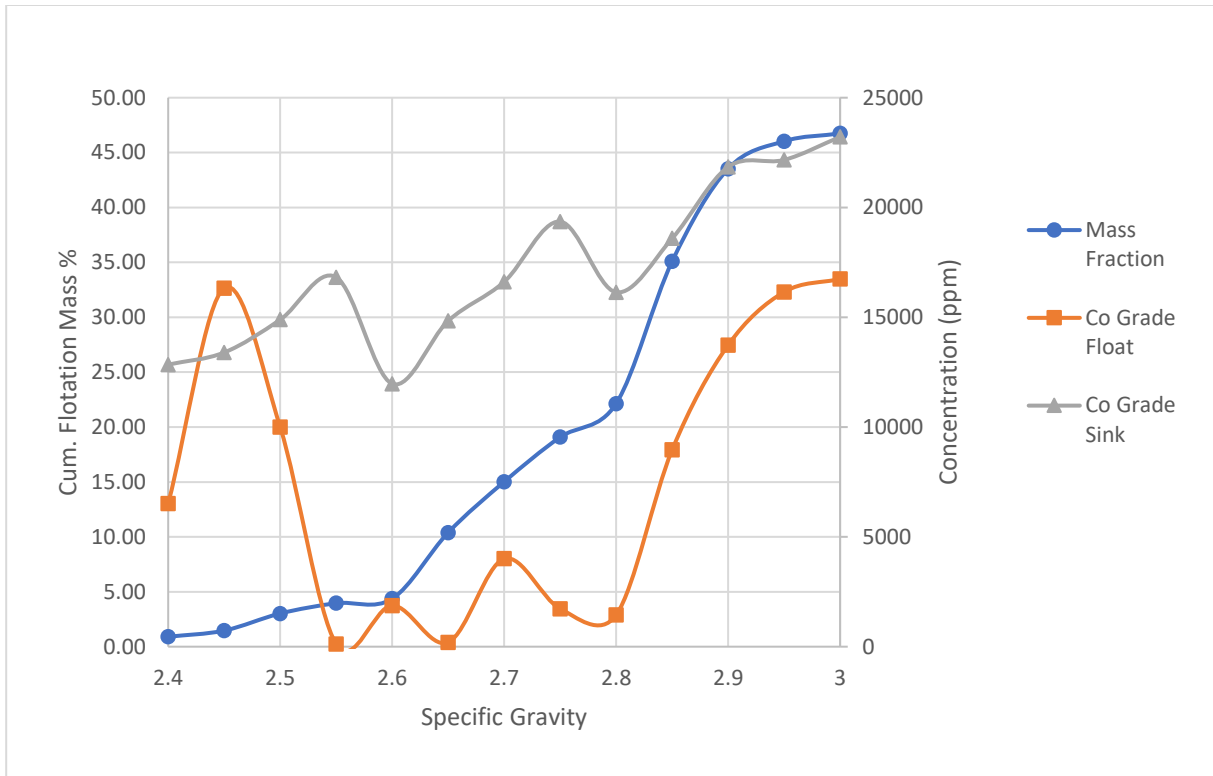


Figure E.5: Bulk Flotation Material Cobalt Grade by Step.

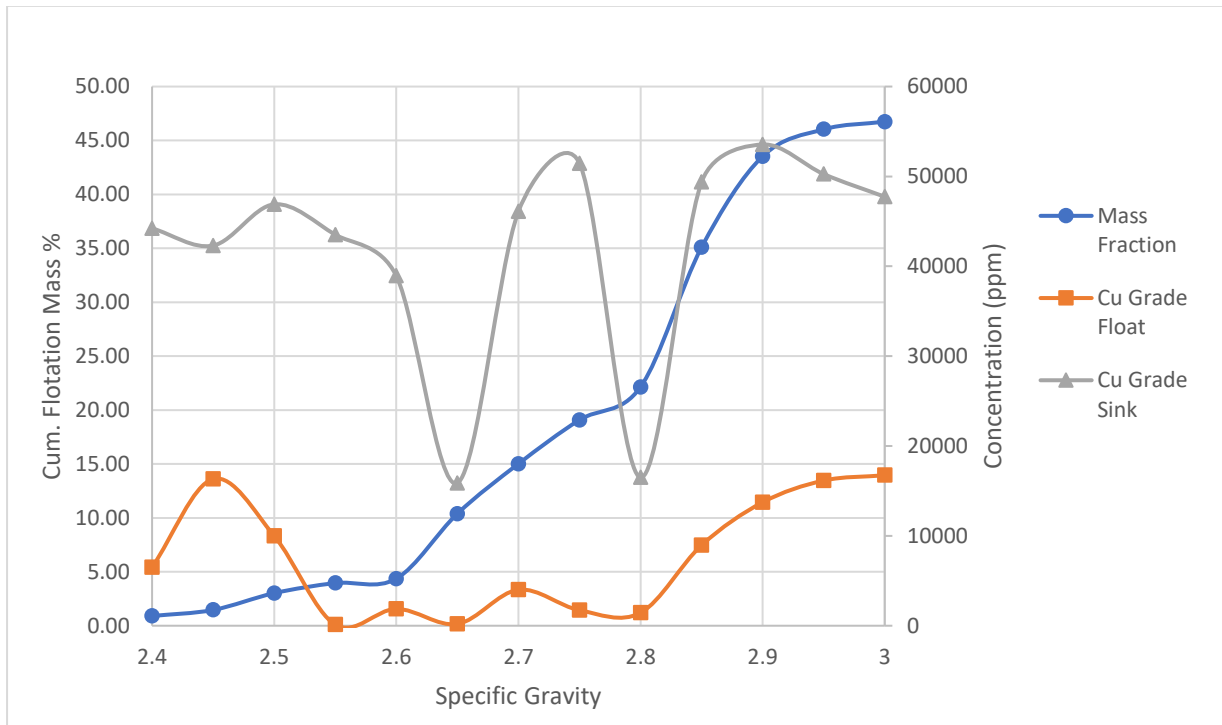


Figure E.6: Bulk Flotation Material Cu Grade by Step.

APPENDIX F. Additional Electrostatic Separation Data

Table F.1: Cobalt grade for splitter angles for various voltages.

Co Concentration (ppm)				
Splitter Angle	Voltage			
	15 kV	20 kV	25 kV	29 kV
20°+	3869	4854	8250	8118
10°-20°	2935	3687	4975	5734
0°-10°	1321	1862	2594	1576
-0°	648	1044	1572	1623

Table F.2: Copper grade for splitter angles for various voltages.

Cu Concentration (ppm)				
Splitter Angle	Voltage			
	15 kV	20 kV	25 kV	29 kV
20°+	2565	3160	4435	4944
10°-20°	2235	2435	3223	3582
0°-10°	1769	1791	1815	1053
-0°	1109	1216	1510	1459

Table F.3: Iron grade for splitter angles for various voltages.

Fe Concentration (wt%)				
Splitter Angle	Voltage			
	15 kV	20 kV	25 kV	29 kV
20°+	21.17	16.73	14.71	23.59
10°-20°	16.60	17.17	18.64	20.86
0°-10°	12.11	13.52	12.77	9.11
-0°	12.27	12.45	9.60	13.24

Table F.4: Cobalt recovery for splitter angles for various voltages.

Co Recovery (%)				
Splitter Angle	Voltage			
	15 kV	20 kV	25 kV	29 kV
20°+	85.36	8.45	37.31	40.64
10°-20°	13.24	10.38	18.76	26.86
0°-10°	0.55	76.99	40.82	29.59
-0°	0.85	4.17	3.11	2.90

Table F.5: Copper recovery for splitter angles for various voltages.

Cu Recovery (%)				
Splitter Angle	Voltage			
	15 kV	20 kV	25 kV	29 kV
20°+	82.18	6.03	31.46	40.64
10°-20°	14.64	7.51	19.06	26.86
0°-10°	1.07	81.14	44.79	29.59
-0°	2.11	5.32	4.69	2.90

Table F.6: Iron recovery for splitter angles for various voltages.

Fe Recovery (%)				
Splitter Angle	Voltage			
	15 kV	20 kV	25 kV	29 kV
20°+	82.94	5.73	18.65	28.77
10°-20°	13.30	86.44	19.71	23.80
0°-10°	0.90	6.57	56.32	41.67
-0°	2.86	1.26	5.33	5.77

APPENDIX G. Additional Electrostatic Separation Washability Curves

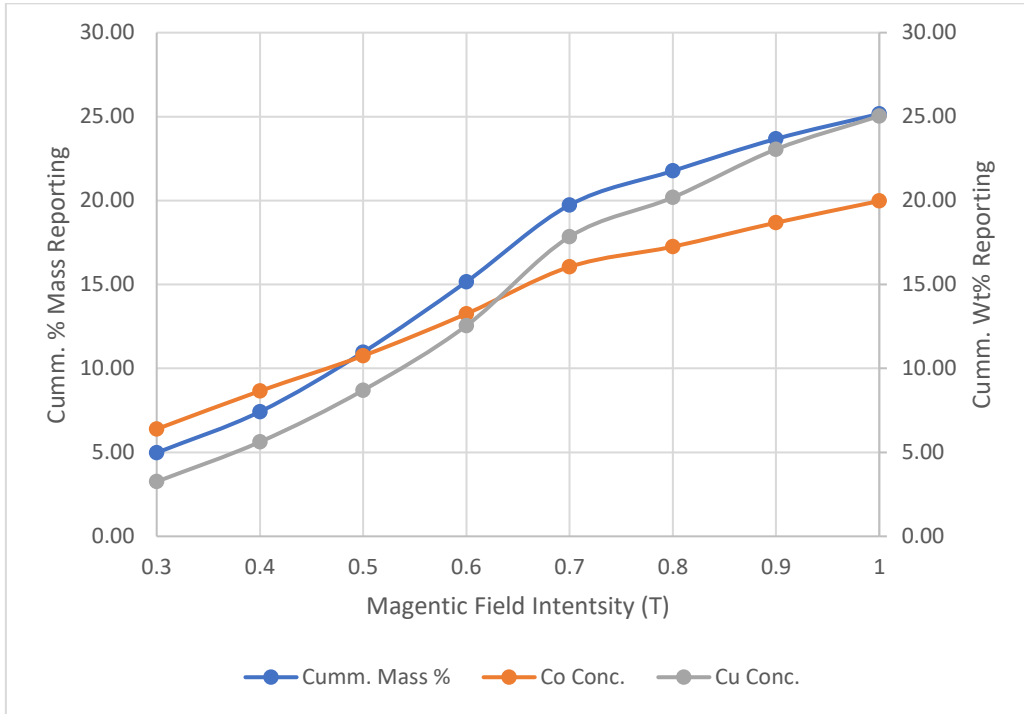


Figure G.1: Feed Material Float Fraction Elemental Concentration Response.

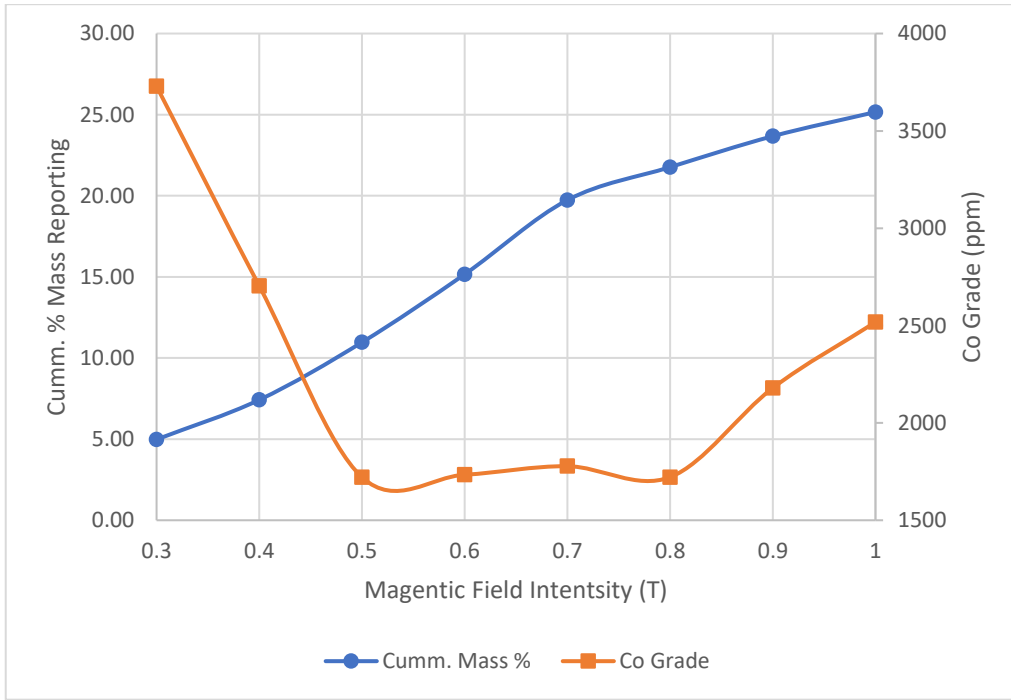


Figure G.2: Feed Material Cobalt Grade by Step.

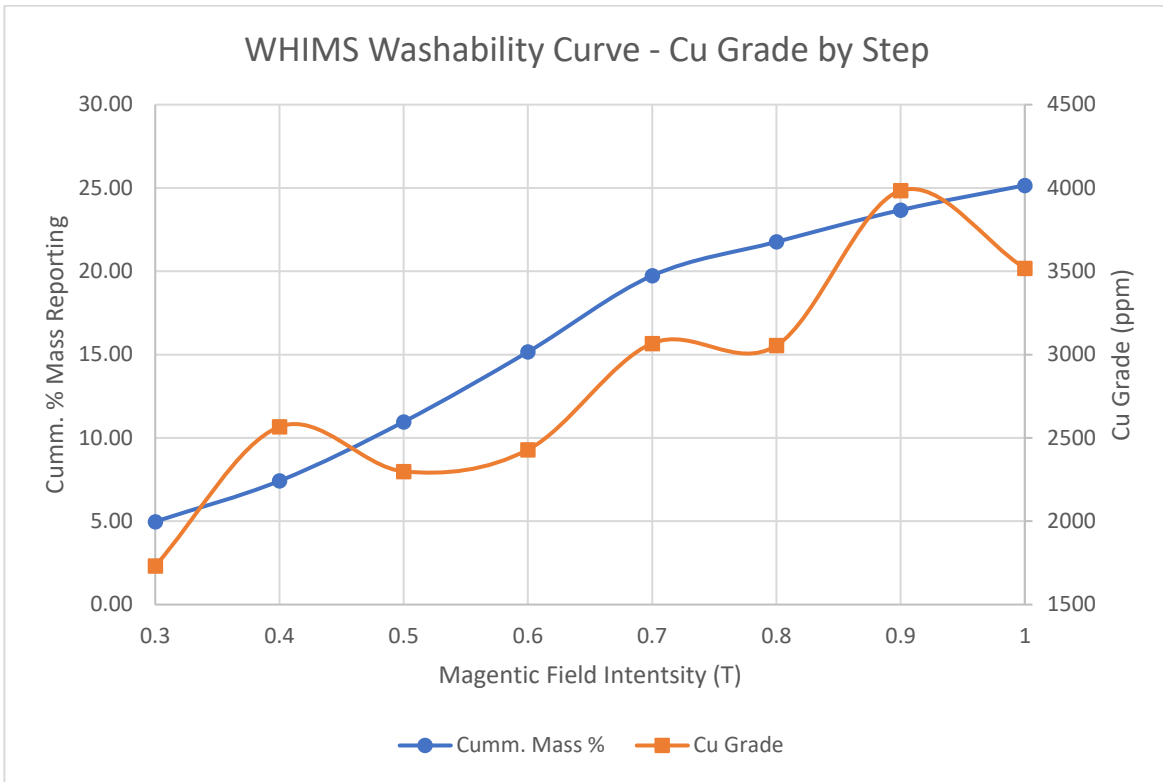


Figure G.3: Feed Material Cu Grade by Step.

APPENDIX H. Grade Calculations

Shown in Equation H.1 is the equation used to calculate the elemental grades using data from the AAS. The concentration of the element in the material is represented by “ C_o ”. “ M_o ” represents the mass of the sample used in the digestion. “ M_{Dg} ” represents the final mass of the digestion. “ M_{Di} ” represents the total mass of the dilution. “ M_{DD} ” represents the mass of the digestion used in the dilution. For example, to determine the cobalt grade in the magnetic fraction of the magnetic separation thermal decomposition of bulk flotation concentrate trial 1, one would take the cobalt concentration measured by the AAS (7.903 ppm), multiple it by the final mass of the dilution (52.3895 g) and divide by the mass of the digestion used in the dilution (2.2 g). This is the concentration of cobalt in the digestion. This concentration is then multiplied by the total mass of the digestion (60.3902 g) divided by the mass of the sample used in the digestion (0.4995g). This results in the cobalt concentration of the magnetic fraction being calculated as 22753 ppm (2.275 wt%) . This is shown in equation H.2.

$$C_o = \frac{C_A * M_{Di}}{M_{DD}} * \frac{M_{Dg}}{M_o} \quad (H. 1)$$

$$C_{Co,mag\ fraction,thermo\ decomp\ bulk\ trial\ 1} = \frac{7.903\ ppm * 52.3895\ g}{2.2\ g} * \frac{60.3902\ g}{0.4995\ g} \quad (H. 2)$$

APPENDIX I. Recovery Calculations

Shown in Equation I.1 is the equation used to calculate the elemental recoveries. Recovery is represented by “R”. “C_f” represents the elemental concentration in the fraction being calculated. “M_f” represents the mass of the fraction being calculated. “M_e” represents the mass of the element in all other fractions of the trial. For example, to determine the cobalt recovery in the magnetic fraction of the magnetic separation thermal decomposition of bulk flotation concentrate trial 1, one would take the cobalt concentration (22753 ppm), divide it by 1000 and then multiply by the mass of the fraction (10.2259 g). This calculates the amount of cobalt in the sample in mg. Then, that mass would be divided by the sum of the mass of the cobalt in target fraction and the mass of the cobalt in the other produced fractions (37 mg), in this case the non-magnetic fraction, in that trial. This sum is the total mass of cobalt in the sample used to run the trial. With the total cobalt in the sample and the cobalt in the target fraction known, a recovery of 0.8616 (86.16%) can be calculated. This is shown in Equation I.2.

$$R = \frac{\left(\frac{C_f}{1000}\right) * M_f}{\left\{\left(\frac{C_f}{1000}\right) * M_f\right\} + M_e} \quad (I.1)$$

$$R = \frac{\left(\frac{22753}{1000}\right) * 10.2259 \text{ g}}{\left\{\left(\frac{22753}{1000}\right) * 10.2259\right\} + 37 \text{ mg}} \quad (I.2)$$

APPENDIX J. Combined Economics Design Criteria and Model Assumptions

Table J.1: Operating Schedule

Period	Value
Days/Year	340
Days/Week	7
Shifts/Day	3
Hours/Shift	8
Hours/Week	168
Availability	87

Table J.2: Feed and Product Characteristics

	Value	Units	Comments
Cobalt Grade (in)	0.19	wt%	Indicated Resource Grade
Copper Grade (in)	0.59	wt%	Back Calculated from Sortation
Cobalt Grade (out)	3.01	wt%	From Magnetic Separation
Copper Grade (out)	6.10	wt%	From Cleaner Differential Flotation
Cobalt Recovery		%	
Copper Recovery	1.55	%	Recovery to Cleaner Differential Flotation
Bond Work Index			
Final Grind	105	micrometer	Feed to Rougher Flotation

Table J.3: Crushing Circuit Schedule.

Crushing Circuit Schedule	Value	Units
Daily	24	Hours/day
Weekly	7	Days/week
Volume of Material	2000	Metric tons/day
Availability	81	%

Table J.4: Sortation Circuit Schedule.

Sortation Circuit Schedule	Value	Units
Daily	24	Hours/day
Weekly	7	Days/week
Volume of Material	1580	Metric tons/day
Availability	97	%

Table J.5: Grinding/Processing Circuit Schedule.

Crushing Circuit Schedule	Value	Units
Daily	24	Hours/day
Weekly	7	Days/week
Volume of Material	1298.5	Metric tons/day
Availability	92	%

Table J.6: Flotation Equipment.

Equipment	Value	Units	Number
Mine Run Ore Bin	38	Cubic meter	1
Conveyor	36	Centimeter	1
Grizzly Feeder	91	Centimeter	1
Conveyor	36	Centimeter	1
Jaw Crusher	25	Horsepower	1
Vibrating Screen	3.0	Square meter	1
Conveyor	36	Centimeter	1
Vibrating Feeder w/ Bin	30	Centimeter	1
Conveyor	36	Centimeter	1
Conveyor	36	Centimeter	1
SAG Mill	4.1	Meter diameter	1
Sump and Pump	627	lpm	1
Vibrating Screen	3.0	Square meter	1
Ball Mill	0.82	Meter diameter	1
Sump and Pump	471	lpm	1
Cyclone	15	Centimeter	6
Sump and Pump	631	lpm	1
Regrind Ball Mill	0.20	Meter diameter	1
Thickener	4.4	Meter diameter	1
Sump and Pump	56	lpm	1
Flotation Cells	0.54	Liter	49
Sump and Pump	56	lpm	1
Sump and Pump	11	lpm	1
Filter	7.0	Square meter	1

Table J.6 Continued

Sump and Pump	49	lpm	1
Flotation Cells	0.53	Liter	41
Cyclone	10	Centimeter	6
Conveyor	36	Centimeter	1
Thickener	4.1	Meter Diameter	1
Sump and Pump	3.7	lpm	1
Dryer	0.91	Meter diameter	1
Sump and Pump	49	lpm	1
Sump and Pump	515	lpm	1
Sump and Pump	7.5	lpm	1
Conveyor	36	Centimeter	1
Filter	7.0	Square meter	1
Thickener	13	Meter diameter	1
Thickener	1.6	Meter diameter	1
Conveyor	36	Centimeter	1
Sump and Pump	515	lpm	1
Sump and Pump	7.5	lpm	1
Dryer	0.91	Meter diameter	1
Conveyor	36	Centimeter	1

Table J.7: Flotation Supplies.

Supplies	Value	Units
Electricity	13,700	kWh/day
Fuel Oil	1,250	liters/day
Grinding Media	522	kilograms/day
Mill Liners	65	kilograms/day
Lime	805	kilograms/day
Collectors	58	kilograms/day
Frothers	50	kilograms/day
Flocculants	9	kilograms/day

Table J.8: Flotation Personal Needed.

Hourly Personnel (per shift)	Value	Units
Control Room Operators	1	Per shift
Crusher System Operators	0	Per shift
Process Machinery Operators	1	Per shift
Leach System Operators	0	Per shift
Tailings System Operators	1	Per shift
Reagent Mixers	0	Per shift
Assayers	0	Per shift
Samplers	0	Per shift
Maintenance Workers	0	Per shift
Mechanics	1	Per shift
Electricians	0	Per shift
Laborers	1	Per shift
Total	5	Per Shift

Table J.9: Personal used in flotation labor calculations.

Salaried Personnel (per day)	Value	Units
Mill Superintendent	0	Per day
General Foreman	1	Per day
Maintenance Foreman	0	Per day
Plant Manager	1	Per day
Senior Metallurgist	0	Per day
Metallurgist	1	Per day
Process Technician	1	Per day
Instrument Technician	0	Per day
Process Foreman	1	Per day
Total	5	Per day

Table J.10: Flotation operating costs.

Operating Cost Category	Cost (\$)/per metric ton	Percent of Total
Equipment Operation	6.94	27.36
Supplies	4.82	19.00
Labor	8.94	35.23
Administration	2.36	9.30
Sundry Items	2.31	9.11
Total	25.37	100.00

Table J.11: Differential flotation capital costs.

Capital Cost Category	Cost (\$)	Percent of Total
Equipment	5,537,700	18.17
Installation Labor	4,505,300	14.78
Concrete	526,400	1.73
Piping	1,736,100	5.69
Structural Steel	541,600	1.78
Insulation	153,100	0.53
Instrumentation	1,089,400	3.57
Electrical	616,100	2.02
Coatings and Sealants	69,200	0.23
Mill Building/Surface Facilities	2,838,200	9.32
Initial Tailings Facility	190,300	0.62
Engineering and Desing	3,916,700	12.86
Construction Management	2,848,500	9.35
Contingency	5,127,300	16.83
Working Capital	769,100	2.52
Total	30,465,000	100.00

Table J.12: Factored Mill Capital Costs.

Component	Sub-Component	Proportion (%)
Equipment	Crushers & Grinding Mills	22.7
Equipment	Concentrator Eq. and Ancillary	8.9
Tailings Pond	Parts, Tires, and Pumps	1.0
Tailings Pond	Fuel and Lubrication	1.4
Tailings Pond	Construction Labor	6.7
Tailings Pond	Synthetic Liner and PVC Pipe	12.9
Buildings and Equipment	Timber	1.5
Buildings and Equipment	Concrete	2.6
Buildings and Equipment	Construction Materials and Steel	11.1
Buildings and Equipment	Purchased Equipment	1.9
Buildings and Equipment	Construction Labor	20.0
Construction Equipment Op	Parts	1.2
Construction Equipment Op	Fuel and Lubrication	4.1
Electrical System	Electrical Systems	4.0
Total		100

Table J.13: Factored Mill Operating Costs.

Component	Sub-Component	Proportion (%)
Fuel	Fuel	3.4
Lubricants	Lubricants	3.9
Electricity	Electricity	17.3
Parts	Crushing and Grinding	3.8
Parts	Concentration and Ancillary	1.6
Reagents	Reagents	24.5
Grinding Media	Grinding Media	21.5
Mill Labor	Mill Labor	24.0
Total		1.0

Table J.14: Thermal decomposition design criteria.

Drying Circuit	Units	Value	Comments
Operating Schedule	[d/y]	365	
	[d/week]	7	
	[shifts/d]	3	
	[h/shift]	8	
	[h/week]	168	
Plant availability	[%]	93.15	340 day per year
Processing design rate	[t/d]	379.3	Wet concentrate
Initial moisture	[%]	12	
Feed temperature	[°C]	25	
Number of conveyors	[unit]	1	
Conveyor capacity	[t/h]	37.9	Plus 20% of the design rate
Conveyor power consumption	[kWh]	75.9	
Furnace temperature	[°C]	100	
Furnace capacity	[t/d]	18.9	Plus 20% of the design rate
Discharge temperature	[°C]	100	
Nitrogen consumption	[Nm ³ /t]	1	Per tonnes of wet feed
Nitrogen temperature	[°C]	25	
Nitrogen discharge temperature	[°C]	100	

Table J.14 Continued

Energy requirement	[kcal/kg]	83.22	Theoretical minimum to dry
Thermal Decomposition Circuit	Units	Value	Comments
Operating Schedule	[d/y]	365	
	[d/week]	7	
	[shifts/d]	3	
	[h/shift]	8	
	[h/week]	168	
Plant availability	[%]	93.15	340 day per year
Processing design rate	[t/d]	333.8	Dry concentrate
Cobalt grade in the feed	[%]	1.84	
Copper grade in the feed	[%]	1.20	
Cobalt grade in the discharge	[%]	2.15	
Copper grade in the discharge	[%]	1.40	
Furnace temperature	[°C]	650	
Rotary kiln capacity	[t/d]	16.7	Plus 20% of the design rate
Feed temperature	[°C]	100	
Discharge temperature	[°C]	650	
Average decomposition of FeS ₂ to Fe ₇ S ₈	[%]	99.58	
Average decomposition of Fe ₇ S ₈ to FeS	[%]	47.31	
Average retention time	[min]	60	
Energy requirement	[kcal/kg]	151.57	Theoretical minimum
Nitrogen consumption	[Nm ³ /t]	2	Per tonnes of dry feed
Nitrogen generator capacity	[cu ft/min]	20	
Nitrogen feed temperature	[°C]	25	
Nitrogen discharge temperature	[°C]	650	
Dust entrainment	[%]	10	Dry feed basis
Number of bag houses	[unit]	1	
Bag house capacity	[cu ft/min]	28.8	

Table J.14 Continued

Number of heat exchangers	[unit]	2	
Condensation in 1 st exchanger	[%]	65	
Condensation in 2 nd exchanger	[%]	35	

Table J.15: Thermal decomposition equipment costs.

Equipment	Capital Cost [USD]
Portable Conveyor	18,428.3
Hollow Flight Dryer	44,000.0
Thermal Decomposition Circuit	
Indirect-Fired Rotary Kiln	2,918,136.3
Bag House for Dust Collection	2,401.4
Bin Collector for Dust	516.2
Shell and Tube - Heat Exchanger #1	125,770.5
Shell and Tube - Heat Exchanger #2	125,770.5
Rotary Cooler - Heat Exchanger #3	245,458.2
Nitrogen Generator	78,000.0
Total	3,558,481.4

Table J.16: Thermal decomposition capital costs.

Expense	Capital Cost [\$]
Capital Cost of Major Equipment	3,558,481
Capital Cost of Minor Equipment and Installation	3,807,575
Construction, Contingencies, and EPC & Management	10,445,068
Total Installed Costs	17,811,125

Table J.17: Thermal decomposition operating costs.

Item	Annual Cost [\$/year]
Electricity	57,781
Natural Gas	646,608
Nitrogen	8,181
Labor and Maintenance	1,781,112
Total Operating Expenses	2,493,682

Table J.18: Magnetic separation factored capital costs.

Expense	Factor	Cost
WHIMS	---	\$ 700,000.00
Dewatering Method	---	\$ 154,100.00
Minor equipment	0.9 equipment	\$ 768,690.00
construction	0.65 all equipment	\$ 1,054,813.50
Contingency	0.3 all equipment + construction	\$ 803,281.05
Installation Labor	0.5 all equipment + construction + contingency	\$ 1,740,442.28
Total		\$ 5,221,326.83

Table J.19: Magnetic separation capital cost proportion.

Component	Sub-Component	Proportion (%)
Equipment	Wet High Intensity Magnetic Separator	13.41
Equipment	Rotary Drum	2.95
Equipment	Minor Equipment	14.72
Buildings	Construction	20.20
Miscellaneous	Installation Labor	33.33
Miscellaneous	Contingency	15.38
Total		100

Table J.20: Magnetic Separation operating costs.

Expense	Cost
Labor	\$ 813.49
Parts Cost	\$ 96.48
Electricity	\$ 21.60
Lubricant	\$ 39.24
Water	\$ 1.00
Total	\$ 971.81

Table J.21: Magnetic separation design criteria.

	Unit	Value
Availability (estimated)		87%
Feed Amount	Tonne/day	273.17
Cobalt Feed Grade	wt%	2.15
Copper Feed Grade	wt%	1.4
Magnetic Field Strength Required	Tesla	1.0
Process Capacity (estimated)	Tonne/hour	12
Concentrate Cobalt Grade	wt%	3.5
Concentrate Copper Grade	wt%	1.71
Concentrate Tonnages	Tonnes	200

Table J.22: Dewatering design criteria.

	Unit	Value
Availability (estimated)		87%
Feed Amount	lb dry concentrate/day	200
Diameter	ft	6
Length	ft	6
Weight	lbs	8,900
Filter Area	sq ft	113
Process Capacity (estimated)	lb dry concentrate/hour	25.63
Final Conc. Water Weight (estimated)	wt%	10
Final Concentrate weight	tonnes/day	220

Table J.23: Cobalt transportation cost calculation.

Transportation Method	Distance (Km)	Cost Per Ton per km (\$)	Tonnes	Total Cost per day (\$)	Total Cost per Year (\$)
Truck	439	0.156	220	\$ 15,078.49	\$ 5,126,685.18
Rail	3516	0.051	220	\$ 39,454.10	\$ 13,414,392.86
				Total	\$ 18,541,078.04

Table J.24: Copper transportation cost calculations.

Transportation Method	Distance (km)	Cost Per Ton per km (\$)	Tonnes	Total Cost per day (\$)	Total Cost per Year (\$)
Truck	694	0.156	2.88	\$ 311.63	\$ 105,954.91
Rail	---	0.051	---	\$ -	\$ -
				Total	\$ 105,954.91

APPENDIX K. Refined Flowsheet with Mass Balances

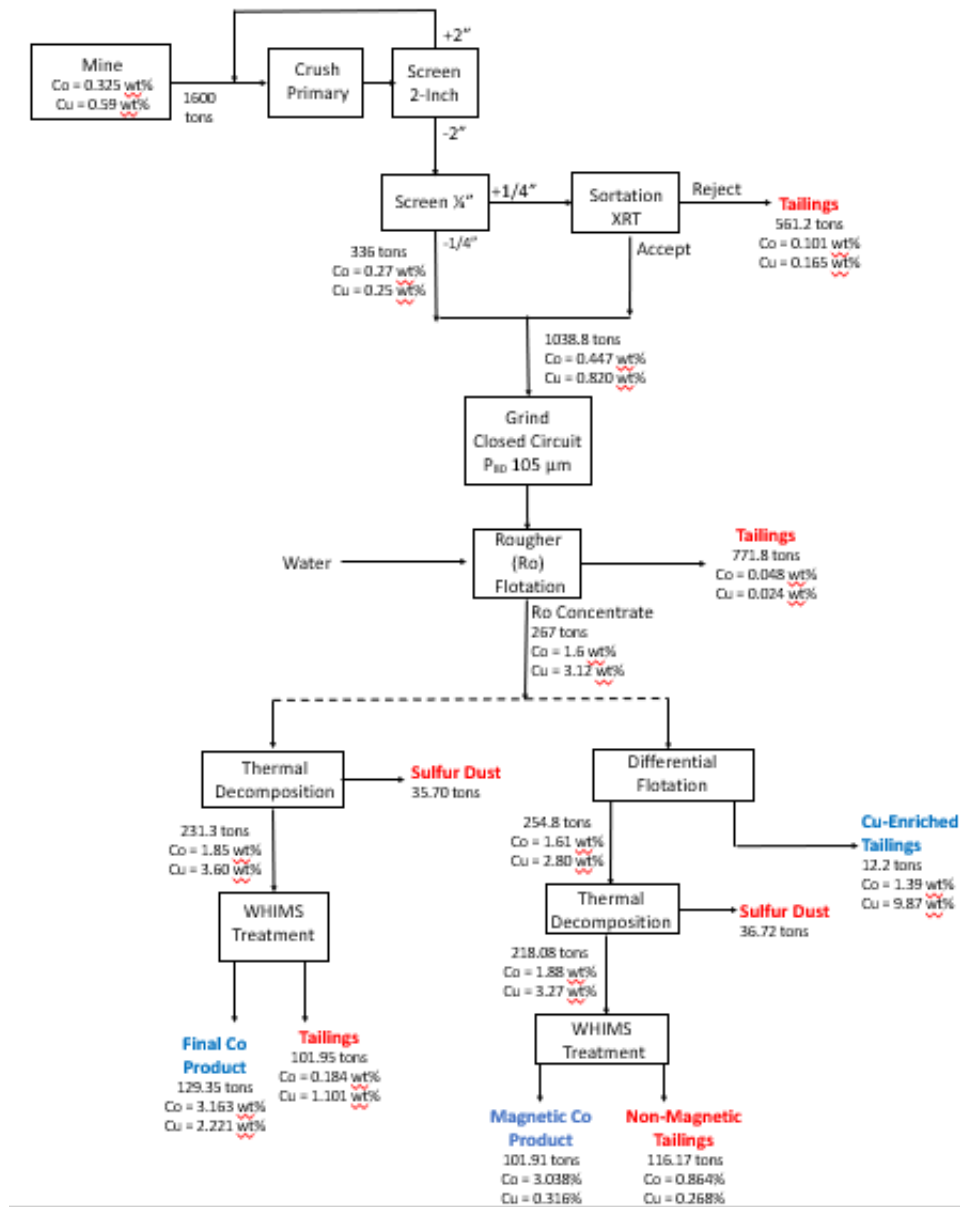


Figure K.1: Refined possible flowsheet with mass balances.